

Time-Frequency Analysis of Waveform Diverse Designs

By

© 2023

Thomas Kramer

Submitted to the graduate degree program in Electrical Engineering and Computer Science and the Graduate Faculty of the University of Kansas in partial fulfillment of the requirements for the degree of Master of Science.

Dr. Shannon Blunt, Chairperson

Committee members

Dr. James Stiles

Dr. Victor Frost

Date Defended:

The thesis committee for Thomas Kramer certifies that this is the approved version of the following thesis:

Time-Frequency Analysis of Waveform Diverse Designs

Chairperson: Dr. Shannon Blunt

Date Approved: _____

Abstract

Waveform diversity desires to optimize the Radar waveform given the constraints and objectives of a particular task or scenario. Recent advances in electronics have significantly expanded the design space of waveforms. The resulting waveforms of various waveform diverse approaches possess complex structures which have temporal, spectral, and spatial extents. The utilization of optimization in many of these approaches results in complex signal structures that are not imagined a priori, but are instead the product of algorithms. Traditional waveform analysis using the frequency spectrum, autocorrelation, and beampatterns of waveforms provide the majority of metrics of interest. But as these new waveforms' structure increases in complexity, and the constraints of their use tighten, further aspects of the waveform's structure must be considered, especially the true occupancy of the waveforms in the transmission hyperspace. Time-Frequency analysis can be applied to these waveforms to better understand their behavior and to inform future design. These tools are especially useful for spectrally shaped random FM waveforms as well as spatially shaped spatial beams. Both linear and quadratic transforms are used to study the emissions in time, frequency, and space dimensions. Insight on waveform generation is observed and future design opportunities are identified.

Acknowledgements

I would like to dedicate this to all the friends, faculty, and coworkers I have met at KU, my colleagues at Sandia, my whole support network scattered throughout north-east Kansas and beyond, and my incredibly supportive wife.

This work was supported in part by the Office of Naval Research under Contract #N00014-20-C-1006 and by Sandia National Laboratories under Contract #2237007. This paper describes objective technical results and analysis. Any subjective views or opinions that might be expressed in the paper do not necessarily represent the views of the U.S. Department of Energy or the United States Government.

Table of Contents

1. Introduction and Background	1
1.1 Intro to Radar Signal Processing	1
1.1.1 Basic Principles	1
1.1.2 Radar Range Equation.....	2
1.1.3 Continuous Wave and Pulsed Operation	3
1.1.4 Radar Ranging.....	4
1.1.5 Coherent Integration.....	5
1.1.6 Pulse Compression.....	5
1.1.7 Doppler Processing	8
1.2 Radar Waveforms	11
1.2.1 Deterministic FM Waveforms	12
1.2.1.1 Linear FM Waveforms	12
1.2.1.2 Deterministic Nonlinear FM	15
1.2.2 Random FM Waveforms.....	18
1.2.2.1 Optimized Random FM Noise	20
1.2.2.2 Process-Based Random FM Noise	20
1.2.2.3 Waveform Diversity	21
1.2.2.3.1 Temporal and Spectral Diversity	21
1.2.2.3.2 Spatial Diversity	22
1.2.2.3.3 Other Forms of Waveform Diversity	22
1.2.2.4 Waveform Agility.....	23
1.2.3 Waveform Designs under Consideration	23
1.2.3.1 PRO-FM Waveforms.....	23
1.2.3.2 FTE and Log-FTE Waveforms.....	25
1.2.3.3 TTE Waveforms.....	26
1.2.3.4 StoWGe Waveforms	27
1.2.3.5 CE-OFDM Waveforms.....	28
1.3 Waveform Analysis Tools.....	29
1.3.1 Fourier Analysis.....	30
1.3.2 Autocorrelation and Cross-Correlation	31
1.3.3 Delay-Doppler Ambiguity Function.....	32

1.3.4	Time-Frequency Analysis	33
1.3.4.1	Linear Time-Frequency Transforms	33
1.3.4.2	Quadratic Time-Frequency Transforms	35
2.	Time-Frequency Analysis of Random FM Waveforms.....	38
2.1	Traditional Analysis of Gaussian spectral shapes.....	38
2.1.1	Time Domain Analysis	38
2.1.2	Frequency Domain Analysis.....	40
2.1.3	Delay Domain Analysis	44
2.2	Joint Time-Frequency Analysis of Gaussian Spectral Shapes.....	46
2.2.1	Angle-Based Instantaneous Frequency Analysis.....	46
2.2.1.1	PRO-FM Instantaneous Frequency	47
2.2.1.2	FTE Instantaneous Frequency.....	48
2.2.1.3	Log-FTE Instantaneous Frequency.....	50
2.2.1.4	TTE Instantaneous Frequency	52
2.2.1.5	CE-OFDM Instantaneous Frequency	54
2.2.1.6	StoWGe Instantaneous Frequency	56
2.2.1.7	Instantaneous Frequency statistical parameters.....	58
2.2.2	Spectrogram Analysis.....	59
2.2.3	Wigner-Ville Distribution Analysis.....	63
2.2.4	Instantaneous Autocorrelation Function Analysis	67
2.2.5	Radon-Wigner Transform Analysis.....	71
2.3	Traditional Analysis of Notched Gaussian Spectral Shapes	72
2.3.1	Time Domain Analysis	73
2.3.2	Frequency Domain Analysis	74
2.3.3	Delay Domain Analysis	77
2.4	Joint Time-Frequency Analysis of Notched Gaussian Spectral Shapes.....	79
2.4.1	Angle-Based Instantaneous Frequency Analysis.....	79
2.4.2	Spectrogram Analysis.....	82
2.5	Traditional FM Design Perspective.....	86
2.6	Waveform Analysis Conclusions	87
3.	Instantaneous Frequency Estimation of Random FM.	89
3.1	Instantaneous Frequency Estimation using the Spectrogram	89

3.1.1 Bayesian Estimation of Instantaneous Frequency using the Spectrogram	89
3.1.2 Reiterative Bayesian Estimation of Instantaneous Frequency using the Spectrogram.	91
4. Conclusions & Future Work.....	96

List of Figures

Figure 1.1: The matched filter pulse compression response of two equal power scatterers..	7
Figure 1.2: The matched filter response of a strong and weak scatterer close in range	8
Figure 1.3: A geometric representation of the radar data cube. [1].....	9
Figure 1.4: Pulse compressed response for each pulse in the CPI.....	10
Figure 1.5: Range-Doppler map after Doppler Processing.....	11
Figure 1.6: Autocorrelation function of a LFM waveform.	13
Figure 1.7: Frequency spectrum of a LFM waveform.	14
Figure 1.8: Ambiguity function of a LFM waveform.	15
Figure 1.9: Instantaneous frequency function of a tangent NLFM waveform.	17
Figure 1.10: PSD of a tangent NLFM waveform.	18
Figure 1.11: Power Spectral Density of a single PRO-FM waveform.....	24
Figure 1.12: Mean power spectral density of 100 PRO-FM waveforms.....	25
Figure 2.1: Comparison of several waveform amplitudes.	39
Figure 2.2: Comparison of several waveform PSDs.	41
Figure 2.3: Comparison of the average PSD of several waveform classes.	42
Figure 2.4: Comparison of mean PSD for each waveform class.....	43
Figure 2.5: Average autocorrelation for different waveform classes.....	45
Figure 2.6: Histogram of 1,000 PRO-FM instantaneous frequency values in simulation....	47
Figure 2.7: Histogram of 1,000 PRO-FM instantaneous frequency values captured in loopback.....	48
Figure 2.8: Histogram of 1,000 FTE instantaneous frequency values in simulation.....	49
Figure 2.9: Histogram of 1,000 FTE instantaneous frequency values captured in loopback.	50
Figure 2.10: Histogram of 1,000 log-FTE instantaneous frequency values in simulation. ..	51
Figure 2.11: Histogram of 1,000 log-FTE instantaneous frequency values captured in loopback.....	52
Figure 2.12: Histogram of 1,000 TTE instantaneous frequency values in simulation.....	53
Figure 2.13: Histogram of 1,000 TTE instantaneous frequency values captured in loopback.	54
Figure 2.14: Histogram of 1,000 CE-OFDM instantaneous frequency values in simulation.	55
Figure 2.15: Histogram of 1,000 CE-OFDM instantaneous frequency values captured in loopback.....	56
Figure 2.16: Histogram of 1,000 StoWGe instantaneous frequency values in simulation. ..	57
Figure 2.17: Histogram of 1,000 StoWGe instantaneous frequency values captured in loopback.....	58
Figure 2.18: Spectrogram of a PRO-FM waveform using a 10% time window.	61
Figure 2.19: Spectrogram of a PRO-FM waveform using a 1% time window.	61
Figure 2.20: Wigner-Ville distribution of a PRO-FM waveform.	64
Figure 2.21: Smoothed Wigner-Ville distribution of a PRO-FM waveform.....	65
Figure 2.22: Instantaneous Autocorrelation of a PRO-FM waveform.	68

Figure 2.23: Smoothed Instantaneous Autocorrelation of a PRO-FM waveform.	68
Figure 2.24: Instantaneous Autocorrelation of a CE-OFDM waveform.	69
Figure 2.25: Smoothed IAF of a CE-OFDM waveform.	70
Figure 2.26: Smoothed WVD of a CE-OFDM waveform.	70
Figure 2.27: Radon-Wigner Transform of a PRO-FM waveform.	71
Figure 2.28: Radon-Wigner transform of a CE-OFDM waveform.	72
Figure 2.29: Comparison of several waveform amplitudes.	73
Figure 2.30: Comparison of several waveform PSDs.	75
Figure 2.31: Comparison of the average PSD of several waveform classes.	76
Figure 2.32: Average autocorrelation for different waveform classes.	78
Figure 2.33: Instantaneous Frequency distribution for notched PRO-FM captured in loopback.	79
Figure 2.34: Instantaneous frequency distribution for notched FTE captured in loopback.	80
Figure 2.35: Instantaneous frequency distribution for notched Log-FTE captured in loopback.	80
Figure 2.36: Instantaneous frequency distribution for notched TTE captured in loopback.	81
Figure 2.37: Spectrogram of a notched PRO-FM waveform using a 20% time window.	83
Figure 2.38: Spectrogram of a notched PRO-FM waveform using a 5% time window.	83
Figure 2.39: Spectrogram of a notched PRO-FM waveform using a 1% time window.	84
Figure 3.1: Estimated spectrum from different estimators on the spectrogram.	90
Figure 3.2: Reiterative spectrum estimate using the $p = 1$ estimator for 10 iterations.	92
Figure 3.3: Reiterative spectrum estimate using the $p = 2$ estimator for 10 iterations.	92
Figure 3.4: Reiterative spectrum estimate using the $p = \infty$ estimator for 10 iterations.	93
Figure 3.5: Comparison of estimators versus iterations on PRO-FM.	94
Figure 3.6: Comparison of estimators versus iterations on PRO-FM.	95

List of Tables

Table 2.1: Comparison of different waveform class amplitudes.	40
Table 2.2: Comparison of different waveform class PSD metrics in loopback.....	43
Table 2.3: Comparison of different waveform class autocorrelation metrics.	46
Table 2.4: Instantaneous frequency metrics for various simulated waveform classes.....	59
Table 2.5: Instantaneous frequency metrics for various waveform classes captured in loopback.	59
Table 2.6: Spectrogram metrics for various waveform classes in simulation.	62
Table 2.7: Spectrogram metrics for various waveform classes captured in loopback.	63
Table 2.8: WVD metrics for various waveform classes in simulation.	65
Table 2.9: WVD metrics for various waveform classes captured in loopback.....	66
Table 2.10: Comparison of different waveform class amplitudes.	74
Table 2.11: Comparison of different waveform class PSD metrics in loopback.....	77
Table 2.12: Comparison of different waveform class autocorrelation metrics.	78
Table 2.13: Instantaneous frequency metrics for various notched waveform classes captured in loopback.	81
Table 2.14: Spectrogram metrics for various notched waveform classes using 10% time window.	85
Table 2.15: Spectrogram metrics for various notched waveform classes using 1% time window.	85

1. Introduction and Background

Since the beginning of the 20th Century, Radar has provided mankind a new way of seeing the physical world. Utilizing the same underlying physics as optical light, Radar has provided us with a means to utilize frequencies far lower than capable of seeing with the human eye. From an initial use of ranging and detecting targets, Radars have been used to search, track, and image environments from across oceans [1] to across the human hand [2]. This diverse set of applications in turn requires a diverse set of background knowledge, including mathematics, electromagnetics, analog and digital electronics, signal processing, and many other disciplines relevant to specific Radar applications. It is impossible to cover over 100 years of radar research in a single paper, let alone a book. Instead, the key concepts relevant to this work will be covered in this chapter. Emphasis will be given to the core signal processing techniques used for radar measurements, the types of waveforms used in radar systems, and means of analyzing radar waveforms.

1.1 Intro to Radar Signal Processing

Here, a basic understanding of the Radar concept and the key measurements made by a radar system is discussed. Specifically, the concepts of pulse compression, Doppler processing, and basic array processing.

1.1.1 Basic Principles

Radars utilize the reflections of electromagnetic waves anywhere from 1 MHz to over 100 GHz to infer properties of the physical entities which reflect the waves back towards the radar. Depending on the energy of the reflection, the delay of an echo, and frequency shifting of the echo all relate

to different mechanical properties of the reflector. These are in turn used to estimate the scatterer's range, velocity, and angular direction relative to the radar system.

1.1.2 Radar Range Equation

Using a Radar, an electromagnetic pulse is emitted from some transmitter, reflected off objects in the environment, and then these reflections of the pulse are absorbed at some receiver. The ability of a receiver to utilize the reflection is primarily a function of the *signal-to-noise ratio* (SNR), which is described by the radar range equation [1], which for a monostatic case (co-located receiver and transmitter) is given as:

$$SNR = \frac{P_t G_t G_r \lambda^2 \sigma}{(4\pi)^3 R^4 k T_0 F B} \quad (1.1)$$

This equation can be broken down into the terms as they appear in the physical emission process. P_t is the power of the transmitted signal, and G_t is the gain from the transmitted antenna in the direction of the target. The transmitter's emission radiates from the transmitter in the shape of a sphere, and the power is spread over the surface of this spherical wavefront. The amount of signal power at the object is divided by the surface area of this wavefront, which is given as $4\pi R^2$. σ is the *radar cross section* (RCS) of the object illuminated by radar a distance R away in meters. The reflection then returns to the receiver, whose power is again divided by the surface area of this wavefront, $4\pi R^2$. The receiving antenna scales the reflection by its effective area, which is given as:

$$A_e = \frac{G_r \lambda^2}{4\pi} \quad (1.2)$$

Losses from the electronics and circuits inside both the transmitter and receiver are quantified in a noise figure F . Finally, the resulting signal power is divided by the thermal noise power, given as:

$$N = kT_0B \quad (1.3)$$

Where k is Boltzmann's constant (1.38×10^{-23} watt-sec/K), T_0 is the temperature of the receiver, and B is the bandwidth of the receiver.

Any additional detrimental effects to the receiver's ability to detect reflections from the transmitter are quantified as interference I . A *signal-to-interference-noise ratio (SINR)* can then be determined as:

$$SINR = \frac{S}{I + N} \quad (1.4)$$

Where S is the signal power at the receiver. Depending on the environment the radar is utilized in, I may or may not be a significant contribution in $SINR$. Interference is a particularly important consideration in environments with multiple spectrum users within the spectral band of operation [1].

1.1.3 Continuous Wave and Pulsed Operation

Radars are operated temporally in one of two ways: *continuous wave (CW)* mode and pulsed mode. In a CW mode, the transmitter continuously illuminates the environment, and the receiver continuously listens for echoes from the transmitter. In a pulsed mode, the transmitter turned on and off periodically for a time τ . While the transmitter is off, the receiver listens for echoes from the transmitter until the transmitter begins emitting the next pulse. The rate at which the transmitter emits a pulse is called the *pulse repetition frequency (PRF)*.

CW mode provides constant power on a target, which can realize higher SNRs. Longer target dwell times enable the detection of small doppler velocities, which is particularly important

in micro-Doppler applications [3]. Conversely, distortion on the receiver can occur if there exists inadequate isolation between the transmitter and the receiver. Alternatively, pulsed operation does not require as much isolation between the transmitter and receiver, as the pulse transmission and reception generally occur at different points in time. In this work, it is assumed the radar is operating in pulsed mode unless otherwise specified.

1.1.4 Radar Ranging

One of the basic measurements a radar system can make is a range measurement. In a monostatic, pulsed radar, the time delay between the transmission of a pulse and the return of an echo is proportional to the radial distance between the radar and the electromagnetic scatterer that produced the echo. The electromagnetic wave travels at the speed of light c (299,792,458 m/s) to and from the scatterer, with the resulting range being [1]:

$$R = \frac{c\Delta T}{2} \quad (1.5)$$

The radar can only measure range unambiguously until the time that the next pulse is emitted from the transmitter. Once a consecutive pulse is emitted from the radar, the echo could be from the old pulse or the new pulse, and these delays correspond to different ranges. The unambiguous maximum range is given as [1]:

$$R_{ua} = \frac{c}{2PRF} \quad (1.6)$$

In order to resolve two closely spaced scatterers, the temporal extent of the radar pulse must be smaller than the time delay between the return of the scatterer echoes. This can be restated as a range resolution, which can be written as [1]:

$$\Delta R = \frac{c\tau}{2} \quad (1.7)$$

Where τ is the temporal extent of the radar pulse. To achieve finer range resolution, the temporal extent of the radar pulse must be shortened. Otherwise, pulse compression techniques must be utilized (see section 1.1.6).

1.1.5 Coherent Integration

One means of obtaining a smaller ΔR is for the transmitter to utilize a very small τ . One consequence of short pulses is that the resulting spectra will be very wide in frequency extent, resulting in a large bandwidth. This large bandwidth will reduce the SNR of the radar according to the radar range equation. One method of improving the SNR is to utilize coherent integration [1]. By performing M_{coh} measurements of the same scene using M_{coh} transmitted pulses, the resulting received, discrete signal from each measurement can be summed sample by sample. For each received signal $y_m[n] = y(nT_s)$, the resulting signal becomes:

$$y_{\text{coh}}[n] = \sum_m^{M_{\text{coh}}} y_m[n] \quad (1.8)$$

It is assumed that the signal component of each measurement is the same, while the noise component is independently and identically distributed Gaussian noise. This process reduces the noise signal by M_{coh}^2 and the noise power by M_{coh} . The radar range equation can now be written as:

$$SNR_{\text{coh}} = \frac{M_{\text{coh}} P_t G_t G_r \lambda^2 \sigma}{(4\pi)^3 R^4 k T_0 F B} = M_{\text{coh}} SNR \quad (1.9)$$

1.1.6 Pulse Compression

Another means of both improving the SNR and achieving finer range resolution is by a process known as pulse compression [1], which decouples the temporal extent of the pulse from range

resolution. By applying a filter to the received signal, the temporal extent of the signals is compressed by converting the received temporal signal into a correlation signal.

The most utilized filter for pulse compression is the matched filter, which is often described as the pulse compression filter which maximizes SNR in the presence of white noise [1]. For a transmitted radar pulse $s(t)$, the matched filter is given as [1]:

$$h(t) = s^*(-t) \quad (1.10)$$

The matched filter response of a point scatterer is equivalent in structure to the autocorrelation of $s(t)$. The width of the mainlobe of this response is inversely proportional to the bandwidth B of the *power spectral density* (PSD) of $s(t)$ according to the Wiener-Khinchin theorem, described as [4]:

$$R_{ss}(\tau) = \int_{-\infty}^{\infty} S(f)e^{j2\pi f\tau} df \quad (1.11)$$

where $R_{ss}(\tau)$ is the autocorrelation of $s(t)$ and $S(f)$ is the PSD of $s(t)$. In order to resolve two closely spaced scatterers in the matched filtered response, such as in figure 1.1, the mainlobe width of the responses must be smaller than the time delay between the scatterer echoes. Thus, the resulting range resolution now becomes:

$$\Delta R = \frac{c}{2B} \quad (1.12)$$

Pulse compression filters other than the matched filter can be used, known as mismatch filters. One consequence of pulse compression is the presence of sidelobes, which can mask nearby scatterers with smaller RCS values, such as in figure 1.2. Mismatch filters can create responses with sidelobes lower than the matched filter. However, because they deviate from the matched filter, they will result in some loss of SNR. Another adverse side effect is a potential broadening of the mainlobe which occurs with some choices of mismatch filters.

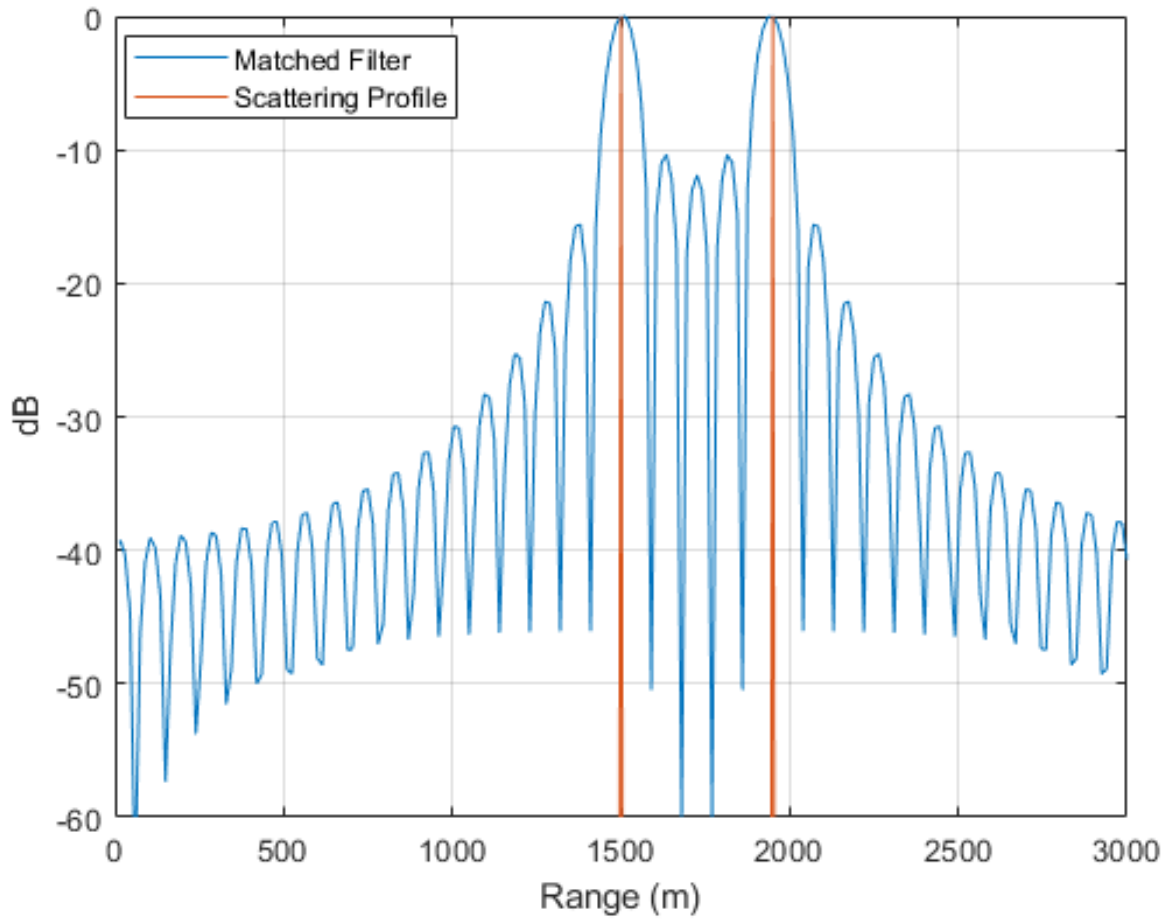


Figure 1.1: The matched filter pulse compression response of two equal power scatterers

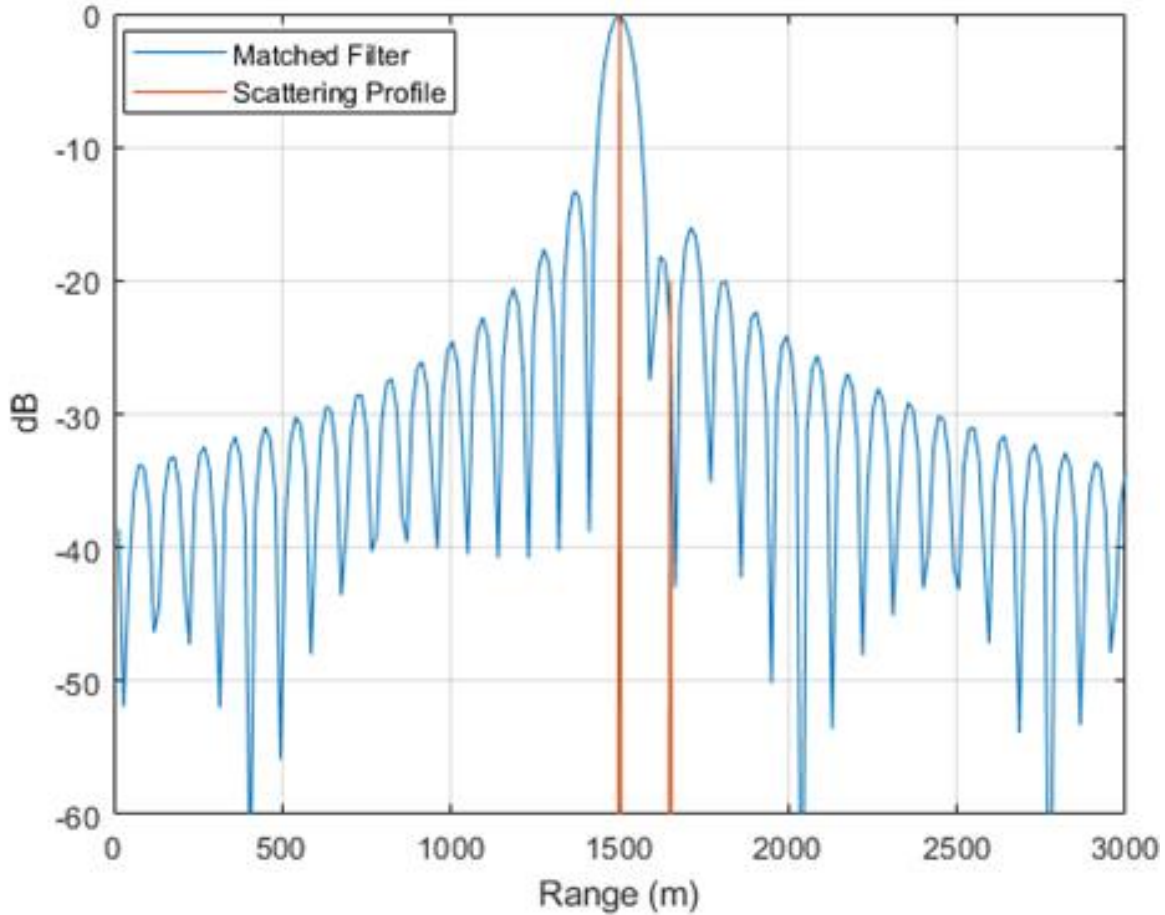


Figure 1.2: The matched filter response of a strong and weak scatterer close in range

1.1.7 Doppler Processing

Another basic measurement a radar can perform is a measure of change in range, or radial velocity relative to the radar. This is accomplished by the Doppler effect, a frequency shift on a reflected electromagnetic wave resulting from a moving scatterer.

Consider a monostatic pulsed radar which transmits a series of M pulses and, after some time delay, receives the set of pulses back from the environment. Traditional Doppler processing operates on this set of M *pulse repetition intervals* (PRI) known as a *coherent pulse interval* (CPI). The set of the M received signal samples form a data grid in fast time (range) and slow time (pulse).

This grid is a single slice of the Radar data cube shown in figure 1.3. The doppler shifts of the scatters are observed across slow time through phase shifts on a pulse-to-pulse basis.

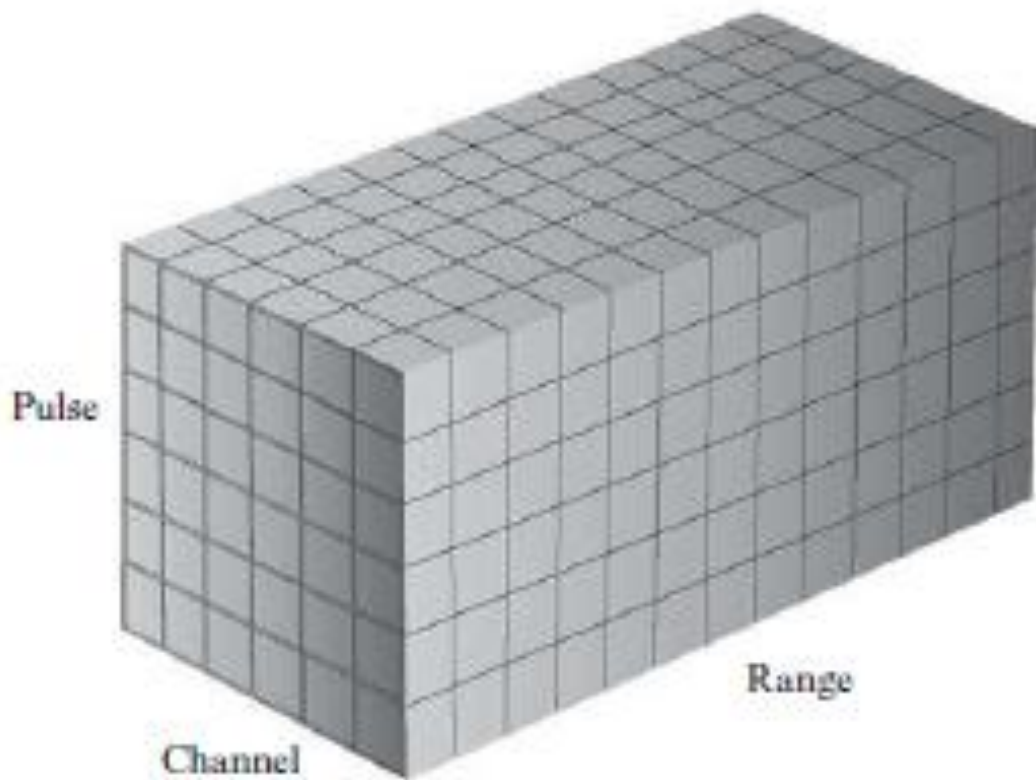


Figure 1.3: A geometric representation of the radar data cube. [1]

First, it is assumed that the scatterers in the CPI, though potentially moving, occupy the same region of space such that they exist within the same range sample (which will be referred to as a range bin) [1]. Secondly, it is assumed that the scatters in the scene are moving at a near constant velocity in range within the CPI (Such that they will be constrained to a single Doppler bin). For a point scatterer, the received echo will have a constant phase shift from pulse to pulse. The resulting slow time samples at the range of that scatter will form a complex tone, represented mathematically as:

$$\mathbf{y}_m = \exp(j2\pi f_d \mathbf{t}_{slow}) \quad (1.13)$$

Where f_d is the doppler frequency shift from the radar's center frequency, and \mathbf{t}_{slow} is a slow time indexing vector, corresponding to the start time of each PRI. Figure 1.4 shows the 2D map of pulse compression responses before Doppler processing.

After performing pulse compression on each pulse, a Fourier transform is applied across slow time at each range bin. This transforms the data grid from fast time by slow time to Range (fast-time) by Doppler.

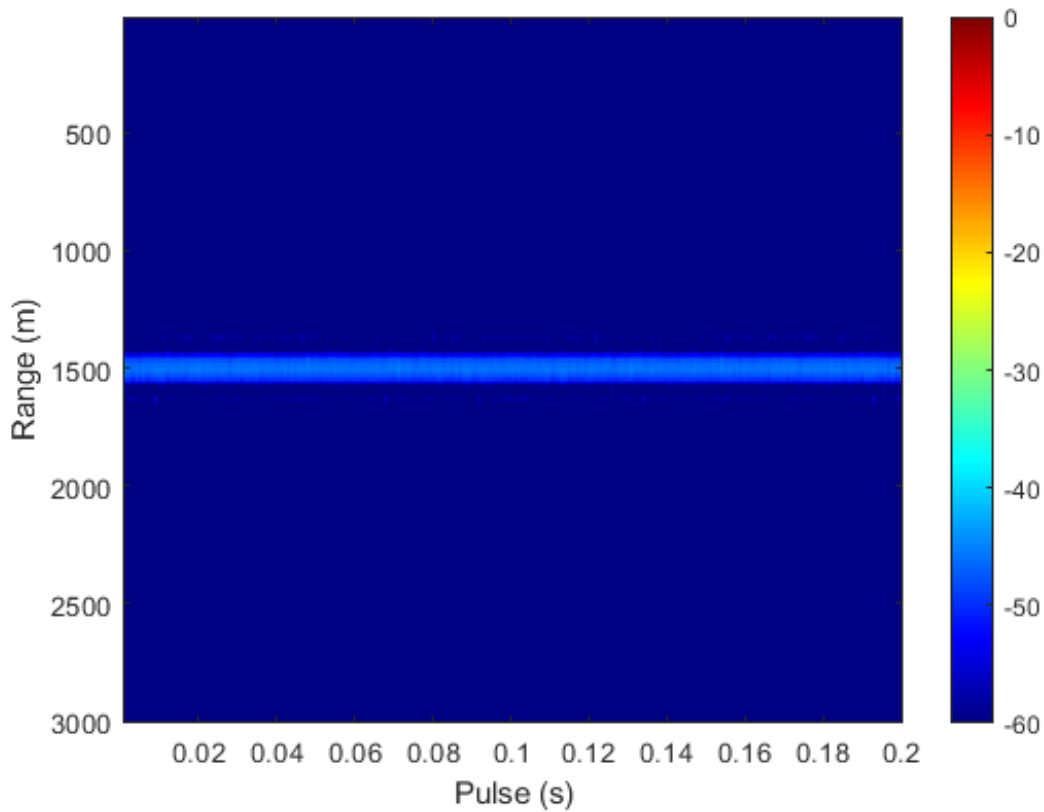


Figure 1.4: Pulse compressed response for each pulse in the CPI.

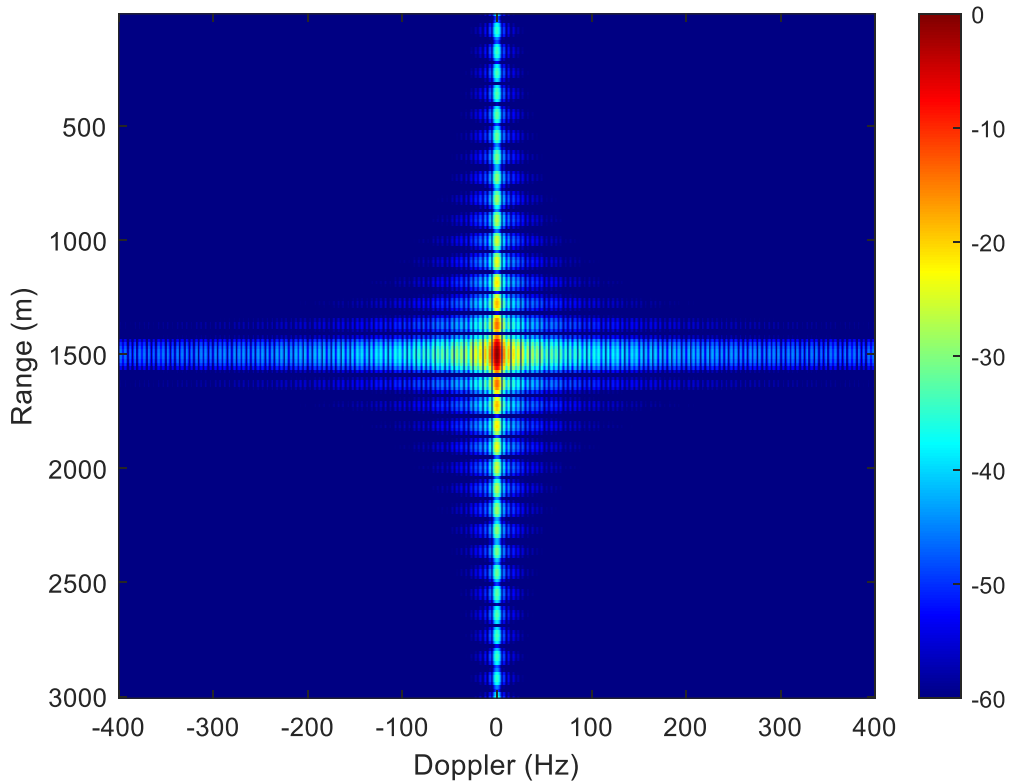


Figure 1.5: Range-Doppler map after Doppler Processing.

Ideally, the point scatterers would resolve as points on the range-doppler map, but the range sidelobes from pulse compression prevent this. Additionally, any variation between the waveforms between pulses will result in a sinc (or a $\sin(x)/x$) structure when Fourier transformed, manifesting as doppler sidelobes in the range-Doppler map. However, much like range sidelobes, a variety of techniques have been developed to reduce doppler sidelobes, including windowing.

1.2 Radar Waveforms

An important consideration in a radar system is the waveform. The waveform has many properties which impact the entire radar system, and its structure can vary depending on available resources and potential application. Here, we provide a brief overview of a subset of Radar waveforms

relevant known as *frequency modulated* (FM) waveforms, as well a short discussion on waveform diversity.

1.2.1 Deterministic FM Waveforms

FM waveforms can be both deterministically and pseudo-randomly generated. Here, we discuss the deterministic FM waveforms.

1.2.1.1 Linear FM Waveforms

The earliest radar systems used a monotone as their waveform, as it was the simplest to generate. However, as discussed in the pulse compression section, waveforms with wider bandwidths can provide increased Radar performance. The easiest method to generate and recreate a waveform with bandwidth was the *linear frequency modulated* waveform (LFM) [4], given as:

$$s(t) = \exp (2\pi(kt + f_i)t) \quad (1.14)$$

Where k is the chirp rate of the waveform, and f_i is the starting frequency. The LFM is by and far the most used Radar waveform [4] and has several defining characteristics. First, the autocorrelation of the LFM has a characteristic sinc structure, with a *peak sidelobe level* (PSL) of about -13dB as shown in figure 1.6. Secondly, the *power spectral density* (PSD) of an LFM has a square band with roll-off, exhibiting a good degree of spectral containment shown in figure 1.7. Lastly, the ambiguity function of the LFM exhibits a ridge in delay-doppler, demonstrating a linear coupling between delay and doppler.

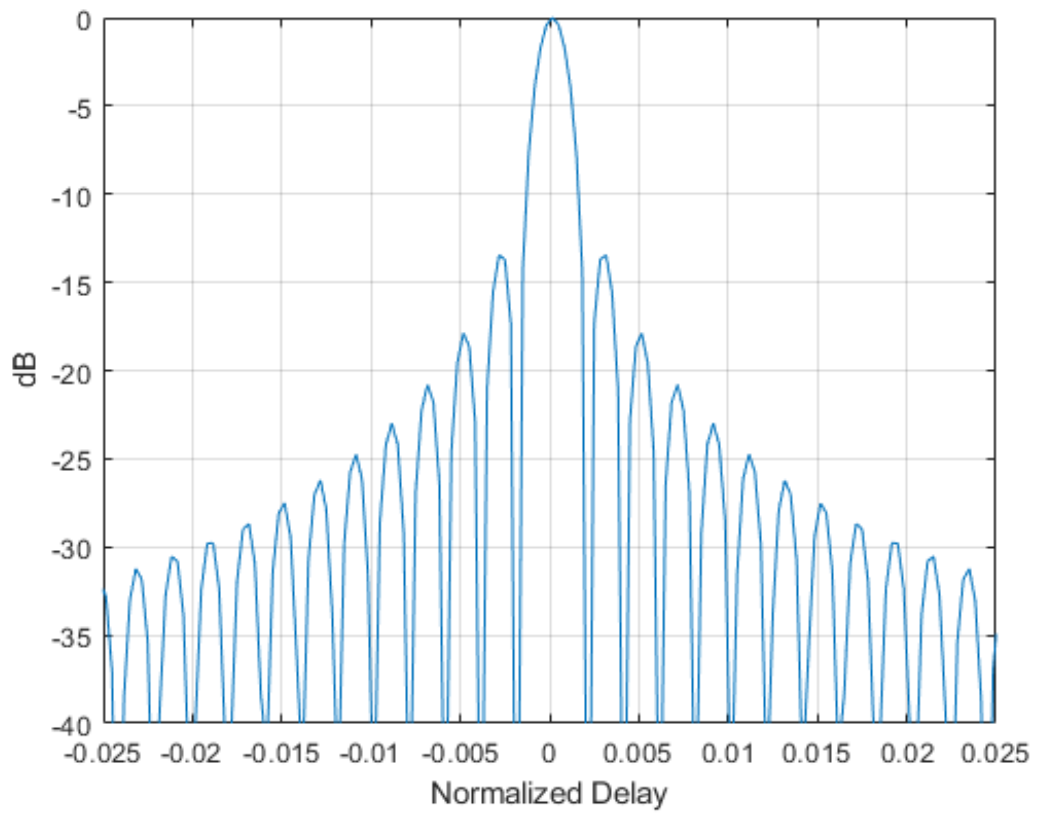


Figure 1.6: Autocorrelation function of a LFM waveform.

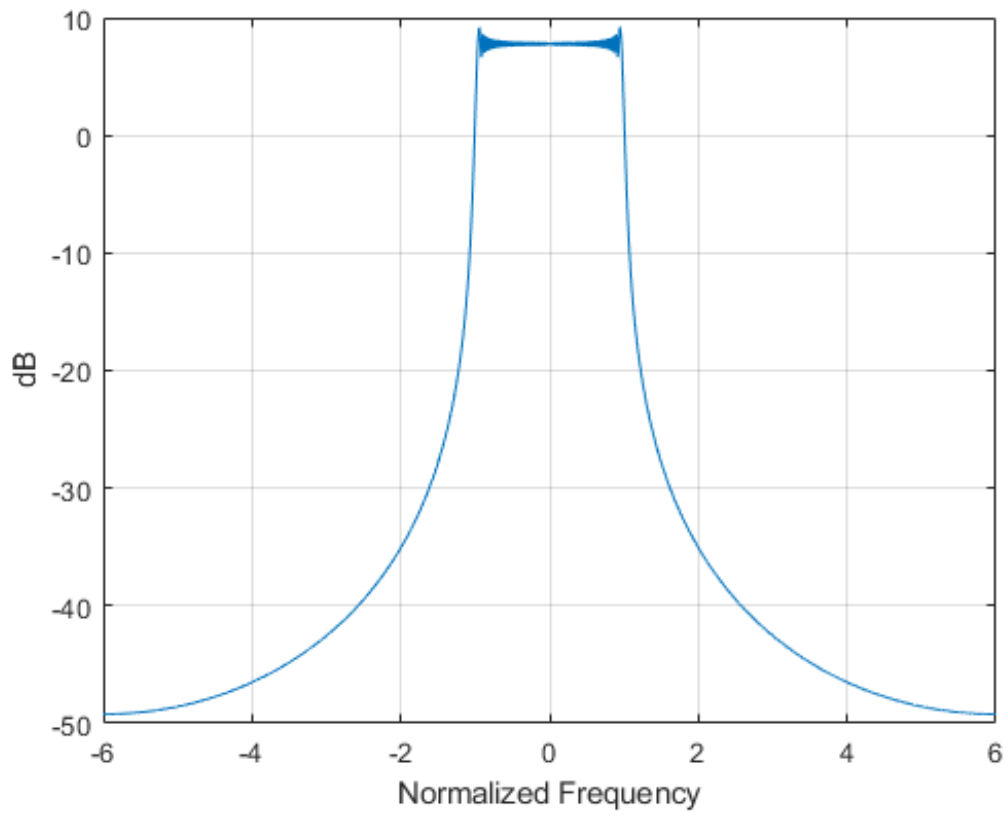


Figure 1.7: Frequency spectrum of a LFM waveform.

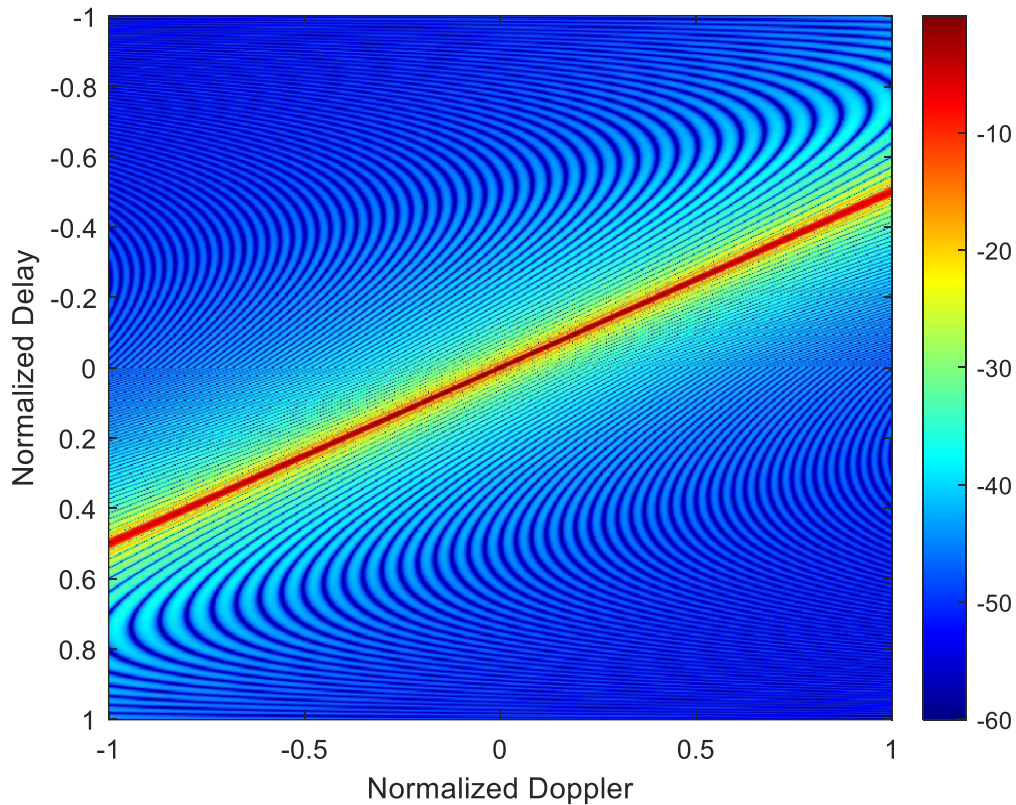


Figure 1.8: Ambiguity function of a LFM waveform.

1.2.1.2 Deterministic Nonlinear FM

While the LFM has been used in many radar systems successfully, other FM waveforms have been developed for various purposes. These waveforms are known as *nonlinear FM* waveforms (NLFM). Some of these waveforms are altered to provide a communication structure. Others attempt to alter the autocorrelation to reduce sidelobe levels, while still utilizing the matched filter to maximize SNR.

The resulting sidelobes from the pulse compression of an LFM are relatively high. However, these sidelobes and the general pulse compression shape of the waveform can be altered by shaping the spectrum due to the Fourier relationship between the PSD and the autocorrelation.

One relatively simple way this can be done is by changing the instantaneous frequency function from linear to nonlinear.

In a linear instantaneous frequency function, the waveform spends an equal amount of time at each frequency (or frequency interval). By deviating from this, the spectrum can be shaped according to the *principle of stationary phase* (PSP) [4].

The PSP describes the relationship between the rate of frequency change, or chirp rate, and spectral energy density as an inverse relationship written as:

$$|U(f_k)|^2 \approx 2\pi \frac{g^2(t_k)}{|\phi''(t_k)|} \quad (1.15)$$

Where $\phi''(t_k)$ is the chirp-rate at time t_k and $g(t_k)$ is the amplitude of the pulse at time t_k (For FM waveforms, this is a constant) [4]. This can be observed by comparing an LFM to a monotonically increasing NLFM. In linear FM, the waveform's spectrum is nearly even within the 3dB bandwidth. The linear FM also spans the same frequency interval for each equal sized time interval. Compare this to a monotonically increasing NLFM with a tangent instantaneous frequency curve shown in figure 1.9. Here, the waveform spends very little time at the lowest and highest frequency intervals while spending the most time at the middle frequency intervals. When one studies the PSD of the tangent NLFM as shown in figure 1.10, the majority of the energy is in the middle frequency interval, thus demonstrating the PSP.

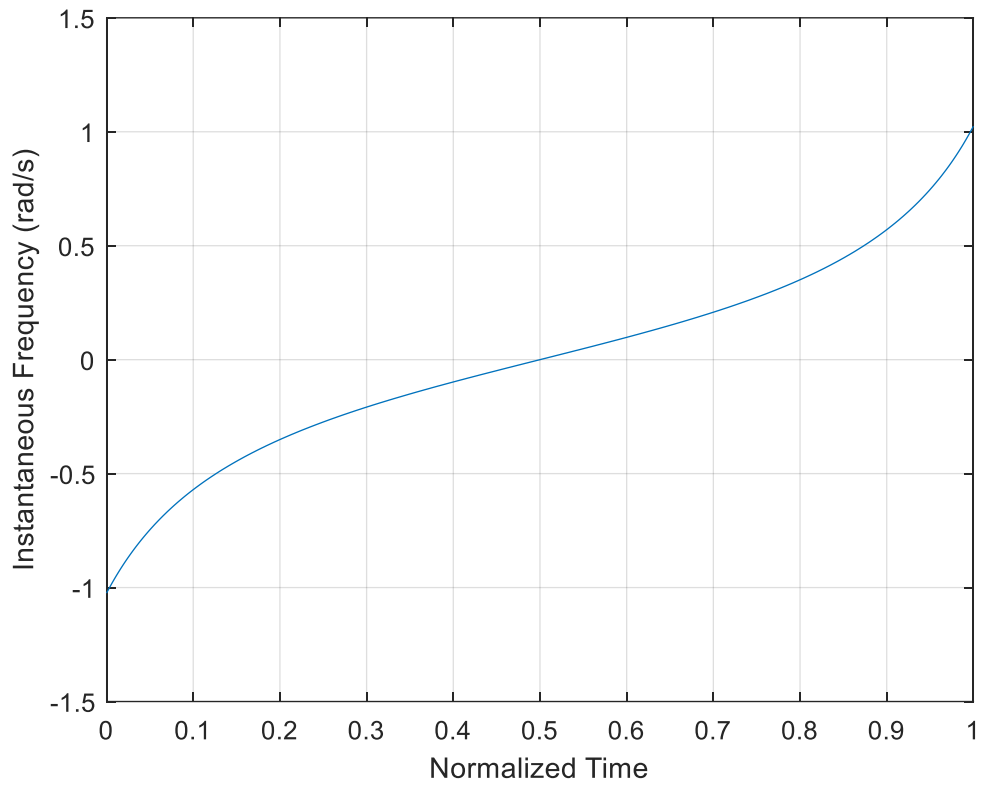


Figure 1.9: Instantaneous frequency function of a tangent NLFM waveform.

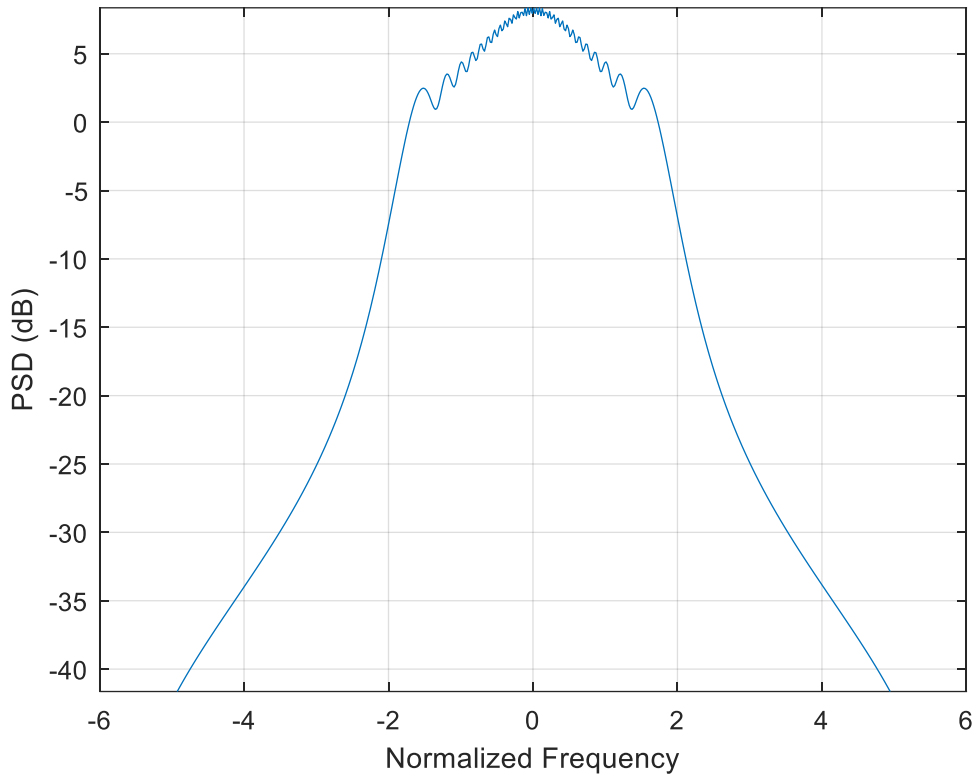


Figure 1.10: PSD of a tangent NLFM waveform.

1.2.2 Random FM Waveforms

The waveforms described above have generally have a deterministic structure. However, not only is it advantageous to shape the spectrum of a waveform, but also to have a waveform structure that allows the generation of non-repeating waveforms. One class of waveforms which enables the generation of a large quantity of unique waveforms are random FM waveforms. These waveforms utilize an FM structure which is derived in part from some stochastic function.

A baseline, non-optimized FM noise waveform, studied in [5-9], can be expressed as

$$s(t) = \exp(j2\pi \int_{-\infty}^t f(\tau) d\tau) = \exp(j\theta(t)) \quad (1.16)$$

for instantaneous frequency $f(\tau)$, the modulating random process that, when integrated, provides a random phase. The random process is generally assumed to be Gaussian, though other distributions may be used. Much like the previous discussed FM techniques, the random FM waveform possesses a single frequency at each instant in time. The form provides, like the previous FM waveforms discussed, a constant envelope and a continuous phase, which is important to providing amenability to high-power amplifiers [10].

While the baseline form of random FM has been around for decades [5-6], it has only been in recent years that spectral shaping has been incorporated. Spectral shaping of random FM provides a means to incorporate spectral containment for the waveforms, and the utilization of spectral shapes which lead to low autocorrelation sidelobes due to the Weiner- Khinchin theorem [3]. Typically, the spectral shape utilized to provide low autocorrelation sidelobes is generally a wideband Gaussian-shaped spectrum. Since the Fourier transform of a wide Gaussian is a narrow Gaussian, this PSD shape will result in an autocorrelation that is nearly impulse like and possessing theoretically no sidelobes. This has been recommended as an ideal template in several recent works [10-15].

In total, random FM waveforms provide a constant amplitude and continuous phase for amenability to high-power transmitters. Their generation via a noise modulation process provides uniqueness which is preserved through spectral shaping. The spectral shaping provides spectral containment and low autocorrelation sidelobes. Lastly, the noise-like structure provides non-repetition and high dimensionality to the waveforms and waveform sets. All of these properties have made random FM an attractive waveform choice not only for traditional radar sensing modes, such as moving target indication and imaging applications, but also for novel sensing modes, including complementary waveform sidelobe cancellation [15] and real-time sense and notch [16].

1.2.2.1 Optimized Random FM Noise

One means of providing spectral shaping for waveforms is through the use of optimization. While the baseline case in 1.2.2 can provide a somewhat effective waveform, often time it is desirable to maximize certain properties of the waveform. Additionally, waveforms for specific applications may be subject to several constraints. Both the maximization of performance and satisfaction of constraints can be accomplished via an optimization approach to Random FM Noise.

The optimization problem has a general structure of:

$$\min_s \{J(s)\}, g_i(s) = c_i, h_j(s) \geq d_j \quad (1.17)$$

for some $i = 1, 2, \dots, n$ and $j = 1, 2, \dots, m$. $J(s)$ is a cost function, which represents properties of the waveform to minimize, subject to the equality constraints $g_i(s)$ and the inequality constraints $h_j(s)$ [17]. The variable s usually corresponds to the waveform itself but can also be formulated where s corresponds to the phase function, instantaneous frequency function, or other compacted waveform representations [18]. Several approaches to optimizing waveforms that have recently been utilized for optimized random FM noise waveforms include a greedy search [19], alternating projections on convex sets [20], and gradient descent methods [21-22].

1.2.2.2 Process-Based Random FM Noise

Sometimes the computational cost of optimization prohibits its use in the generation of Random FM waveforms. As an alternative, various processes and algorithms can be used to shape the baseline random FM in 1.2.2 to provide a more effective waveform. These approaches can vary as widely, but their general operation involves an input random distribution which is then transformed

into a well-behaved random FM waveform. These approaches can utilize an optimized transform structure, or they can simply exploit the mathematical behavior of the phase functions.

1.2.2.3 Waveform Diversity

A higher-level goal of optimizing waveforms is waveform diversity. Waveform Diversity, as defined by the IEEE Standard 686-2008 definition, is “Optimization of the radar waveform to maximize performance according to particular scenarios and tasks.” [23]. As the RF spectrum becomes increasingly crowded with users, and the desire for improved radar performance grows, it is important to consider the occupancy of the waveform emission within the transmission hyperspace [24], and how best to utilize it. Here, several dimensions of the transmission hyperspace are covered.

1.2.2.3.1 Temporal and Spectral Diversity

Two of the most important dimensions to consider are time and frequency dimensions. The temporal extent, or pulse width of a waveform T , and the spectral extent, or bandwidth of a waveform B , combine with the initial time t_0 and center frequency f_c provide a means to measure a waveforms occupancy in time and frequency respectively. The time-bandwidth product, BT , provides a measure of a dimensionality of a waveform, and the degrees of freedom available.

Several considerations must be made when describing a waveforms temporal and spatial extent with its time-bandwidth product. One, there exist multiple definitions for both pulse width and bandwidth. The most commonly used is the 3dB width, but can also include the null-to-null width, RMS power, 99% power width, and others. Secondly, the waveforms under consideration (FM) can only truly occupy a single frequency at a single point in time. Therefore, the spectral

extent over a smaller time interval is not the same as over a temporal extent T . Later, we will consider time and frequency jointly, and provide a joint measure of temporal and spectral extent.

1.2.2.3.2 Spatial Diversity

Another set of dimensions to consider are the spatial dimensions. Since most RF emissions are not uniform in power in all directions, some signals are stronger in some regions of space than others. From a transmission perspective, spatial diversity is controlled by beamforming and steering, either mechanically or electronically. The spatial extent of waveform is provided by the beamwidth in both azimuth and elevation angles, and the direction of the beam, provided by β_{az} , β_{el} , θ_{az} , and θ_{el} . Similar considerations to the temporal and spectral extent of the physical emission must be considered for the azimuth and elevation dimensions. Additionally, a joint measure of the spatial extent and either temporal or spectral extent can be formed as will be seen later in this thesis.

1.2.2.3.3 Other Forms of Waveform Diversity

There exist other dimensions in which to consider waveform diversity. When utilizing a code sequence or a phase pattern, code diversity can be considered. This is a particularly important dimension to consider in a joint Radar-Communications waveform, or when utilizing the coherent integration gain of noise waveform autocorrelation sidelobes. Another dimension for consideration is polarization diversity. By utilizing any two antipodal points on the Poincare sphere, the resulting emissions should be orthogonal [23]. This has recently been demonstrated with FM noise waveforms [25].

1.2.2.4 Waveform Agility

Often, the transmission hyperspace with respect to other spectrum users is not static, but dynamic. This results in smaller unoccupied subspaces of the transmission hyperspace throughout the entire CPI. One way to compensate for a dynamically changing environment is waveform agility. By changing the waveform on a pulse-to-pulse basis, greater subspaces of the transmission hyperspace will be open for the waveform to occupy. While these waveforms are often generated and chosen in advance, it is possible to adapt some features of the waveform based on the environment. This usually requires some form of cognitive sensing, in which the RF environment is sensed, a determination of the other spectrum users is made, and then future waveforms are modified to adapt to the updated RF environment. This can be an important factor when considering the use of a non-repeating waveform.

1.2.3 Waveform Designs under Consideration

Recently, there has been substantial active research on different random FM waveforms. Due to the large volume of random FM design approaches, it would be impossible to cover them all in a single work. Rather, a subset of waveforms will be considered which have properties that are amenable to high power emission and good range sidelobe performance.

1.2.3.1 PRO-FM Waveforms

The first waveform type to be considered are Pseudo Random Optimized FM waveforms (PRO-FM). PRO-FM waveforms are generated via alternating projections on convex sets optimization approach [20]. The PRO-FM process begins by specifying an ideal frequency template U . Next, a random phase waveform is generated and is projected into the frequency domain, where it is

shaped to the magnitude U . After spectral shaping, the resulting spectrum is transformed back into the time domain, and the phase of the shaped waveform is used as the phase trajectory of a new FM waveform. This approach is repeated for K iterations until it converges. The optimized waveform will generally follow the template closely within a couple normalized frequencies, but will not closely follow the template for frequencies farther away from the center frequency. Figures 1.11 and 1.12 show the optimized waveform relative to a spectral template.

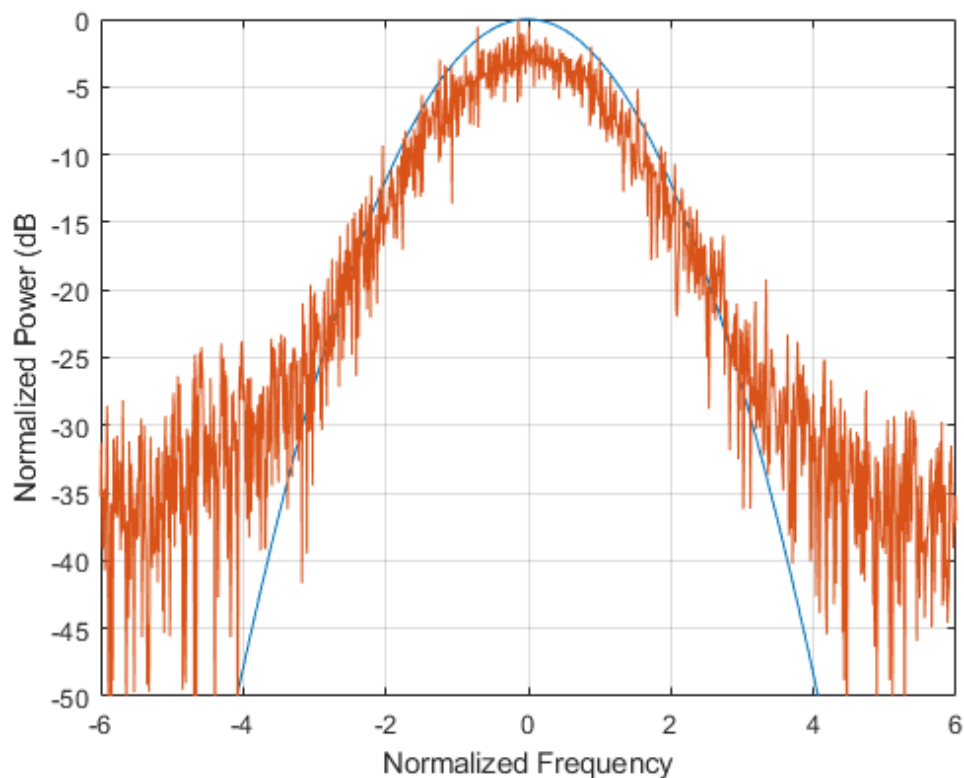


Figure 1.11: Power Spectral Density of a single PRO-FM waveform.

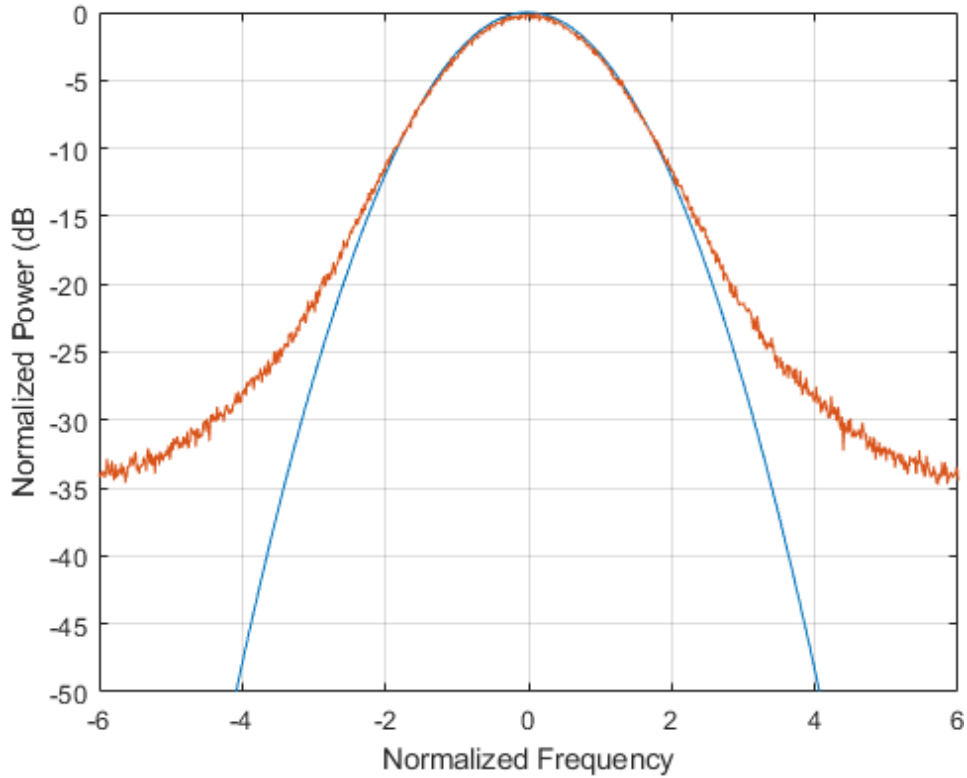


Figure 1.12: Mean power spectral density of 100 PRO-FM waveforms.

1.2.3.2 FTE and Log-FTE Waveforms

The second waveform type to be considered are frequency template error (FTE) waveforms [21].

Unlike PRO-FM, FTE attempts to minimize a cost function. The FTE cost function is written as:

$$J = \|(As)^2 - \mathbf{u}^2\|^2 \quad (1.18)$$

The cost function is a scalar function of an input signal vector \mathbf{s} , where the vector representation of the power spectral density is computed via \mathbf{A} , an $L \times N$ discrete Fourier transform matrix. The cost function becomes the Frobenious norm squared of the difference in the computed PSD and the ideal template PSD.

One advantage FTE has over PRO-FM is, by having a cost function, a wide variety of optimization methods can be utilized to minimize the objective function. The norm squared

operation in the cost function enforces a convex structure on the function, making a local minimizer possible. One method that has been demonstrated to work well with FTE [21] is a conjugate gradient descent. To minimize J , the gradient is computed with respect to the input signal \mathbf{s} . The next iteration of \mathbf{s} is obtained by subtracting off a scaled version of the gradient, written as:

$$\mathbf{s}_{n+1} = \mathbf{s}_n - \alpha_n \nabla_{\mathbf{s}^*} \{J(\mathbf{s})\} \quad (1.19)$$

Where α_n is the step size at the n th iteration. A fixed step size can be used, but it is recommended to adjust the step size with each iteration to improve convergence speed. The heavy ball method, discussed in [21], is recommended to avoid converging to poor local minima of J .

A modified version of this approach is log-FTE, where the cost function is modified to:

$$J = \|\log((\mathbf{A}\mathbf{s})^2) - \log(\mathbf{u}^2)\|^2 \quad (1.20)$$

Where \log is the logarithm function with base 10. By evaluating a difference on a log (or dB) scale, this modified cost function allows for faster convergence to minimizers of J . The tradeoff is that smaller, more subtle details in the spectrum will not be emphasized as strongly as it would with the linear FTE cost function.

1.2.3.3 TTE Waveforms

The design approach used with FTE and Log-FTE waveforms started with an unoptimized random FM waveform and attempted to minimize the difference between the optimized waveform's PSD and the desired PSD. Another approach is to start off with the desired PSD template and shape the temporal envelope to be constant modulus. These waveforms are known as temporal template error (TTE) waveforms. The cost function for the TTE waveforms is written as:

$$J = \|\mathbf{s}^* \odot \mathbf{s} - \mathbf{u}\|^2 \quad (1.21)$$

where \mathbf{u} is some desired temporal envelope from 0 to T [22]. This approach serves as a time-domain equivalent of FTE and is effective when small amounts of AM are acceptable. Even if the waveform must possess a constant amplitude envelope, a recommended final step in the optimization process is a projection of the phase of s onto the desired temporal magnitude.

1.2.3.4 StoWGe Waveforms

While optimization can be an effective approach to generate high fidelity waveforms, the non-recurrent nature of random FM means that the real-time computational costs are important to consider. One way to mitigate the computational cost is an approach known as Stochastic Waveform Generation (StoWGe) [26]. Instead of optimizing a single waveform or a set of waveforms, a set of basis vectors and a mean vector are optimized instead.

First, a phase vector is defined as a linear function written as:

$$\boldsymbol{\varphi} = \mathbf{B}\mathbf{x} + \boldsymbol{\mu} \quad (1.22)$$

where \mathbf{B} is a matrix whose columns \mathbf{b}_i are basis vectors, \mathbf{x} is a random seed vector, and $\boldsymbol{\mu}$ is mean vector. This phase vector is used to generate a new StoWGe waveform for each new random phase vector \mathbf{x} . The optimization process then involves minimizing the following cost function:

$$J = \left\| E \left[|s_f|^2 \right] - \mathbf{u} \right\|_2^2 \quad (1.23)$$

where \mathbf{u} is the desired spectral template, such as ones used in FTE and log-FTE waveforms. Rather than minimize the difference between the waveform's PSD and a desired PSD, StoWGe aims to minimize the difference between the expected PSD and a desired PSD. This results in waveforms that, though their individual PSD's might not be particularly close to a desired PSD, the average PSD will be very close to the desired PSD, a property that works well with coherent integration.

To accomplish this, the optimization algorithm attempts to find both a \mathbf{B} and a $\boldsymbol{\mu}$ that minimizes J . Gradient-descent based methods [26] such as used for FTE and TTE waveforms are recommended.

Regardless of the method used, instead of optimizing N values as required in FTE and TTE, StoWGe requires the optimization of $N(M+1)$ values, where M is the size of the random seed vector \mathbf{x} . This naturally results in a higher computational cost for StoWGe optimization compared to the previous methods. However, once \mathbf{B} and $\boldsymbol{\mu}$ have been optimized, new waveforms can be generated with the desired spectral template, with the only limit being the number of values available in the random number generator. Thus, the real-time computation required for StoWGe is only the composition of the phase from \mathbf{B} , \mathbf{x} , and $\boldsymbol{\mu}$.

1.2.3.5 CE-OFDM Waveforms

While StOWGe is an effective means to avoid optimization in the real-time computational costs, its representation is not particularly compact. Another approach to avoiding optimization while also maintaining a compact representation is Constant Envelope Orthogonal Frequency Division Multiplexing (CE-OFDM) [27-30]. CE-OFDM is a process-based random FM waveform which uses the Orthogonal Frequency Division Multiplexing (OFDM) signal structure often utilized in communication systems to generate the phase of the waveforms. The use of CE-OFDM as a random FM radar waveform has recently been shown [31] to be an effective random FM radar waveform.

OFDM is composed of a sum of complex sinusoids each modulated with a complex valued communication symbol pulled from some constellation [27]. Each individual subcarrier can be written as:

$$u_n(t) = \beta_n \exp(j2\pi f_n t) \quad (1.24)$$

Where β_n is the n th communications symbol at the subcarrier frequency f_n . A minimum difference in frequency is maintained between each subcarrier to ensure orthogonality. The OFDM signal structure is utilized to generate the FM phase trajectory for the CE-OFDM waveform using the following expression:

$$s(t) = \exp\left(j2\pi h \Re\left\{\sum_{n=1}^N u_n(t)\right\}\right) \text{ for } 0 \leq t \leq T \quad (1.25)$$

As noted in [31], the resulting waveforms phase is composed of a repeated sum of cosine functions. The non-linear complex exponentiation transforms the sum of cosines into a repeated product of non-linear FM functions with limited bandwidth. Further, this repeated product in the time domain becomes a repeated convolution in the frequency domain, and provided the carriers have been properly selected, will result in a Gaussian spectral envelope in a like manner to the central limit theorem in statistics. While the waveforms autocorrelation performance is not as good as other optimized RFM waveform designs, the lack of optimization greatly reduces the computational complexity of CE-OFDM's generation relative to other methods. Additionally, by only needing the subcarrier locations and modulation value to recreate a waveform, the waveforms are generally more compact than methods requiring a full temporal representation of the waveform.

1.3 Waveform Analysis Tools

In order to evaluate waveforms, a set of tools for analysis is required. Both linear and quadratic representations of the waveform are needed to understand many of the critical aspects of a waveform.

1.3.1 Fourier Analysis

Besides considering the time evolution of a waveform, the most commonly used way to analyze a waveform is by studying its frequency spectrum generated by a *Fourier transform* (FT). The FT of a signal can be written as

$$F[s(t)] = \int_{-\infty}^{\infty} s(t) \exp(-j2\pi ft) dt \quad (1.26)$$

and its inverse can be written as

$$F^{-1}[S(f)] = \int_{-\infty}^{\infty} S(f) \exp(+j2\pi ft) df \quad (1.27)$$

Where $S(f)$ is the Fourier transform of $s(t)$. Computing the FT of a time-domain signal provides a frequency-domain representation of the signal, which provides a magnitude and phase of each frequency that composes the time-domain signal. The FT is a linear transform and as a result it satisfies the principle of superposition.

The *power spectral density* (PSD) of a waveform can also be computed from the FT by

$$PSD(f) = |S(f)|^2 \quad (1.28)$$

where $S(f)$ is the FT of the waveform $s(t)$. The PSD provides a measure of the waveform's power at each frequency. Additionally, the PSD is a quadratic transform of $s(t)$ as compared to the FT which is a linear transform. This distinction is important, as two different waveforms can be used in the computation of (equation of PSD), which results in a cross-power spectral density. The cross-power spectral density is sometimes used to correlate between two different spectra.

1.3.2 Autocorrelation and Cross-Correlation

Similar to how the PSD is a quadratic representation of the waveform in frequency, quadratic representations of the signals can be provided in the time domain. Autocorrelation is a quadratic representation of a waveform $s(t)$ defined as

$$R_{ss}(\tau) = \int_{-\infty}^{\infty} s(t+\tau)s^*(t)dt \quad (1.29)$$

where τ is a measure of time called delay [3]. The autocorrelation provides a measure of the self-similarity of a waveform and a time-delay shifted, complex conjugated copy of itself. The shape of a waveform's autocorrelation is equivalent to its matched filter response and is therefore a useful representation of the waveform for evaluating a waveforms performance in range measurements.

Another way of computing the autocorrelation is via the Weiner-Khinchin theorem, which relates the autocorrelation to the PSD by

$$R_{ss}(\tau) = \mathcal{F}^{-1}[PSD(f)] \quad (1.30)$$

where \mathcal{F}^{-1} is the inverse FT [3]. Thus, the spectral shape of the PSD has a direct impact on the autocorrelation (and as an extent, the Radar performance) of the waveform.

Two different signals can be utilized in a way similar to the autocorrelation with the cross-correlation function, written as

$$R_{sv}(\tau) = \int_{-\infty}^{\infty} s(t+\tau)v^*(t)dt = \int_{-\infty}^{\infty} v(t+\tau)s^*(t)dt \quad (1.31)$$

where $s(t)$ and $v(t)$ are two different signals. Cross-correlation provides a measure of similarity of two different signals, one of which is time-delayed and complex conjugated. Just as the autocorrelation has the shape of a matched filter response, the cross-correlation provides the shape of a mismatched filter response, which can be useful in determining how interference responds to

the matched filter, or how a waveform behaves depending on the structure of the mismatched filter. Further, the cross-correlation of two waveforms provides an effective measure of their separability in a radar sense. Just as the cross-correlation provides the shape of a mismatch filter between a waveform and filter, and the reduction in peak provides a measure of mismatch, the peak of the cross-correlation of two waveforms provides a measure of mismatch, or separability, between the two waveforms.

1.3.3 Delay-Doppler Ambiguity Function

Just as the relationship of the delay-shifted versions of a signal with itself can be represented by a function like autocorrelation, the relationship of frequency-shifted versions of a signal with itself can be considered. The combination of both delay-shifts and frequency-shifts can be described via the Delay-Doppler Ambiguity function, written as

$$\chi(\tau, f) = \int_{-\infty}^{\infty} s(t)s^*(t-\tau)\exp(j2\pi ft)dt \quad (1.32)$$

which is both a function of delay and a frequency-shift referred to as Doppler. Like autocorrelation and PSD, the ambiguity function is a quadratic transform of $s(t)$. However, unlike autocorrelation and PSD, the ambiguity is a two-dimensional function, considering both delay and doppler. The ambiguity function has been described as a measure of the performance of a radar waveform. The delay dimension provides a measure of the range performance, and the doppler dimension provides a measure of the doppler performance of a waveform for Range-Doppler maps. Again, just like with cross-correlation and cross-power spectral density, a cross ambiguity function can be defined between two signals.

1.3.4 Time-Frequency Analysis

The ambiguity function provides a way to consider both the effect of delay and doppler shift of a waveform jointly. In a similar manner, one can consider the time and frequency behavior of a waveform jointly. Since Random FM waveforms by their nature have a time-varying, non-stationary instantaneous frequency, it is useful to utilize the toolkit provided by time-frequency analysis. Time-Frequency transforms will be used to study a variety of random FM waveforms with different generation methods and different spectral profiles.

When analyzing a time-varying signal, particularly a non-stationary signal such as random FM waveforms, the time-domain representation does not clearly show what frequencies are present at a particular period of time. Conversely, the frequency representation does not easily describe at what periods of time particular ranges of frequency are present in the signal. Evaluation of this relationship necessitates the use of a joint time-frequency representation [32-33].

1.3.4.1 Linear Time-Frequency Transforms

When the FT is applied to a time-limited signal, a measurement of the frequencies present during the temporal extent of the signal is provided. A simple approach to obtaining a joint time-frequency approach is to consider the FT over different periods of time. This approach is formalized as the Short-Time Fourier Transform, written as

$$STFT_s(t, f) = \int_{\tau} [s(\tau)\gamma^*(\tau - t)] \exp(-j2\pi f \tau) d\tau \quad (1.33)$$

where $\gamma(t)$ is a window function with some specified time support. In this thesis, a rectangular window whose extent is a fraction of the pulse width will be used unless otherwise specified. Similar to the relationship between the frequency spectrum of a waveform and the PSD, a spectrogram can be computed by obtaining the squared magnitude of the STFT.

The STFT is a linear transform, applied over different time swaths. Several other linear time-frequency transforms have been used in literature before, including wavelet transforms (with a wide variety of wavelets) [34]. Regardless of the transform used, linear TF transforms generally involve a trade-off between temporal resolution and spectral resolution and, depending on the sampling rate, can hinder the characterization of sophisticated intra-pulse behavior [35].

Many other linear transforms exist. Generally, these are formulated as piecewise linear operations which are then composed in a 2-dimensional structure, such as the STFT. The other transforms are usually linear transforms, where the transform has an adjustable variable. Most of these transforms can be written as an integral transform, where they are integrated over the entire domain $(-\infty, \infty)$ and transformed into another domain (just like the Fourier Transform goes from time domain to the frequency domain). These transforms can be defined by their *kernel*, or a function in the integrand which can be varied to achieve different transforms.

One integral transform of interest is the Fractional Fourier Transform, which can be written mathematically as

$$\mathcal{F}_{t \rightarrow u}^{\alpha} \{s(t)\} = \sqrt{\frac{1-j\cot(\alpha)}{2\pi}} \exp\{j0.5 \cot(\alpha) u^2\} \int_{-\infty}^{\infty} \exp \{j(0.5\cot(\alpha) t^2 - \csc(\alpha) ut)\} s(t) dt \quad (1.34)$$

where $\cot(\cdot)$ and $\csc(\cdot)$ are the cotangent and cosecant operators respectively, and α and u correspond to the angle and radial variables of the Fractional Transform. The Fractional Fourier Transform rotates the signal about the time-frequency plane by an angle α . A classical Fourier Transform performs a 90° rotation of the time-frequency plane and a classical inverse Fourier transform performs a -90° rotation of the time-frequency plane. These in-between domains behave where time and frequency couplings amplitudes are represented, instead of a purely time of frequency amplitude.

The fractional Fourier transform can be used to generate a 2-dimensional time-frequency distribution known as the Radon-Wigner transform (RWT). The RWT can be written mathematically as:

$$R_s(\alpha, u) = \mathcal{F}_{t \rightarrow u}^\alpha \{s(t)s^*(t)\} \text{ for } 0^\circ \leq \alpha \leq 180^\circ \quad (1.35)$$

The resulting transform manifests as a series of rotations about the time-frequency plane, showing transition from time to frequency and back. The specific portion of the RWT corresponding to the Fourier transform is 90° , which also corresponds to the rotation of the time-frequency plane as previously discussed.

1.3.4.2 Quadratic Time-Frequency Transforms

Another class of joint time-frequency transforms are quadratic (or bilinear) time-frequency transforms. Instead of a tradeoff between time and frequency resolutions, quadratic TF transforms trade off joint time-frequency resolution ($\Delta t \Delta f$) and interference cross-terms [32].

A popular quadratic TF representation is the Wigner-Ville distribution (WVD), as many other TF transforms can be easily derived from it [34]. The WVD of a waveform $s(t)$ is defined mathematically as

$$W_s(t, f) = \mathbb{F}_{\tau \rightarrow f} [s(t + \frac{\tau}{2})s^*(t - \frac{\tau}{2})] \quad (1.36)$$

and provides a TF transform that is well-suited for analyzing signals at full temporal and spectral resolution. Several of the nice properties of the WVD include:

- Integrating over the entire WVD in both time and frequency results in the energy of the waveform.
- Integrating over the time dimension results in the PSD of the waveform.

- Integrating over the time dimension results in the power of the waveform over time.

Naturally, the WVD cannot be fully represented in the digital world, and thus a discretization must be applied to the WVD. The same is true for all other quadratic time-frequency transformation which are defined analytically. However, with adequate sample support, these transforms can be accurately represented in the digital domain.

Along with these integration properties, many other joint distributions can be derived from the WVD. By applying a Fourier Transform across the time dimension, a different distribution called the spectral correlation function (SCF) is obtained, and is mathematically written as:

$$SCF(\nu, f) = \mathcal{F}_{t \rightarrow \nu} \{WVD(t, f)\} \quad (1.37)$$

This transform provides a measure of the frequency of the WVD across time. This can be useful for visualizing spectral nulls in the waveform that can be difficult to pick out in the WVD.

If instead an inverse Fourier transform is taken across frequency, then the instantaneous autocorrelation function is obtained, which is written mathematically as:

$$IAF(t, \tau) = \mathcal{F}^{-1}_{f \rightarrow \tau} \{WVD(t, f)\} \quad (1.38)$$

Where τ is delay. This provides a measure of the autocorrelation of the signal as it varies in time. Just as a random FM waveform is in theory only at a single frequency at a given point in time, each time interval of the IAF should in theory be constant across delay, much like the Fourier relationship between a constant and an impulse, integrating over the time dimension results in the autocorrelation of the waveform.

If a Fourier transform is also taken over the time dimension of the IAF, then the ambiguity function discussed in chapter 1 will be obtained. In a similar way, an inverse Fourier transform across the frequency dimension of the SCF will also result in the ambiguity function (AF). This

creates a relationship between the WVD, SCF, IAF, and AF, all connected by Fourier relationships across the 2 dimensions, shown as:

$$AF(v, \tau) = \mathcal{F}_{t \rightarrow v} \{IAF(t, \tau)\} = \mathcal{F}_{f \rightarrow \tau}^{-1} \{SCF(v, f)\} = \mathcal{F}_{t \rightarrow v} \{ \mathcal{F}_{f \rightarrow \tau}^{-1} \{WVD(t, f)\} \} \quad (1.39)$$

Understanding the Fourier relationships between the AF and the WVD provides a means to better interpret the results of the WVD. Consider the case of AWGN; the ambiguity function will be a thumbtack. If the WVD is a thumbtack, then the WVD should be constant amplitude across all of time and frequency. Wideband signals will result in narrow doppler in the AF, and long temporal signals will have narrow delay in the AF. Another important aspect of the Fourier relationships is that the delay-doppler domain is the natural domain for designing filters for the WVD. Many quadratic time-frequency transforms can be viewed as a filtered WVD, with a structured filter considered in the ambiguity domain. This is often done to reduce the impact of interference cross-terms in the WVD at the cost of a reduction in resolution.

2. Time-Frequency Analysis of Random FM Waveforms

While random FM have been studied in detail on an individual basis in classical time and frequency representations, little attention has been given to their joint time-frequency representations. Here, six random FM waveform classes (PRO-FM, CE-OFDM, FTE, Log FTE, TTE, and StoWGe) are studied first with one dimensional representations, and later with joint time-frequency representations. The waveforms compared have all been generated with $BT=100$ and an oversampling factor of 6 (such that $f_s = 6B$). The statistical measurements are performed over 1,000 waveforms of each class unless specified otherwise.

2.1 Traditional Analysis of Gaussian spectral shapes

Typically, waveforms are analyzed based on their linear and quadratic representations in the time and frequency domains. In this work, the one dimensional domains that the waveforms will be studied in are their time representation, frequency representation, autocorrelation, and PSD.

2.1.1 Time Domain Analysis

In the time domain, the primary consideration for the linear representation using temporal sinc basis functions is the waveform's amplitude. This is primarily used to validate that these random FM waveforms are constant amplitude. While this normally is the case for all the waveforms by the fact that they are all FM, once the waveform signals reach the transmit antenna, they will likely obtain some degree of AM due to distortions along the transmit chain. As a metric for determining the degree of constant amplitude, peak-to-average power ratio (PAPR) is generally used as a figure of merit. The PAPR of the waveform is defined as:

$$\text{PAPR} = \frac{\max\{|s(t)|^2\}}{\frac{1}{T} \int_0^T |s(t)|^2 dt} \quad (2.1)$$

For a waveform $s(t)$ that is defined between $0 < t < T$.

Figure 2.1 shows a comparison of the envelopes of each of the waveforms in loopback. While they may not appear completely flat, they have been measured after amplification where the constant amplitude constraint is not nearly as necessary. Table 2.1 shows the resulting PAPR for each of the waveform classes in both simulation and in loopback measurements. As expected, the simulated have perfect PAPR of 1 with 0 variance due to their FM structure. While the loopback results do possess a degree of AM, their PAPR values are relatively small.

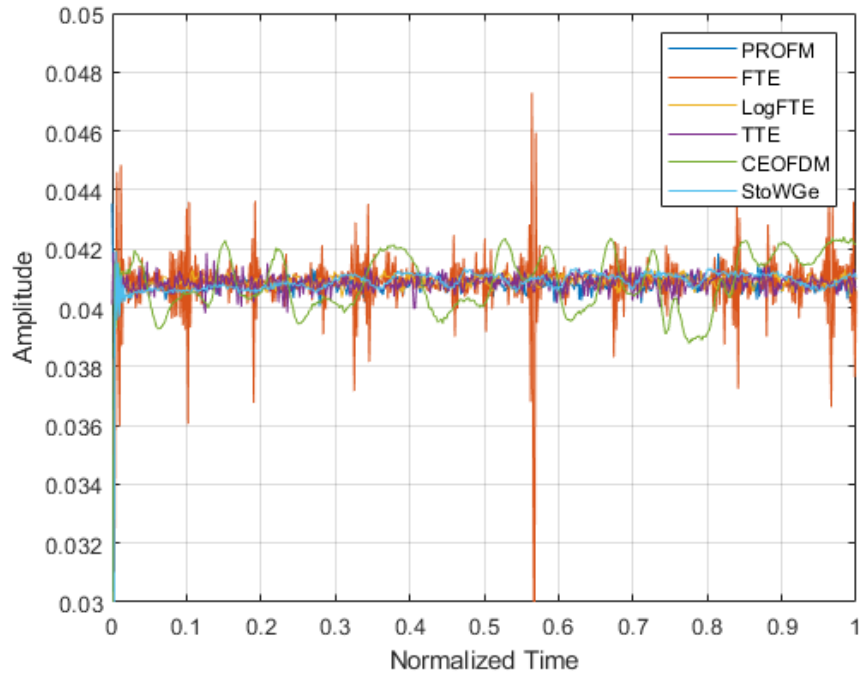


Figure 2.1: Comparison of several waveform amplitudes.

Table 2.1: Comparison of different waveform class amplitudes.

Waveform	PRO-FM	FTE	Log-FTE	TTE	CE-OFDM	StoWGe
Mean PAPR	1.0000	1.0000	1.0000	1.0000	1.0000	1.0000
PAPR Variance	0.0000	0.0000	0.0000	0.0000	0.0000	0.0000
Mean PAPR (Loopback)	1.0636	1.1492	1.0653	1.0256	1.0393	1.0115
PAPR Variance (Loopback)	3.65E-04	9.87E-04	5.79E-04	1.98E-05	8.05E-06	6.75E-06

2.1.2 Frequency Domain Analysis

In terms of the waveform's spectrum and PSD, two factors are of primary importance with a Gaussian template: Gaussian shape and spectral containment. Validation of the Gaussian shape is best measured via the autocorrelation, since the Gaussian shape is what provides the low sidelobe autocorrelation structure. The second property to consider is spectral containment. If the waveform is not well contained spectrally, it could interfere with other spectrum users. Good spectral containment prevents with nearby users and prevents aliasing onto the mainband of the waveform. Three performance metrics are utilized: roll-off level, percent out-of-band (OOB), and the OOB ratio. The roll-off level is defined as the PSD values at $\pm f_s/2$. Percent OOB is the energy within the 3dB bandwidth relative to the total energy of the waveform. OOB ratio is the energy outside the 3dB bandwidth over the energy within the 3dB bandwidth.

For each waveform class, figure 2.2 shows the PSD of a single waveform from each class in simulation. On an individual basis, the waveforms have significant magnitude variation across

frequency but their average is relatively smooth. Figure 2.3 shows the average PSD across a set of 1,000 waveforms from each waveform class. Varying degrees of spectral containment is present.

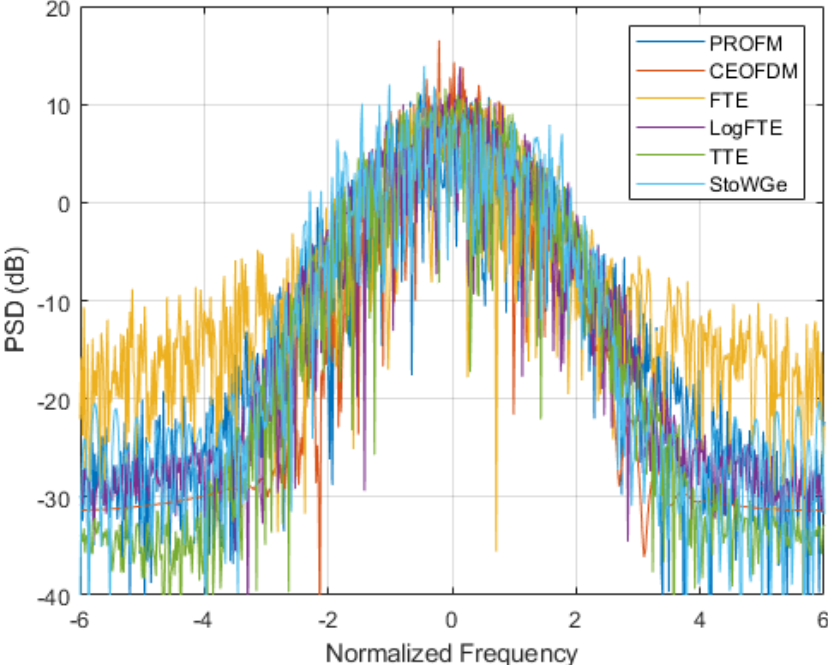


Figure 2.2: Comparison of several waveform PSDs.

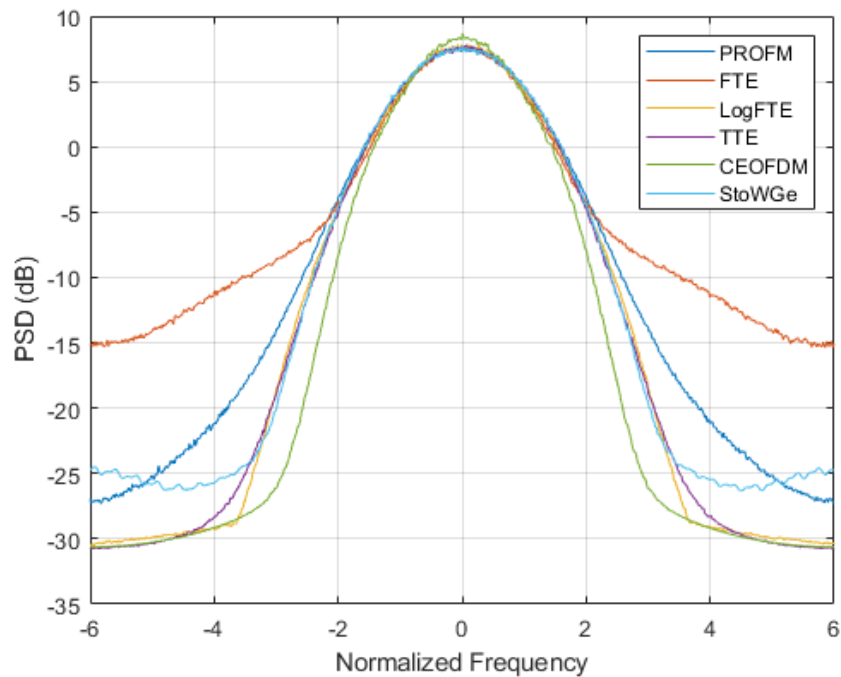


Figure 2.3: Comparison of the average PSD of several waveform classes.

For each waveform class, figure 2.4 shows the mean PSD of 1,000 loopback-captured waveforms. While on an individual basis, the waveforms can appear to have a significant amount of magnitude variation in their power spectral density, on average they all map very closely to the desired template, especially within 3dB bandwidth. While some differences between each class can be distinguished individually, such as their roll-off pattern, the use of metrics may be more illuminating.

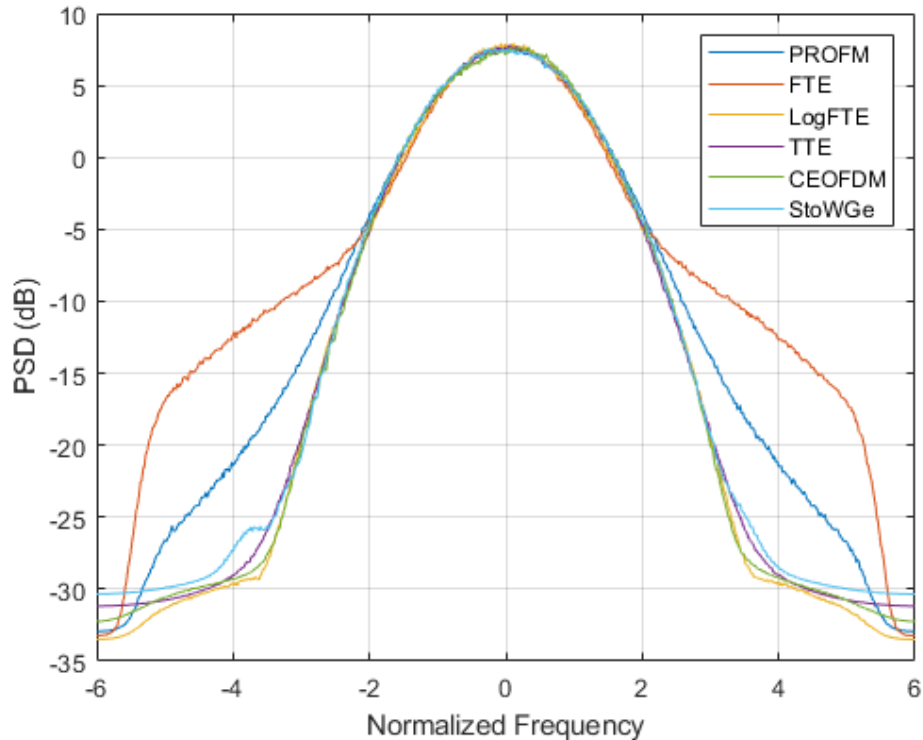


Figure 2.4: Comparison of mean PSD for each waveform class.

Table 2.2 shows the various PSD metrics for each of the different waveform classes captured in loopback. Most of these metrics are consistent across waveform class, which shows that all of these approaches, in terms of spectral containment, are fairly equivalent once applied to real hardware. Certainly, the impact of the filter and amplifier distortion should not be ignored when interpreting the loopback results, as that is certainly a limiting factor in the fidelity of the comparison. However, it is interesting to note that the roll-off level variance is the most different amongst the waveform classes. Specifically, Log-FTE shows extreme consistency in roll-off level, while StoWGe shows drastically varying levels on a waveform-to-waveform basis. Nonetheless, they all, on average, tend to have the same level of spectral roll-off.

Table 2.2: Comparison of different waveform class PSD metrics in loopback

Waveform (Loopback)	PRO-FM	FTE	Log-FTE	TTE	CE-OFDM	StoWGe

Mean Roll-off Level (dB)	-33.39	-33.39	-33.53	-33.44	-33.53	-33.06
Roll-off Level Variance (dB)	4.3938	1.5182	0.4857	33.9136	15.4010	50.4555
Mean Percent OOB	24.89%	24.18%	21.45%	23.01%	23.63%	23.89%
Percent OOB Variance	0.0588%	0.0509%	0.0347%	0.0372%	1.16%	1.33%
Mean OOB Ratio	0.3328	0.3201	0.2739	0.2998	0.3388	0.3479
OOB Ratio Variance	0.0018	0.0015	0.0009	0.0011	0.0460	0.0535

2.1.3 Delay Domain Analysis

In terms of the autocorrelation, the performance of the waveforms can be judged based on how closely their autocorrelation approaches an impulse. To quantify this, we can measure the peak sidelobe levels (PSL) and integrated sidelobe levels (ISL). Both of these metrics can be represented by:

$$GISL = \frac{\|w_{SL} \odot r\|^p}{\|w_{ML} \odot r\|^p} \quad (2.2)$$

which is known as Generalized Integrated Sidelobe Level (GISL) [26]. When $p = 2$, the function is equivalent to the ISL, and when p approaches infinity (generally, 7 is appropriate for optimization implementation), the function approaches the PSL. ISL is useful in quantifying the average sidelobe level relative to the mainlobe level. PSL is useful in quantifying the level of the mainlobes. Ideally, an impulse like autocorrelation has an extremely narrow mainlobe. But sometimes, when optimizing waveforms, the mainlobe is either wider than an impulse, or the mainlobe has a wider region at a lower level known as shoulder lobes.

The other consideration for autocorrelation performance is its coherently combined response. Because the phase of the autocorrelation sidelobe levels should be relatively random, when the autocorrelation of a set of random FM waveforms are coherently integrated, they should provide an improvement of M to the mainlobe-sidelobe ratio, where M is the number of waveforms whose autocorrelations are coherently combined. If the waveforms are truly random, this is always the case. But because optimized random FM waveforms are not entirely random, the improvement due to coherent combination will be sublinear, even if the performance is very close to linear.

Figure 2.5 shows the average autocorrelation response of each waveform class captured in loopback, while Table 2.3 shows the PSL and ISL metrics mean and variance for the loopback waveforms.

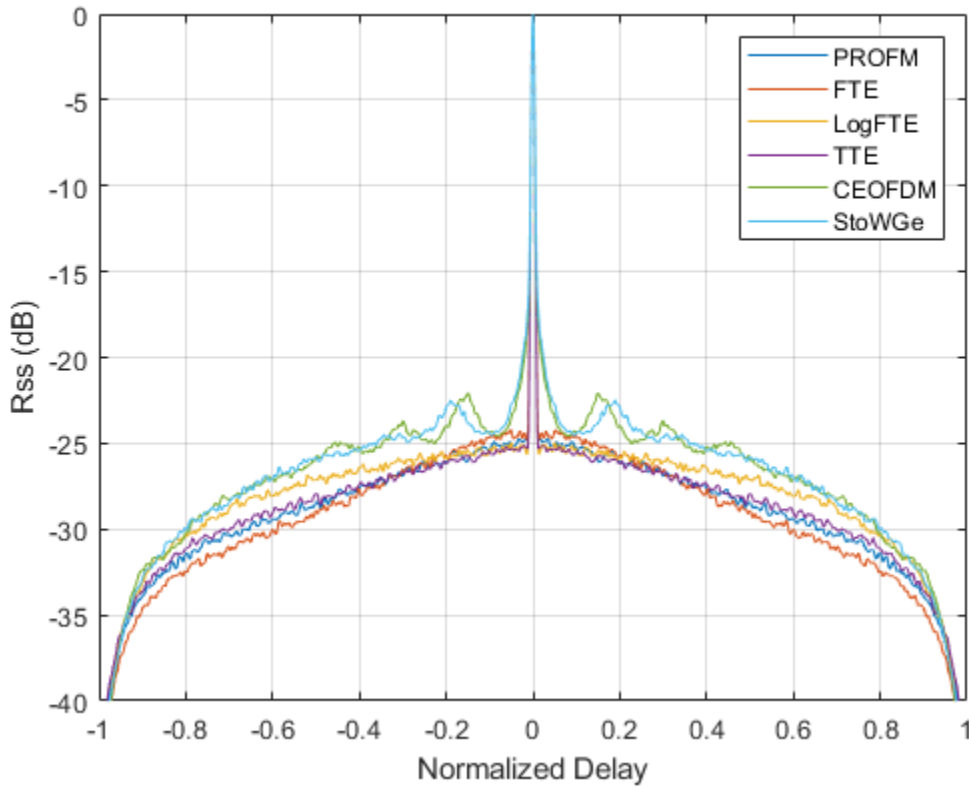


Figure 2.5: Average autocorrelation for different waveform classes.

Table 2.3: Comparison of different waveform class autocorrelation metrics.

Waveform (Loopback)	PRO-FM	FTE	Log-FTE	TTE	CE-OFDM	StoWGe
PSL Mean (dB)	-17.79	-17.39	-17.7	-18.04	-14.7	-14.48
PSL Variance (dB)	1.05	1.09	1.21	1.05	3.49	3.7
ISL Mean (dB)	-28.74	-28.91	-28.01	-28.65	-26.68	-26.66
ISL Variance (dB)	0.0942	0.0945	0.0252	0.0681	1.3765	1.5537

2.2 Joint Time-Frequency Analysis of Gaussian Spectral Shapes

With a traditional, single-domain analysis completed, it is time to consider a joint time-frequency of these waveform classes. The spectral template that tends to be used most for these waveforms is a wide Gaussian spectral shape. Here, the Gaussian spectrally shaped waveforms are analyzed with various time-frequency perspectives.

2.2.1 Angle-Based Instantaneous Frequency Analysis

FM waveforms can have their instantaneous frequency can be accurately estimated from the phase angle of the waveforms, provided there is minimal distortion, other interfering signals, or noise. While the overall instantaneous frequency values may vary significantly on a per-waveform basis, the distribution of values across a waveform set is relatively stationary. For each class, a histogram is generated from the entire waveform set's instantaneous frequency values.

2.2.1.1 PRO-FM Instantaneous Frequency

Figure 2.6 shows the histogram of instantaneous frequency values for PRO-FM in simulation. While the observed distribution technically best fits a truncated normal distribution, it is observed that the distribution of values is close enough to zero that the truncation is of minimal impact.

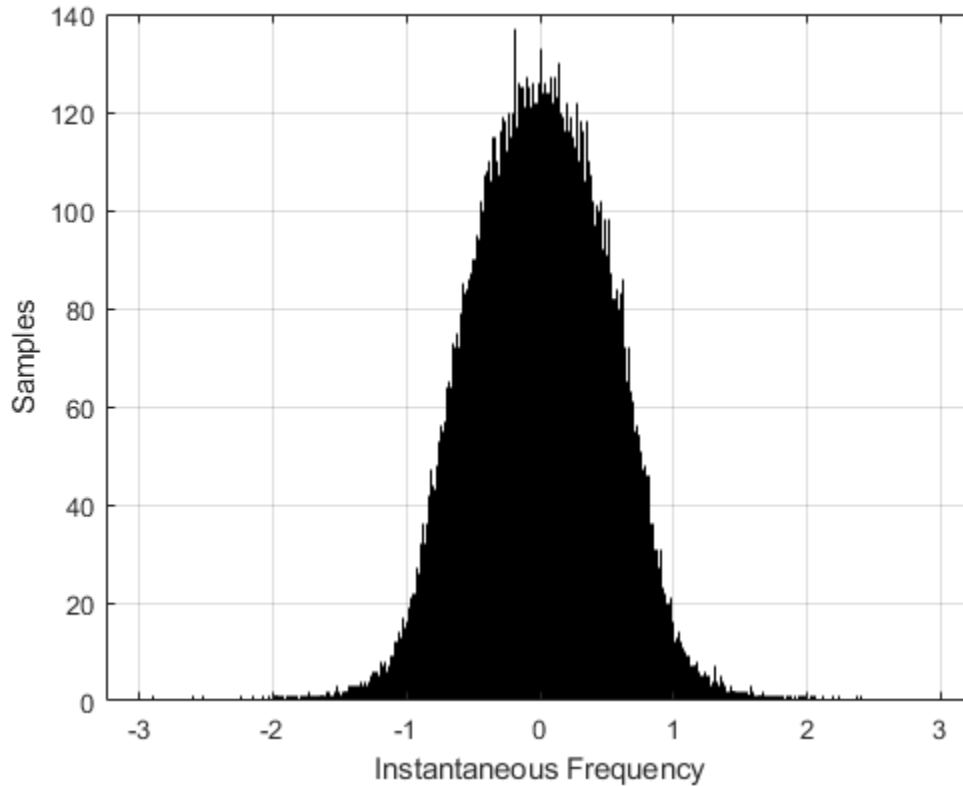


Figure 2.6: Histogram of 1,000 PRO-FM instantaneous frequency values in simulation.

Figure 2.7 shows the histogram of instantaneous frequency values for PRO-FM captured in loopback. While the normal distribution shape is still present with a similar standard deviation, heavier tails are present in this distribution, with a rise around $\pm \pi$. The heavier ends of the distribution are likely due to the pulse edges, which exhibit the most AM behavior of the pulse. This can be visually observed from (PAPR Figure) where an oscillation can be seen at the beginning of the pulse.

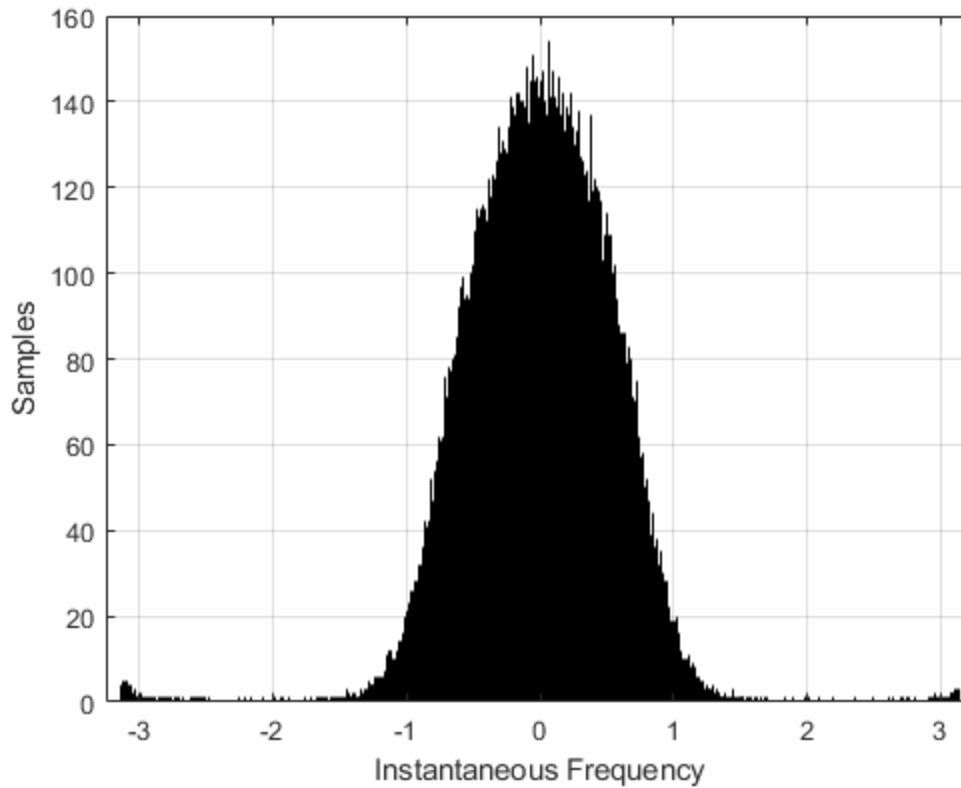


Figure 2.7: Histogram of 1,000 PRO-FM instantaneous frequency values captured in loopback.

2.2.1.2 FTE Instantaneous Frequency

Figure 2.8 shows the histogram of instantaneous frequency values for FTE in simulation. While the observed distribution technically best fits a truncated normal distribution, it is observed that the distribution of values is more spread out than with PRO-FM.

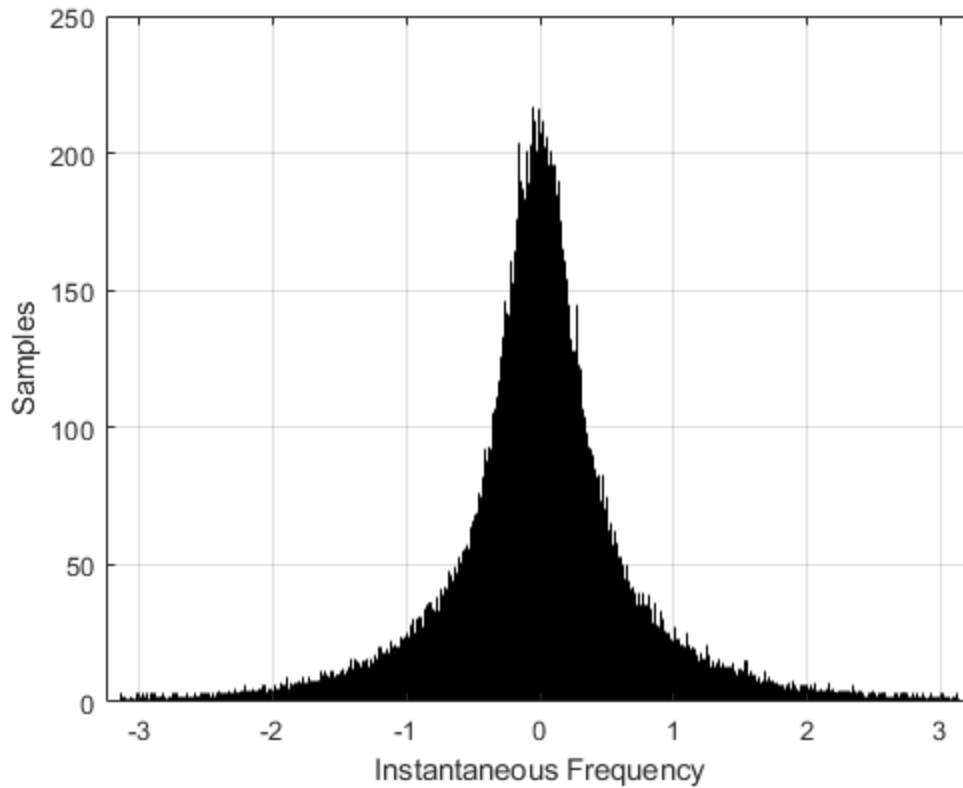


Figure 2.8: Histogram of 1,000 FTE instantaneous frequency values in simulation.

Figure 2.9 shows the histogram of instantaneous frequency values for FTE captured in loopback. Like PRO-FM loopback results, a slight rise is present on the tails of the distribution.

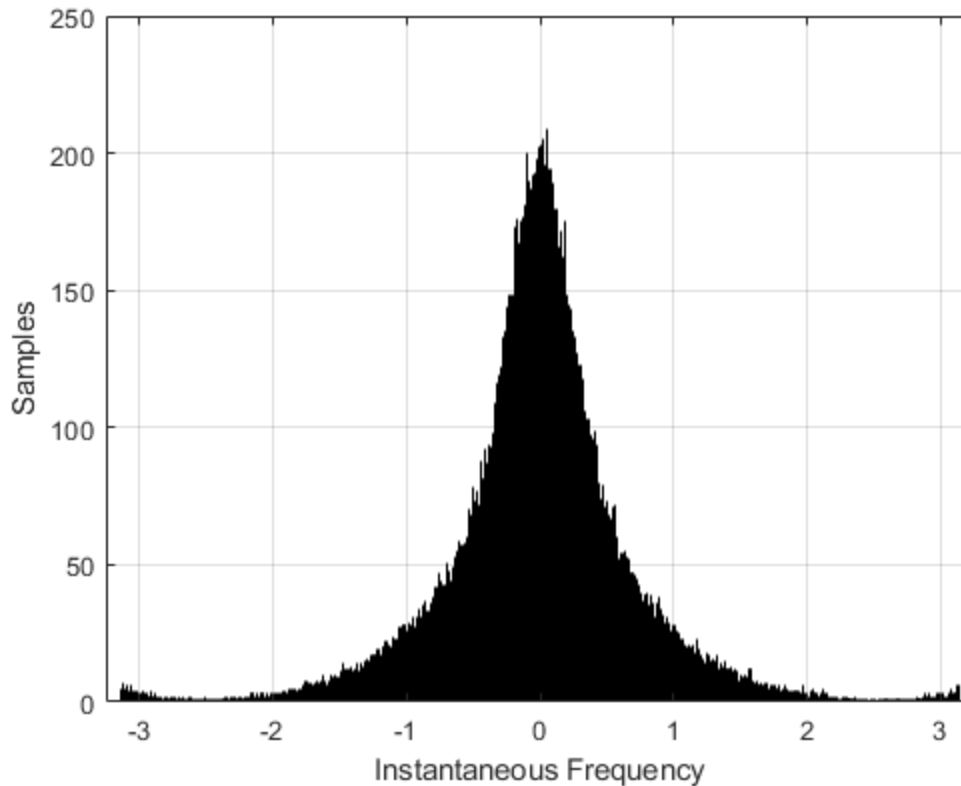


Figure 2.9: Histogram of 1,000 FTE instantaneous frequency values captured in loopback.

2.2.1.3 Log-FTE Instantaneous Frequency

Figure 2.10 shows the histogram of instantaneous frequency values for Log-FTE in simulation. Here, the instantaneous frequency values have a much harder roll-off, ending around ± 1 . This is likely due to the log-FTE creating a stronger emphasis on the spectral roll-off than the mainband, given the logarithmic scaling of the cost function.

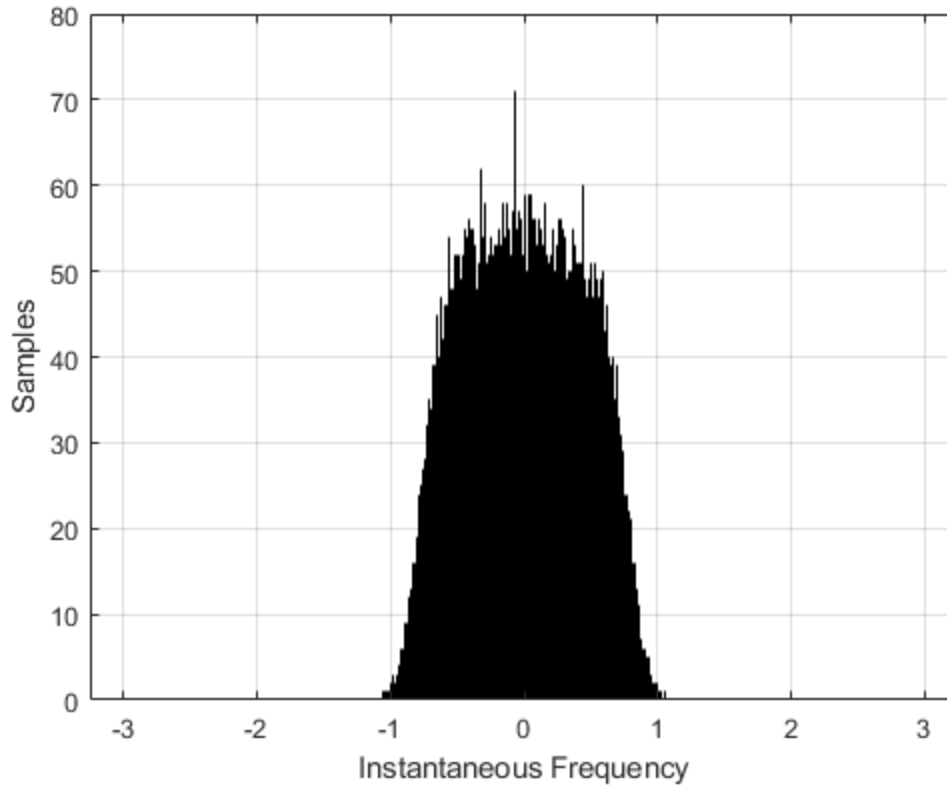


Figure 2.10: Histogram of 1,000 log-FTE instantaneous frequency values in simulation.

Figure 2.11 shows the histogram of instantaneous frequency values for log-FTE captured in loopback. Similar to previous results, the main distribution from simulation is preserved, but the raised tails from the transmit and receive chain is still present.

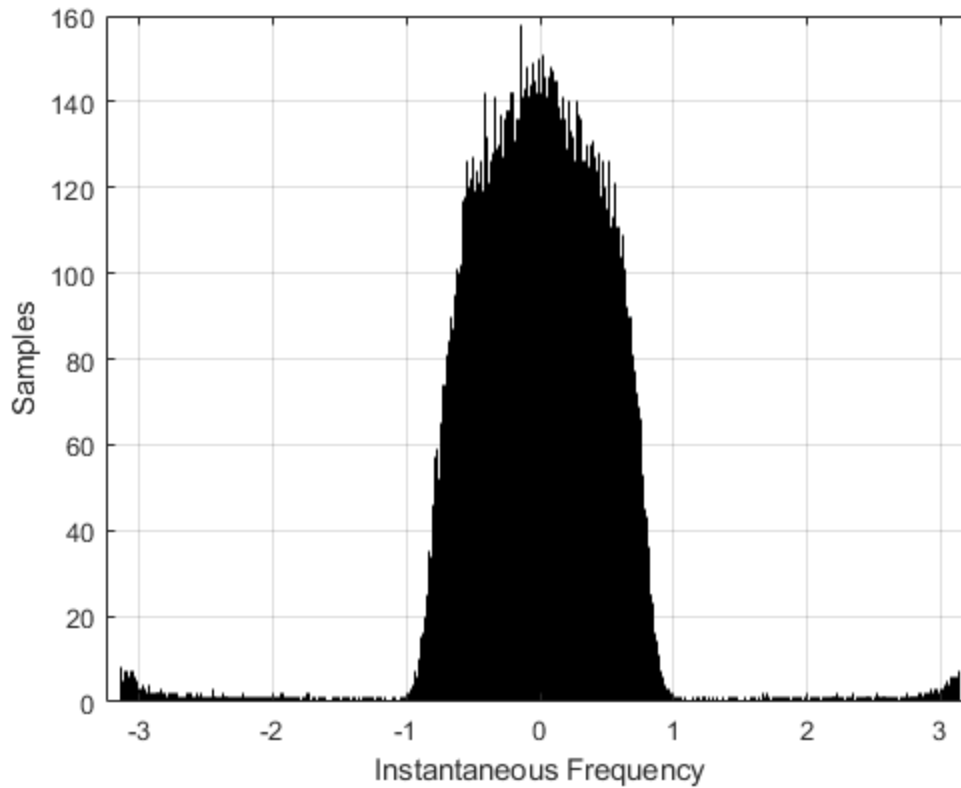


Figure 2.11: Histogram of 1,000 log-FTE instantaneous frequency values captured in loopback.

2.2.1.4 TTE Instantaneous Frequency

Figure 2.12 shows the histogram of instantaneous frequency values for TTE in simulation. The results here are similar to those seen for log-FTE, with TTE resembling a uniform distribution more than a Gaussian one.

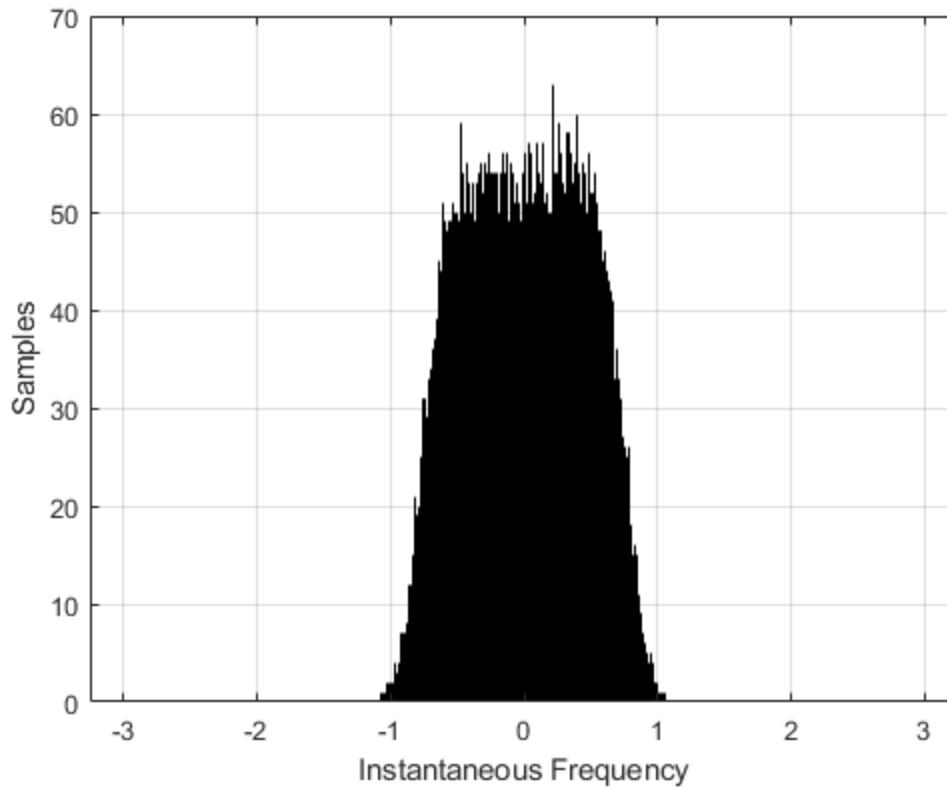


Figure 2.12: Histogram of 1,000 TTE instantaneous frequency values in simulation.

Figure 2.13 shows the histogram of instantaneous frequency values for TTE captured in loopback. Results similar to previous waveforms are observed, while also noting a small dip in the values around 0.

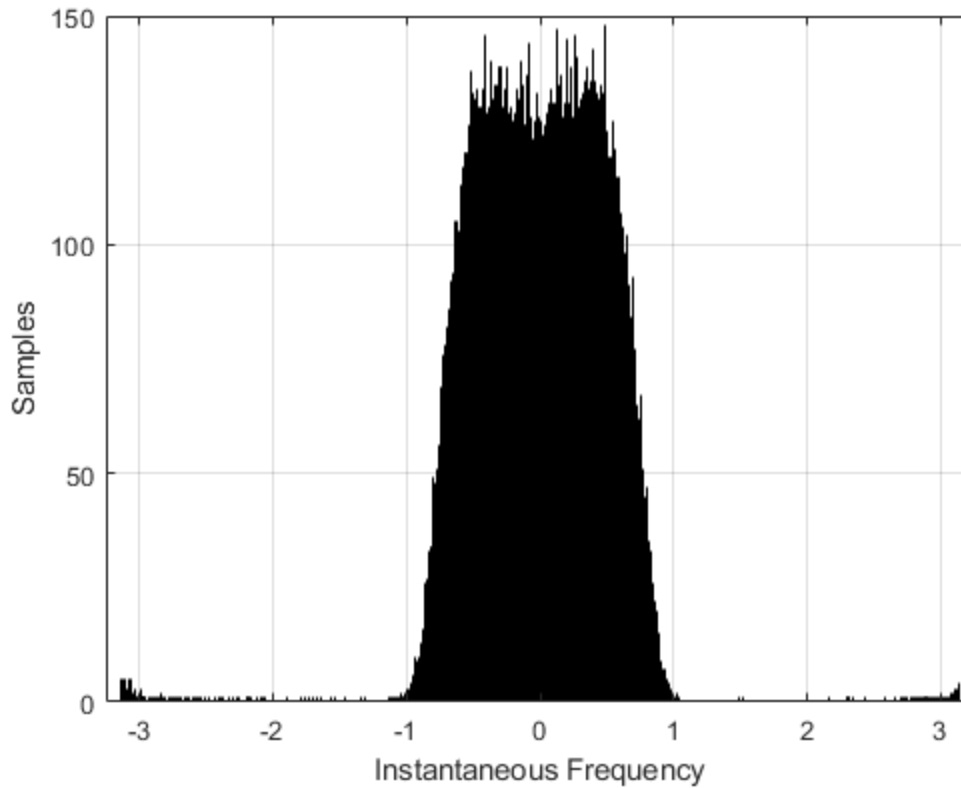


Figure 2.13: Histogram of 1,000 TTE instantaneous frequency values captured in loopback.

2.2.1.5 CE-OFDM Instantaneous Frequency

Figure 2.14 shows the histogram of instantaneous frequency values for CE-OFDM in simulation.

The results resemble the gaussian distribution of FTE.

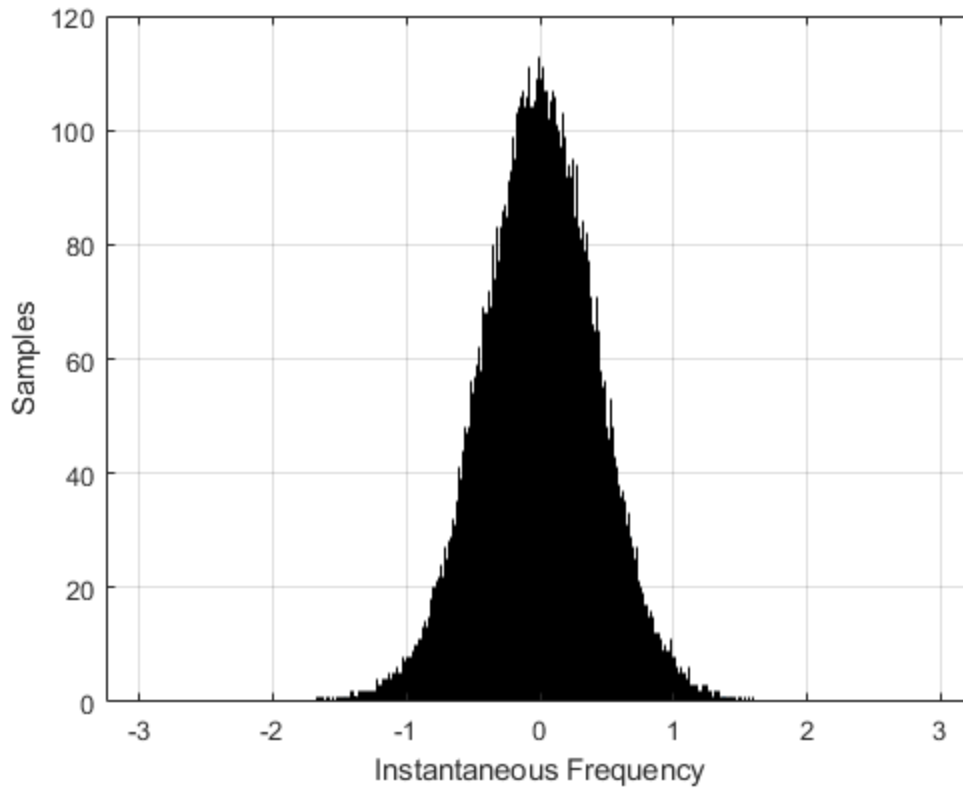


Figure 2.14: Histogram of 1,000 CE-OFDM instantaneous frequency values in simulation.

Figure 2.15 shows the histogram of instantaneous frequency values for CE-OFDM captured in loopback. Notably a spike in values can be observed at DC. It is possible this is due to the summation nature of CE-OFDM.

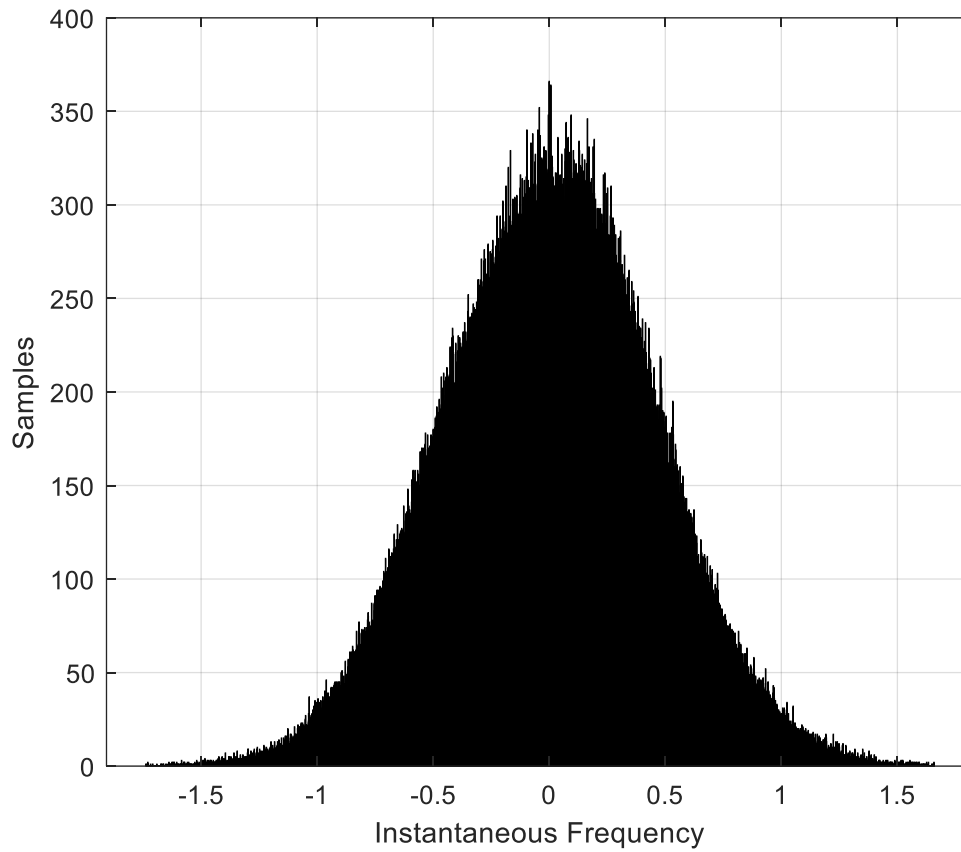


Figure 2.15: Histogram of 1,000 CE-OFDM instantaneous frequency values captured in loopback.

2.2.1.6 StoWGe Instantaneous Frequency

Figure 2.16 shows the histogram of instantaneous frequency values for StoWGe in simulation.

Notably, a tail can be seen present in the simulation values, albeit a small one.

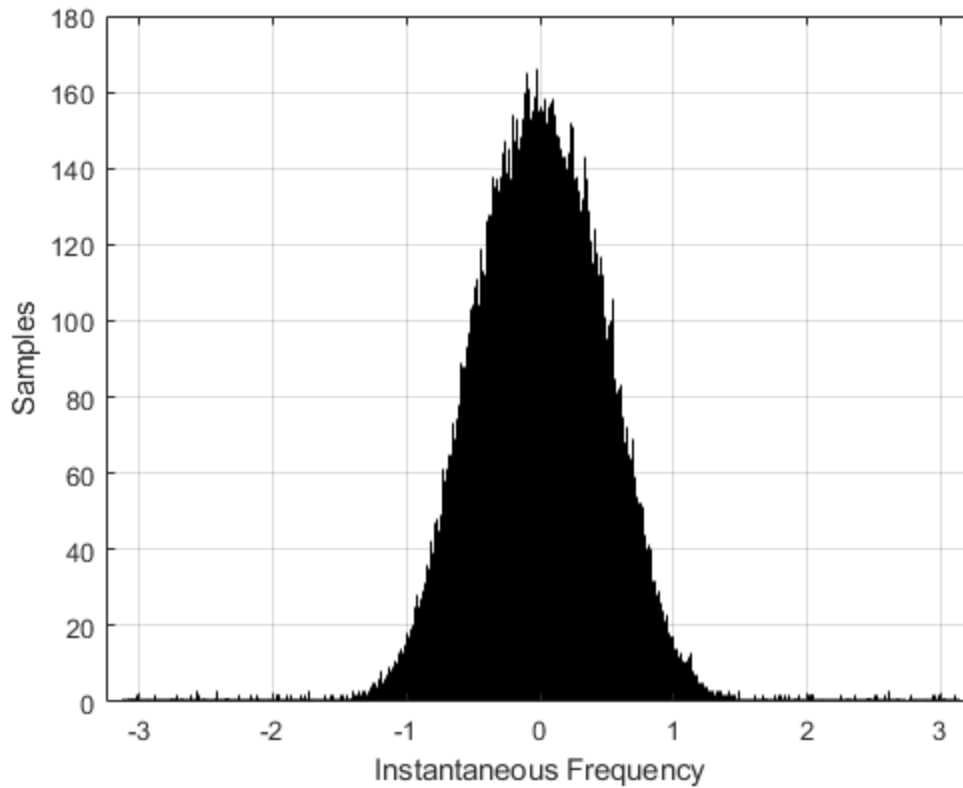


Figure 2.16: Histogram of 1,000 StoWGe instantaneous frequency values in simulation.

Figure 2.17 shows the histogram of instantaneous frequency values for StoWGe captured in simulation. Notably, unlike all the other cases, there isn't a heavy tail or spike around $\pm\pi$. It is possible that, due to the CW context of StoWGe, rising and falling edges do not impact the waveform fidelity as much as the other classes of waveform.

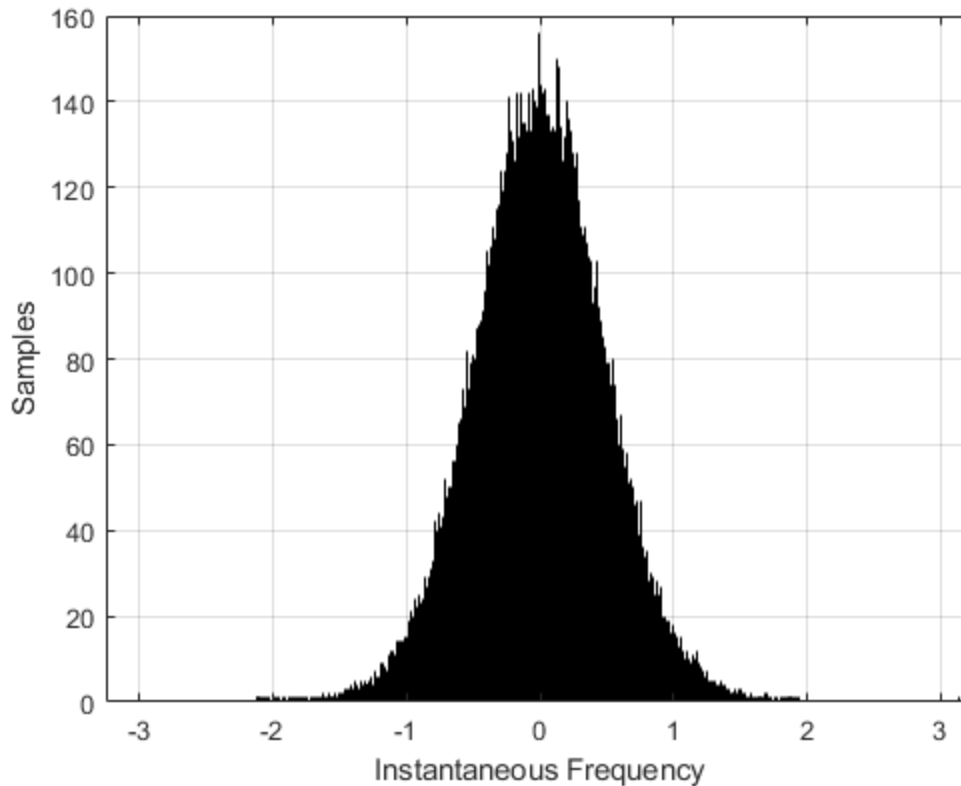


Figure 2.17: Histogram of 1,000 StoWGe instantaneous frequency values captured in loopback.

2.2.1.7 Instantaneous Frequency statistical parameters

It is useful to compute basic statistical parameters for each of the previously discussed waveform class histograms. Tables 2.4 and 2.5 show the mean, variance, and 99th percentile values for each of the distributions in simulation and loopback respectively. All the means of the distribution are effectively zero, although CE-OFDM and StoWGe have a much smaller mean. The variance of the waveforms also varies from class to class. Notably, even though the higher tails can be seen present in the loopback results, the 99th percentile of the distributions barely changes from simulation to loopback. Strangely, in some of the cases with a raised tail, the actual distribution tightens, leading to a lower 99th percentile value.

Table 2.4: Instantaneous frequency metrics for various simulated waveform classes.

Waveform (Simulation)	PRO-FM	FTE	Log-FTE	TTE	CE-OFDM	StoWGe
Mean	-1.42E-3	-1.17E-3	2.16E-4	-7.00E-5	-3.36E-5	8.20E-4
Variance	0.2159	0.3409	0.1850	0.1867	0.1619	0.2005
99th Percentile	1.135	2.122	0.8537	0.8578	1.06	1.20

Table 2.5: Instantaneous frequency metrics for various waveform classes captured in loopback.

Waveform (Loopback)	PRO-FM	FTE	Log-FTE	TTE	CE-OFDM	StoWGe
Mean	-3.46E-3	-3.81E-3	-2.92E-3	-1.92E-3	2.26E-4	-5.06E-4
Variance	0.2258	0.3141	0.2186	0.1981	0.1959	0.1936
99th Percentile	1.144	1.887	1.241	0.9386	1.166	1.173

2.2.2 Spectrogram Analysis

While the instantaneous frequency computed from angle difference can provide a joint time frequency representation at the smallest time window for a single signal, it is not particularly effective in the presence of noise and interference. Therefore, it is worth looking at the waveforms in a fully 2D joint time frequency transform. Firstly, the waveforms are studied using the most commonly utilized joint time-frequency representation, the spectrogram obtained from the Short-Time Fourier Transform (STFT).

The settings used in the spectrogram initially will be a rectangular window, with sample-by-sample overlap. The temporal extent of the window will be varied to provide different degrees

of temporal and spectral resolution. For random FM waveforms, three regimes of behavior exist depending on the window size used.

- Large window size: When the window is large enough, the waveform mimics the PSD of the waveform. Since a sufficient number of samples are included in each Fourier Transform in the STFT that generates the spectrogram, it will match up closely to the Fourier Transform of the entire waveform i.e. the PSD.
- Medium window size: When the window size decreases, the frequency extent of the waveform begins to contract and expand at certain times, correlating with the instantaneous frequencies around that particular time.
- Small window size: When the window size decreases further, the spectrogram will match up to the instantaneous frequency of the waveform with a particular amount of bandwidth at each time slice, corresponding to the available frequency resolution.

Depending on the sampling frequency, not all of these domains may be present. Just as the sampling rate must be high enough to capture the full band of interest, so must the sampling rate be high enough to transition between these three window size domains. For the results of this section, a 10% time window and a 1% time window are used.

Figure 2.18 shows an example spectrogram of a PRO-FM waveform using a 10% of pulse width wide window, where the horizontal axis is time and the vertical axis is frequency. Though the waveform's energy varies across time, it is relatively constrained within the 3dB bandwidth. Conversely, figure 2.19 shows a spectrogram of a PRO-FM waveform using a 1% of pulse width wide window. While the frequency resolution of the spectrogram has been degraded by a factor of 10, the energy now varies significantly across frequency, and closely resembles the angle-based instantaneous frequency profile of the waveform.

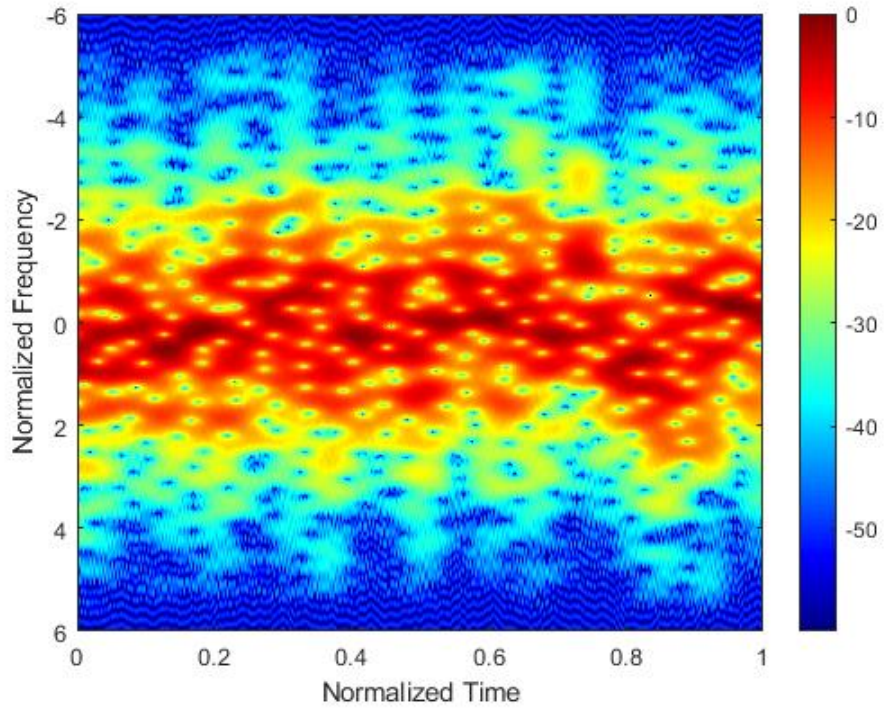


Figure 2.18: Spectrogram of a PRO-FM waveform using a 10% time window.

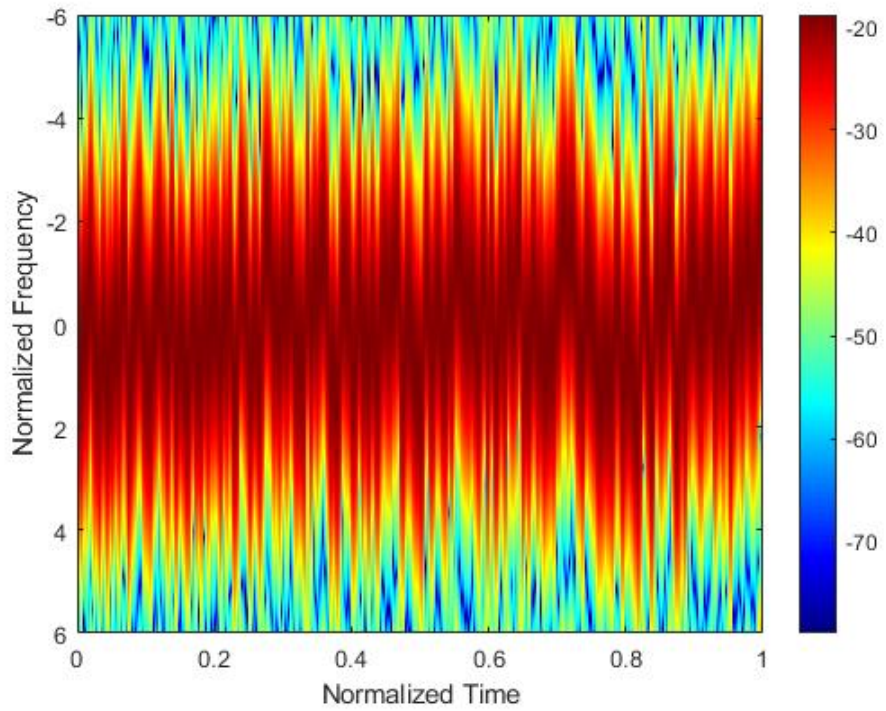


Figure 2.19: Spectrogram of a PRO-FM waveform using a 1% time window.

To further quantify the results, similar metrics to those used in section (spectral analysis section) are utilized to characterize the spectrograms. First, the average roll-off level across time at the edges in frequency are computed. Secondly, the percent OOB energy is computed by finding the ratio of energy in the spectrogram outside of the 3dB bandwidth over the total energy in the spectrogram. Table 2.6 shows the results of the analysis for simulation waveforms, while Table 2.7 shows the results for waveforms captured in loopback. Notably, as the time window of observation becomes smaller, the percent OOB energy increases. This is consistent with what we have seen earlier with the instantaneous frequency values; as the observation time interval decreases, the FM waveform appears to more closely resemble a single tone at the value of instantaneous frequency. Since the instantaneous frequency isn't inherently constrained, combined with degraded frequency resolution, results in decreased spectral containment.

Table 2.6: Spectrogram metrics for various waveform classes in simulation.

Waveform (Simulation)	PRO-FM	FTE	Log-FTE	TTE	CE-OFDM	StoWGe
(10%) Mean Roll-off Level (dB)	-47.03	-33.63	-52.54	-54.34	-55.11	-52.76
(10%) Roll-off Level Variance (dB)	1.59	2.48	0.19	0.14	0.28	0.46
(10%) Mean Percent OOB	43.99%	49.68%	39.85%	39.89%	30.23%	36.99%
(10%) Percent OOB Variance	0.023%	0.026%	0.02%	0.02%	0.30%	0.14%
(1%) Mean Roll-off Level (dB)	-54.16	-49.02	-54.29	-54.81	-59.43	-57.63
(1%) Roll-off Level Variance (dB)	0.36	0.54	0.16	0.21	1.62	0.99
(1%) Mean Percent OOB	61.37%	63.30%	60.66%	60.68%	59.92%	60.67%

(1%) Percent OOB Variance	~0%	0.01%	~0%	~0%	~0%	0.01%
----------------------------------	-----	-------	-----	-----	-----	-------

Table 2.7: Spectrogram metrics for various waveform classes captured in loopback.

Waveform (Loopback)	PRO-FM	FTE	Log-FTE	TTE	CE-OFDM	StoWGe
(10%) Mean Roll-off Level (dB)	-55.00	-54.60	-55.06	-55.07	-54.85	-55.07
(10%) Roll-off Level Variance (dB)	0.16	0.16	0.16	0.16	0.22	0.20
(10%) Mean Percent OOB	43.61%	46.98%	38.93%	39.81%	27.90%	27.54%
(10%) Percent OOB Variance	0.03%	0.03%	0.02%	0.02%	0.86%	0.96%
(1%) Mean Roll-off Level (dB)	-53.30	-48.78	-54.79	-54.69	-58.11	-58.27
(1%) Roll-off Level Variance (dB)	61.33%	62.66%	60.54%	60.68%	60.51%	60.48%
(1%) Mean Percent OOB	61.33%	62.66%	60.54%	60.68%	60.51%	60.48%
(1%) Percent OOB Variance	~0%	~0%	~0%	~0%	0.02%	0.02%

2.2.3 Wigner-Ville Distribution Analysis

As seen above with the spectrogram, linear time-frequency transforms require a trade off between temporal and spectral resolution. However, with a quadratic transformation, there is no trade off between the finest temporal and spectral frequencies. Here, the waveform classes are analyzed using the WVD.

Figure 2.20 shows the WVD for a PRO-FM waveform. The distribution appears to be extremely noisy, but it is in fact self-interference. Figure 2.21 shows a smoothed WVD for the

same PRO-FM waveform. The smoothed WVD is a filtered version of the WVD, and is similar to using longer time windows in the spectrogram. Here, the cross-terms have been heavily suppressed, but at the cost of coarser time and frequency resolutions.

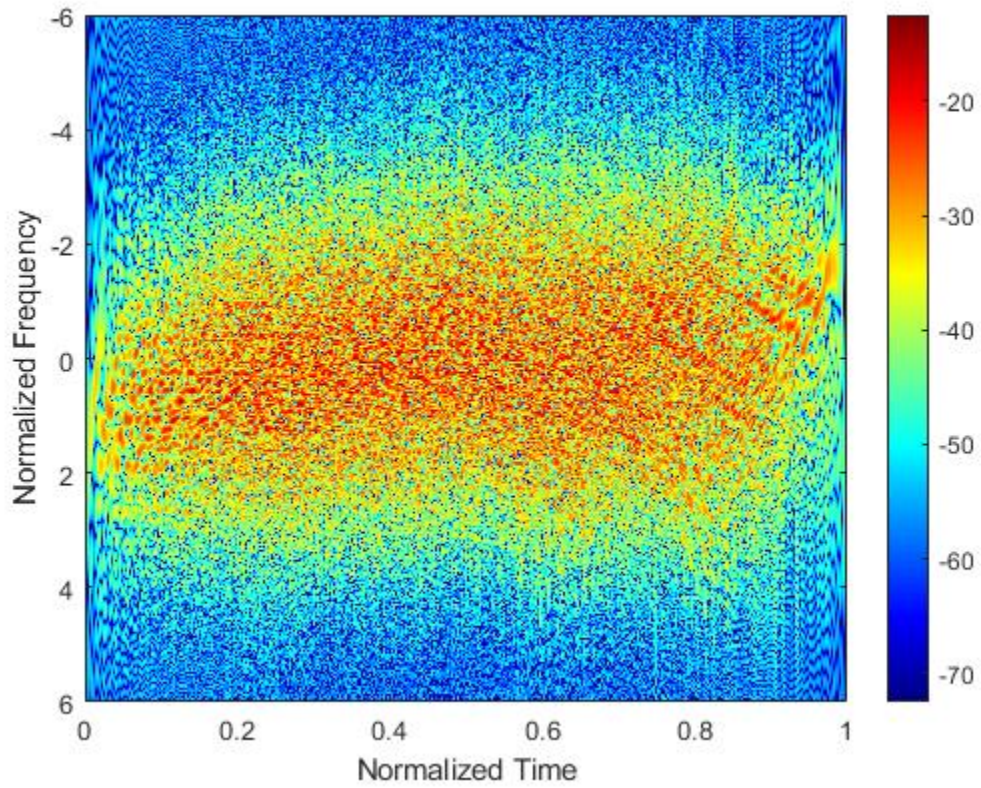


Figure 2.20: Wigner-Ville distribution of a PRO-FM waveform.

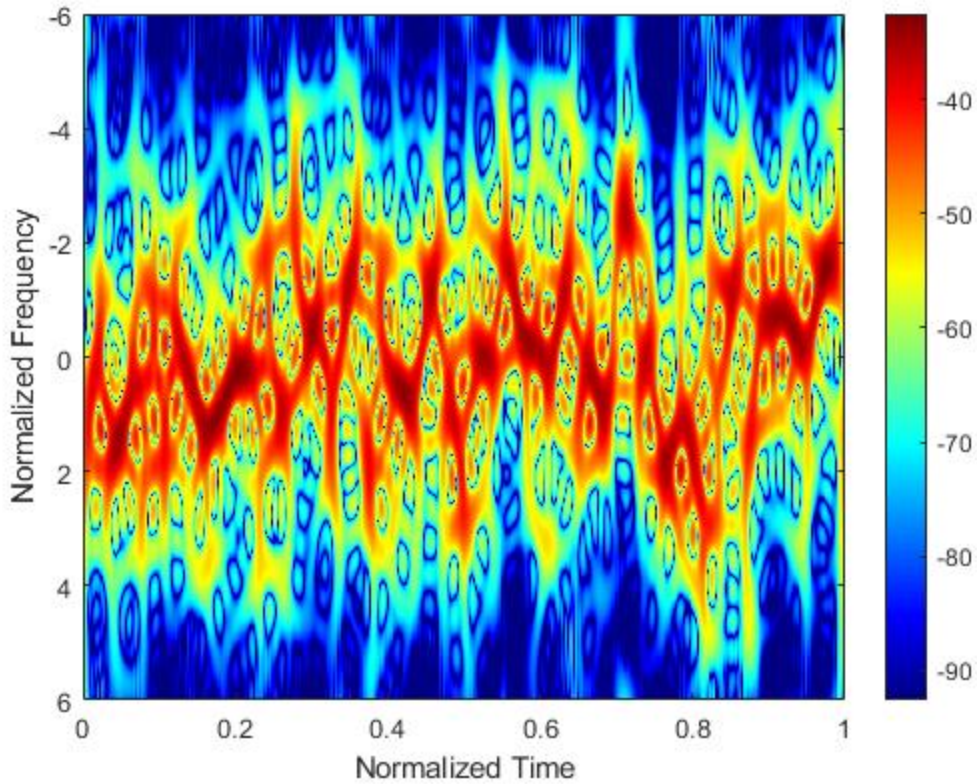


Figure 2.21: Smoothed Wigner-Ville distribution of a PRO-FM waveform.

Table 2.8 shows the results of the waveform classes for the WVD, and table 2.9 shows the results of the waveform classes for the smoothed WVD. Notably, while the spectral containment results for the WVD and smoothed WVD match up with our expected results in the 1% time window spectrogram, the actual roll-off level is significantly lower in the smoothed WVD. Thanks to the finer resolution in time and frequency, this regime more closely follows the instantaneous frequency while providing a much sharper roll-off, unlike the 1% time window spectrogram which has a very slow, broad roll-off across frequency.

Table 2.8: WVD metrics for various waveform classes in simulation.

Waveform (Simulation)	PRO-FM	FTE	Log-FTE	TTE	CE-OFDM	StoWGe

WVD Mean Roll-off Level (dB)	-47.03	-33.63	-52.54	-54.34	-55.11	-52.76
WVD Roll-off Level Variance (dB)	1.59	2.48	0.19	0.14	0.28	0.46
WVD Mean Percent OOB	43.99%	49.68%	39.85%	39.89%	30.23%	36.99%
WVD Percent OOB Variance	0.023%	0.026%	0.02%	0.02%	0.30%	0.14%
Smooth WVD Mean Roll-off Level (dB)	-54.16	-49.02	-54.29	-54.81	-59.43	-57.63
Smooth WVD Roll-off Level Variance (dB)	0.36	0.54	0.16	0.21	1.62	0.99
Smooth WVD Mean Percent OOB	61.37%	63.30%	60.66%	60.68%	59.92%	60.67%
Smooth WVD Percent OOB Variance	~0%	0.01%	~0%	~0%	~0%	0.01%

Table 2.9: WVD metrics for various waveform classes captured in loopback.

Waveform (Loopback)	PRO-FM	FTE	Log-FTE	TTE	CE-OFDM	StoWGe
WVD Mean Roll-off Level (dB)	-59.64	-53.59	-61.93	-61.09	-60.23	-59.39
WVD Roll-off Level Variance (dB)	0.4499	0.7046	0.0786	0.6167	0.1787	0.1173
WVD Mean Percent OOB	58.13%	60.81%	54.85%	55.66%	49.95%	49.46%
WVD Percent OOB Variance	0.0177%	0.0157%	0.0141%	0.0115%	0.5946%	0.6615%

Smooth WVD Mean Roll-off Level (dB)	-89.05	-80.62	-99.97	-98.93	< -300	< -300
Smooth WVD Roll-off Level Variance (dB)	1.747	2.162	1.164	1.185	>10	>10
Smooth WVD Mean Percent OOB	56.45%	54.70%	53.59%	55.19%	56.53%	56.36%
Smooth WVD Percent OOB Variance	0.0177%	0.01%	~0%	~0%	~0%	0.01%

2.2.4 Instantaneous Autocorrelation Function Analysis

As noted before in section 1.3.4.2, the instantaneous autocorrelation can provide a measure of randomness at different points throughout the pulse. Figure 2.22 shows the IAF of a single PRO-FM waveform. The hexagon pattern can be seen, implying that the WVD has such large amounts of oscillating cross-terms that the vertical slices are not particularly random at such a small time-scale. However, figure 2.23 shows the smoothed IAF of a single PRO-FM waveform. Here, a mainlobe can be clearly seen across the horizontal axis, providing a useful measure of randomness throughout the waveform.

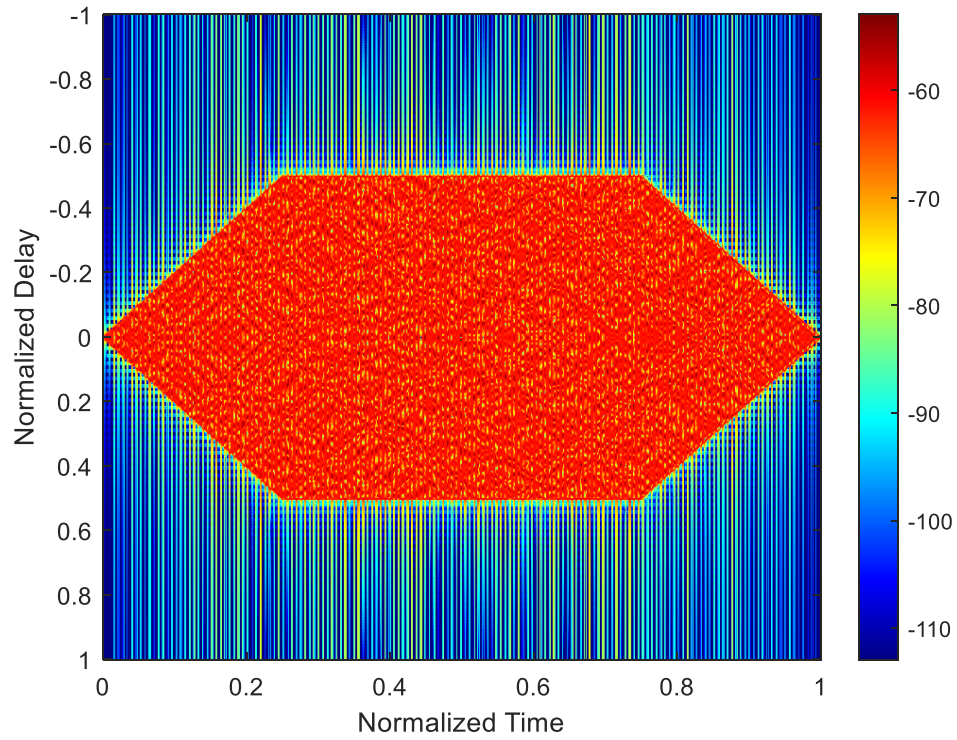


Figure 2.22: Instantaneous Autocorrelation of a PRO-FM waveform.

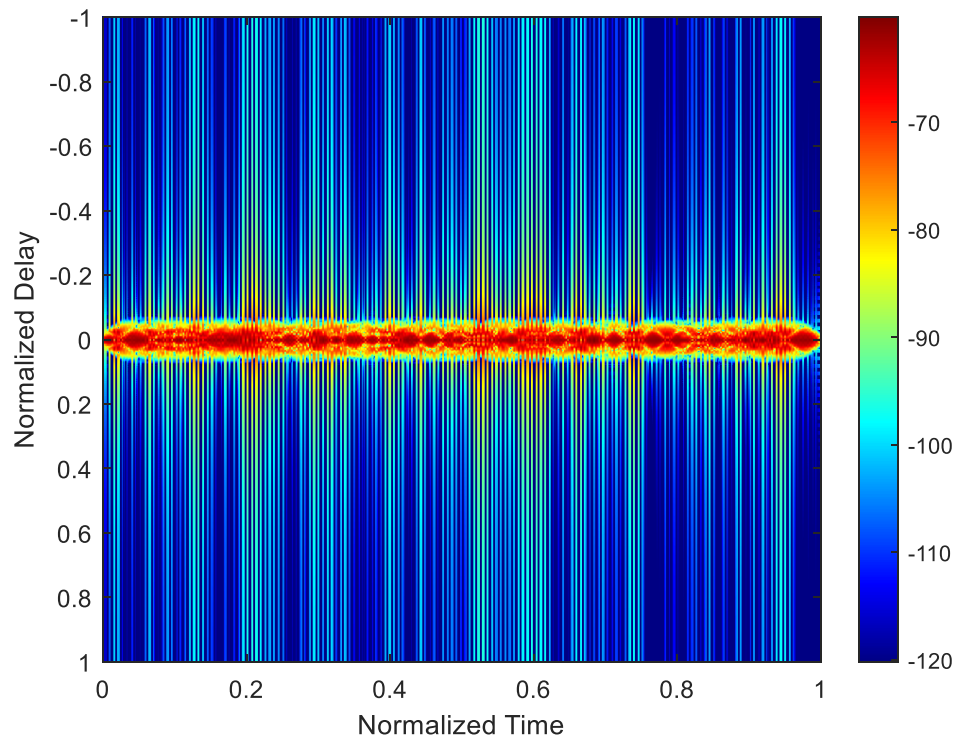


Figure 2.23: Smoothed Instantaneous Autocorrelation of a PRO-FM waveform.

While it is difficult with PRO-FM to interpret the IAF and smoothed IAF, CE-OFDM provides some intuition about the function. Figure 2.24 shows the IAF of a single CE-OFDM and figure 2.25 shows the smoothed IAF of a single CE-OFDM waveform. Notably, a smoothed pattern can be seen within the hexagon of the IAF. But perhaps more intuitive is the smoothed IAF, where the mainlobe widens and narrows relative to time, and has less occurring “sidelobe flashes”. But when compared side to side with the smoothed WVD, shown in figure 2.26, the sidelobe flashes in the smooth IAF correspond to zero crossings in the smooth WVD, and the mainlobe narrows as the chirp rate increases. The narrowing is consistent with the idea that higher chirp rates correspond to instantaneous bandwidths, resulting in narrower autocorrelation.

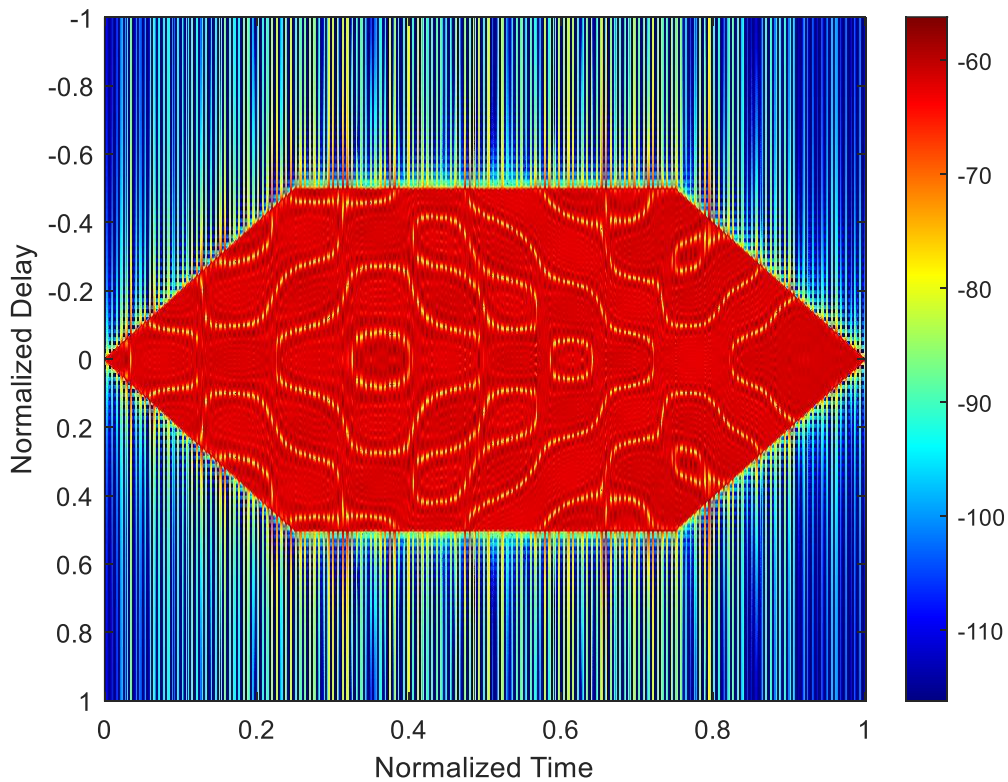


Figure 2.24: Instantaneous Autocorrelation of a CE-OFDM waveform.

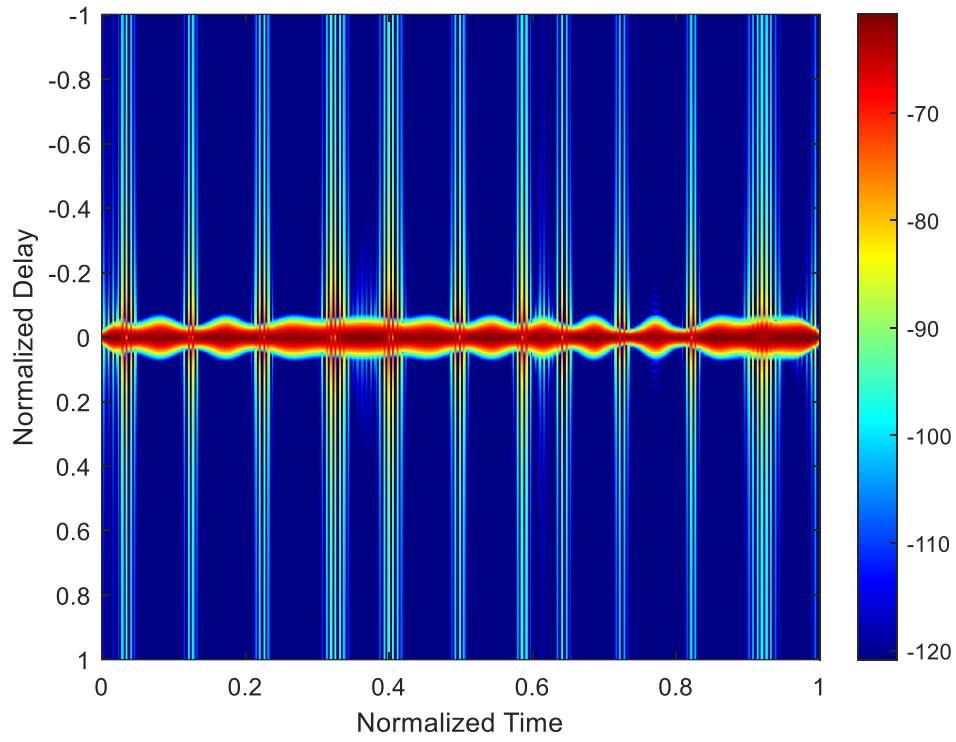


Figure 2.25: Smoothed IAF of a CE-OFDM waveform.

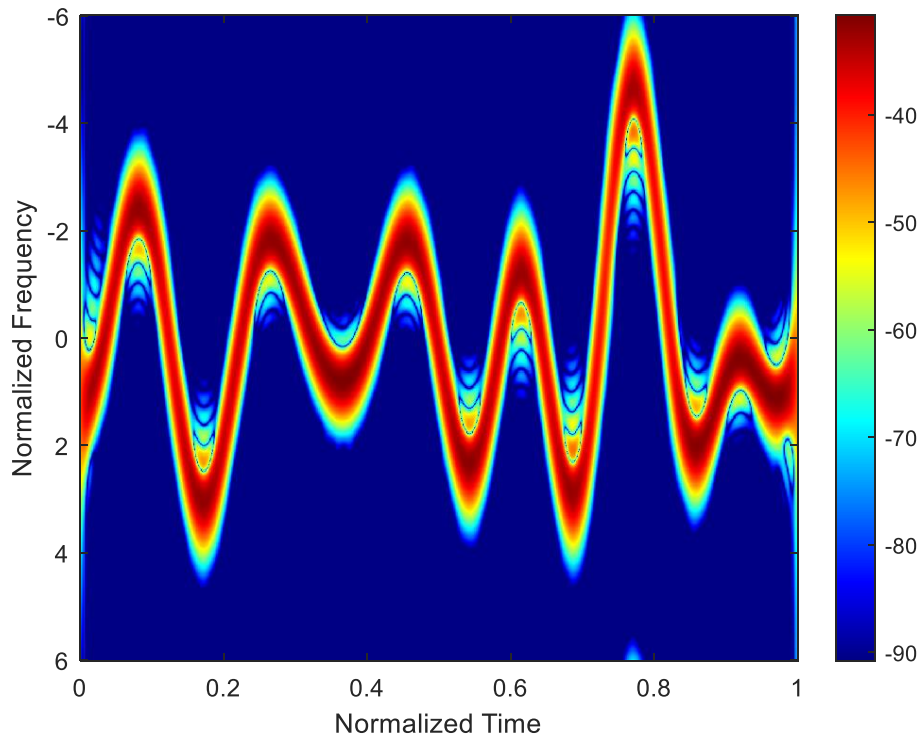


Figure 2.26: Smoothed WVD of a CE-OFDM waveform.

2.2.5 Radon-Wigner Transform Analysis

Lastly, it is useful to briefly consider the Radon-Wigner Transform as a means of viewing the waveform. Figure 2.27 shows the RWT of a PRO-FM Waveform.

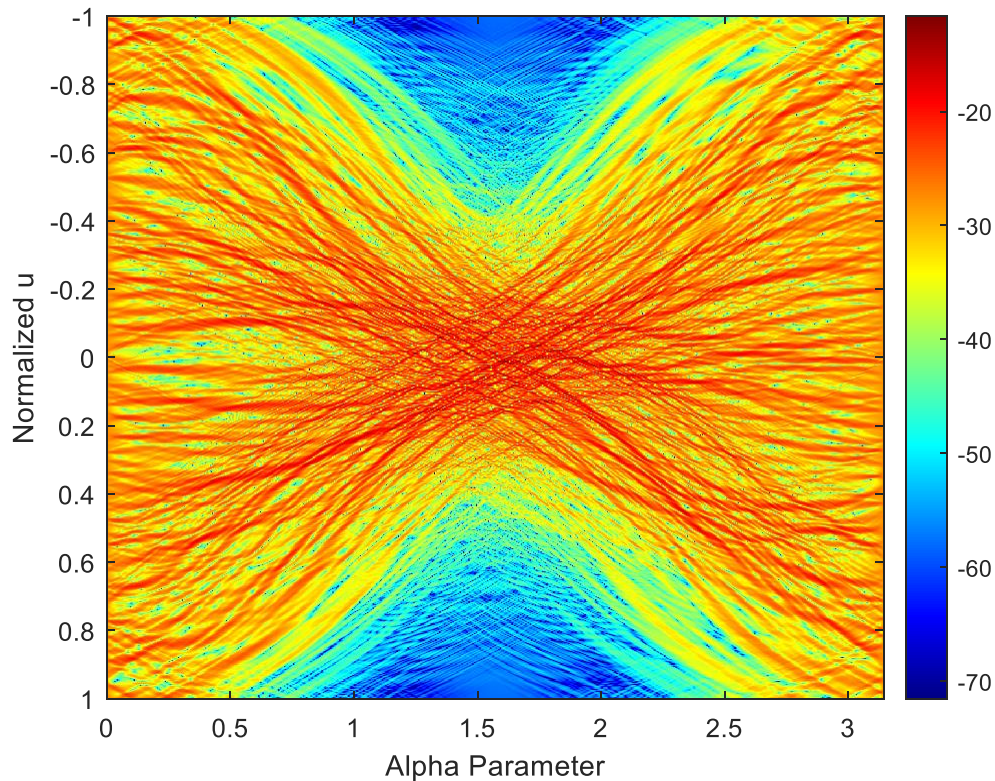


Figure 2.27: Radon-Wigner Transform of a PRO-FM waveform.

Given that the column at $\alpha = 0$ is the time domain, and the column at $\alpha = \pi/2$ is the frequency domain, the RWT shows which portions in time correspond to a given frequency bin in the PSD. Since PRO-FM can have a different instantaneous frequency at each time sample, many curves can be seen from each time sample to its contribution in the frequency domain. Conversely, figure 2.28 shows the RWT for a CE-OFDM waveform. Here the smoother instantaneous frequency function results in broadened curves, with more temporally isolated areas of a given instantaneous frequency value or range.

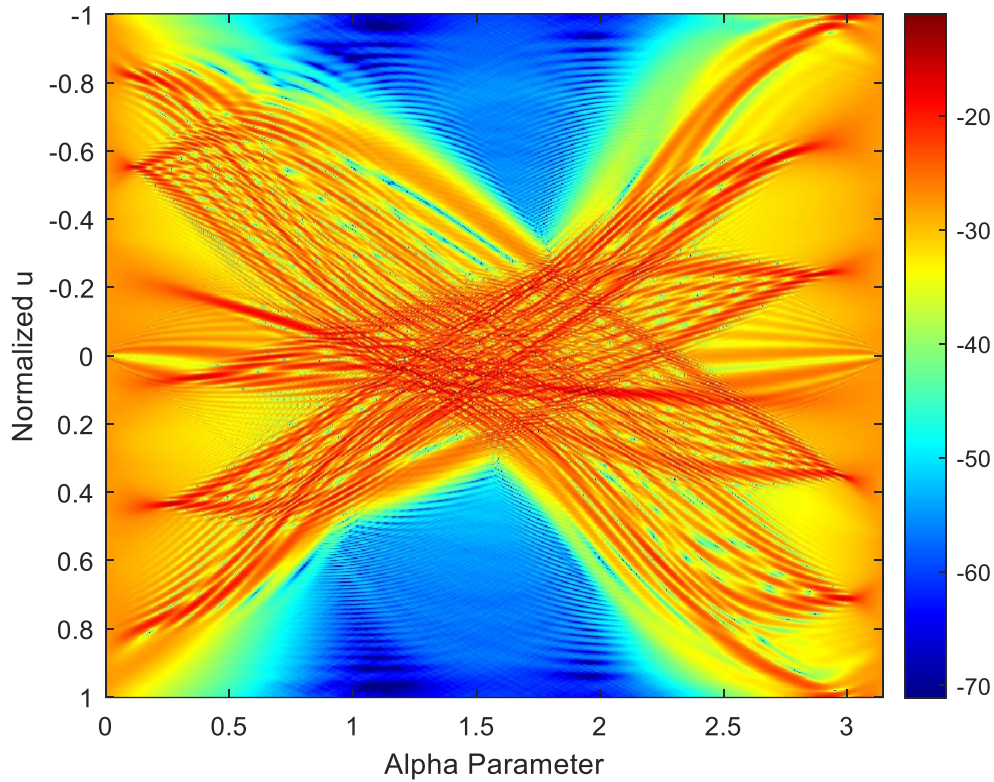


Figure 2.28: Radon-Wigner transform of a CE-OFDM waveform.

2.3 Traditional Analysis of Notched Gaussian Spectral Shapes

While the metrics previously discussed are effective for waveforms with symmetric spectrum, additional metrics should be considered with asymmetric spectra. One particularly interesting shape is a notched Gaussian spectral shape, where a gap is placed within the mainband. These can be particularly deep given the optimization capabilities of some classes of random FM [16, 33, 36-38]. As with the Gaussian spectral shape waveforms, the one dimensional domains that will be studied are their time representation, frequency representation, autocorrelation, and PSD. However, for this particular shape, CE-OFDM and StoWGe will be excluded from the analysis. Additionally, only the loopback captured results will be considered for this particular section.

2.3.1 Time Domain Analysis

Figure 2.29 shows a comparison of the envelopes of each of the waveforms in loopback. While they may not appear completely flat, they have been measured after amplification where the constant amplitude constraint is not nearly as necessary. Table 2.10 shows the resulting PAPR for each of the waveform classes in both simulation and in loopback measurements. As expected, the simulated have perfect PAPR of 1 with 0 variance due to their FM structure. While the loopback results do possess a degree of AM, their PAPR values are relatively small.

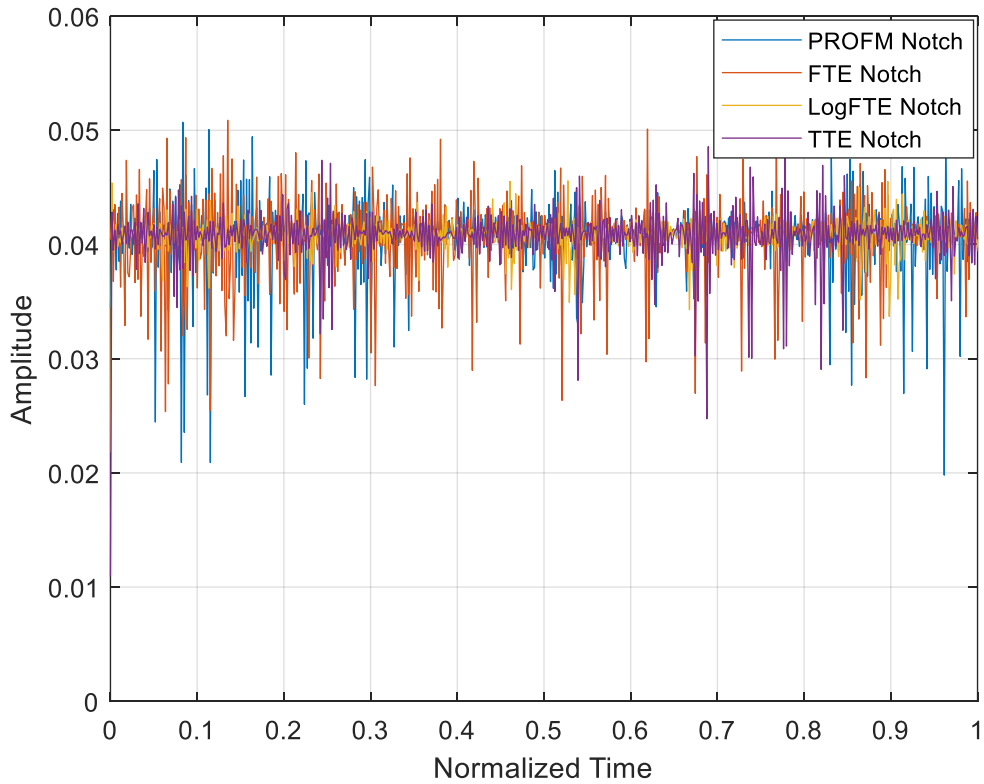


Figure 2.29: Comparison of several waveform amplitudes.

Table 2.10: Comparison of different waveform class amplitudes.

Waveform	PRO-FM	FTE	Log-FTE	TTE
Mean PAPR	1.2840	1.2481	1.1927	1.2014
PAPR Variance	0.0016	0.0015	0.0030	0.0027

2.3.2 Frequency Domain Analysis

For each waveform class, figure 2.30 shows the PSD of a single waveform from each class. On an individual basis, the waveforms have significant magnitude variation across frequency but their average is relatively smooth. Figure 2.31 shows the average PSD across a set of 1,000 waveforms from each waveform class. While the notch for FTE isn't particularly deep, the other 3 classes are fairly close together.

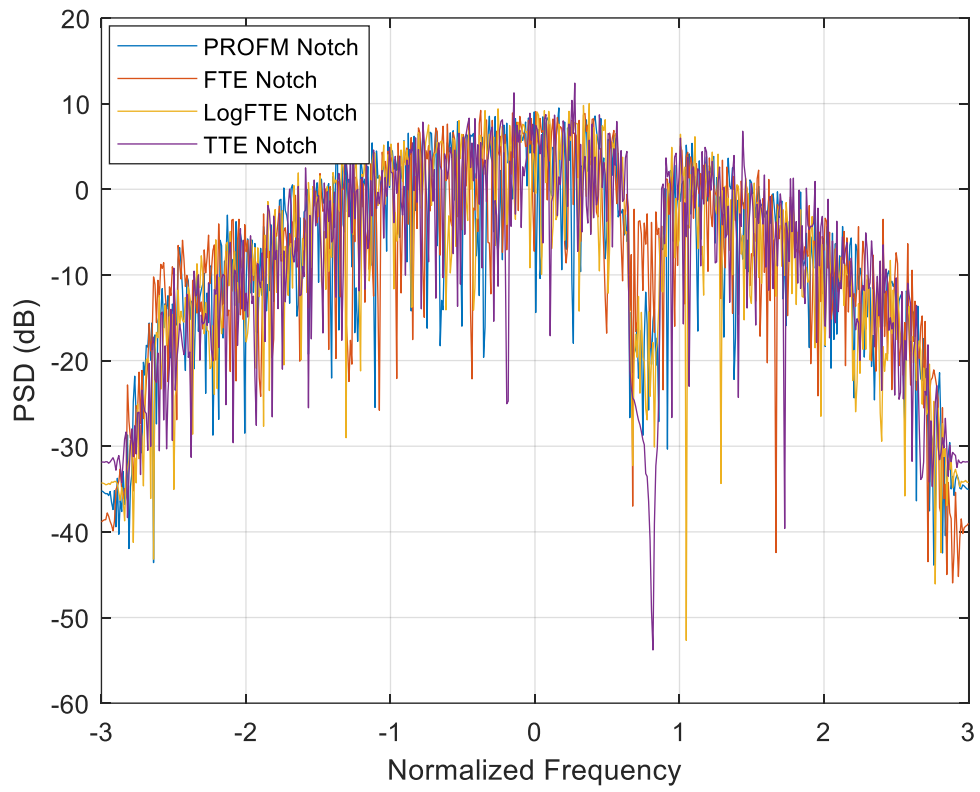


Figure 2.30: Comparison of several waveform PSDs.

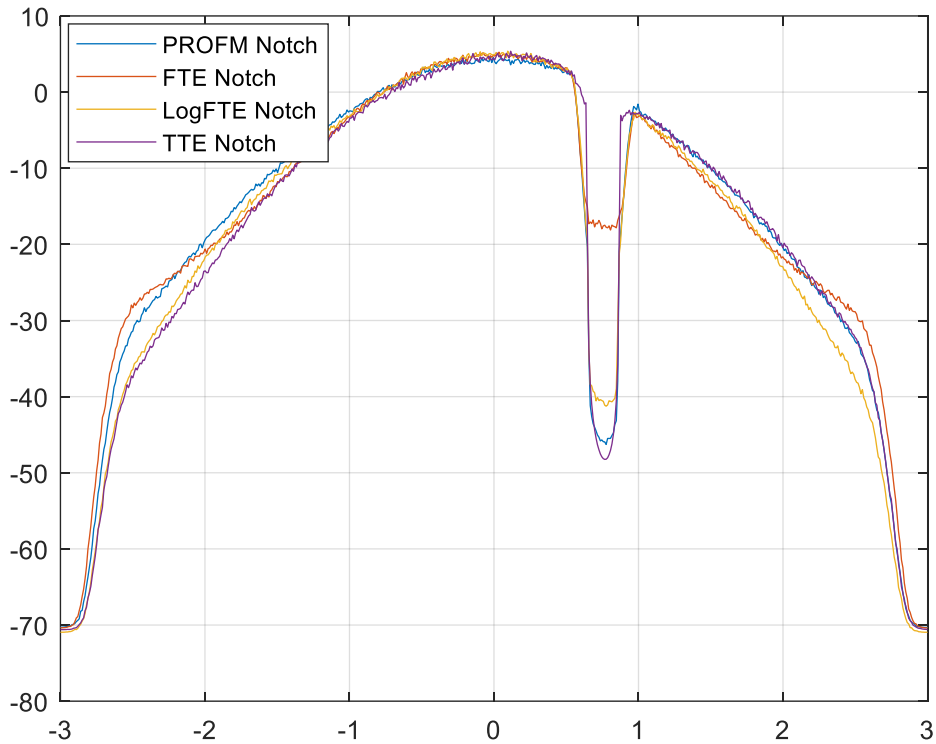


Figure 2.31: Comparison of the average PSD of several waveform classes.

Along with the previous metrics used for the frequency domain, two additional metrics are utilized for the notched waveforms: notch depth and notch width. For these metrics, the notched portion of the spectrum is compared to the mirrored unnotched region for reference. The notch depth is the mean difference from the unnotched levels throughout the notched region. The notch width is the effective width of the notch below a notch depth threshold of -10dB, and is reported as a percentage of the 3dB bandwidth. It is expected that other means of computing the notch depth and width could be considered, but these two metrics will be sufficient for this analysis.

Table 2.11 shows the various PSD metrics for each of the different waveform classes captured in loopback. Notably, even though PRO-FM, Log-FTE, and TTE all have relatively

similar notch depth and widths, the variation on a pulse to pulse basis is significantly different between them.

Table 2.11: Comparison of different waveform class PSD metrics in loopback

Waveform (Loopback)	PRO-FM	FTE	Log-FTE	TTE
Mean Roll-off Level (dB)	-32.71	-32.84	-32.81	-32.67
Roll-off Level Variance (dB)	5.4146	6.3111	3.0293	3.3071
Mean Percent OOB	25.54%	21.66%	22.14%	22.70%
Percent OOB Variance	0.0399%	0.0327	0.0279%	0.0521%
Mean OOB Ratio	0.3440	0.2771	0.2850	0.2949
OOB Ratio Variance	0.0013	0.0008	0.0008	0.0015
Mean Notch Depth (dB)	37.73	17.39	34.95	36.63
Notch Depth Variance (dB)	16.07	5.33	11.36	38.43
Mean Notch Width	12.58%	6.82%	12.48%	11.52%
Notch Width Variance	1.31%	3.56%	1.17%	0.81%

2.3.3 Delay Domain Analysis

Figure 2.32 shows the average autocorrelation response of each waveform class captured in loopback, while Table 2.12 shows the PSL and ISL metrics mean and variance for the loopback waveforms.

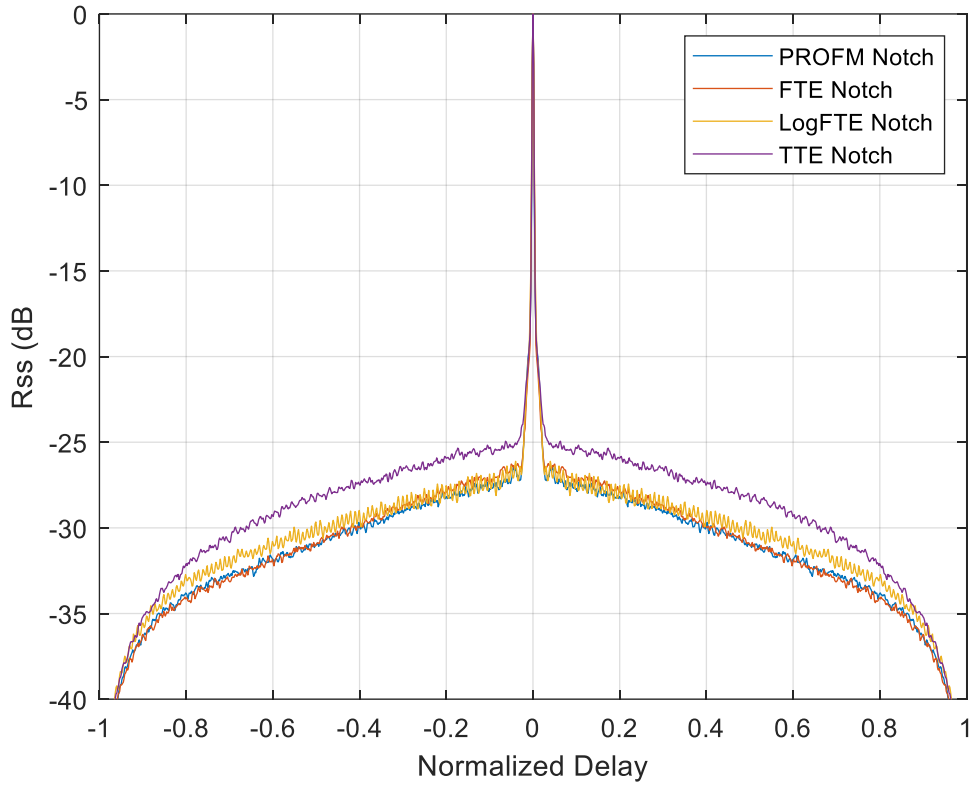


Figure 2.32: Average autocorrelation for different waveform classes.

Table 2.12: Comparison of different waveform class autocorrelation metrics.

Waveform (Loopback)	PRO-FM	FTE	Log-FTE	TTE
PSL Mean (dB)	-18.51	-18.53	-18.55	-17.12
PSL Variance (dB)	1.78	1.54	1.50	1.32
ISL Mean (dB)	-30.97	-30.82	-30.49	-28.79
ISL Variance (dB)	0.06	0.07	0.08	0.28

2.4 Joint Time-Frequency Analysis of Notched Gaussian Spectral Shapes

With a traditional analysis of notched Gaussian waveforms completed, it is time to consider the various joint time-frequency domains as was done in 2.2.

2.4.1 Angle-Based Instantaneous Frequency Analysis

For each class, a histogram is generated from the entire waveform set's instantaneous frequency values. Figures 2.33, 2.34, 2.35, and 2.36 show the histograms of PRO-FM, FTE, Log-FTE, and TTE notched waveforms respectively.

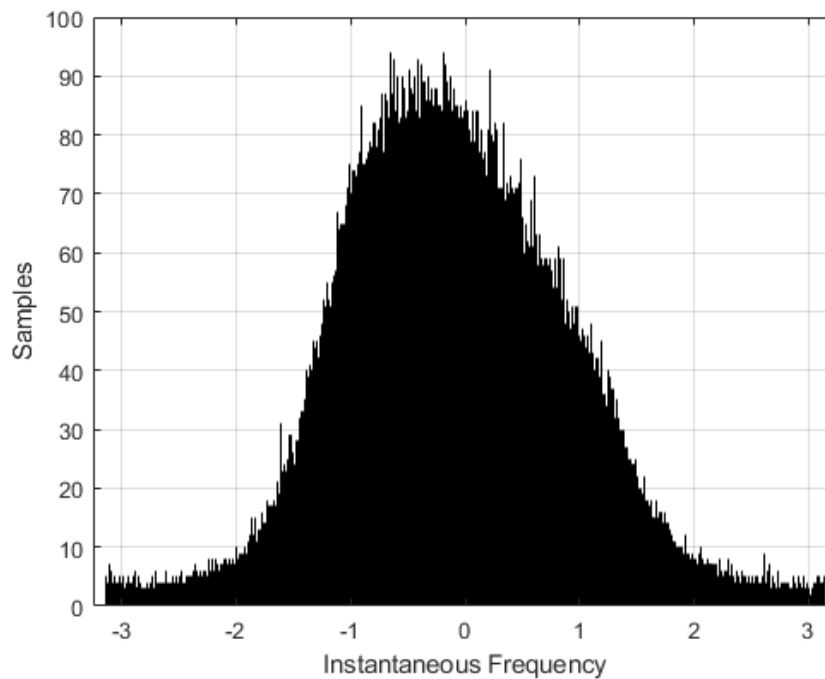


Figure 2.33: Instantaneous Frequency distribution for notched PRO-FM captured in loopback.

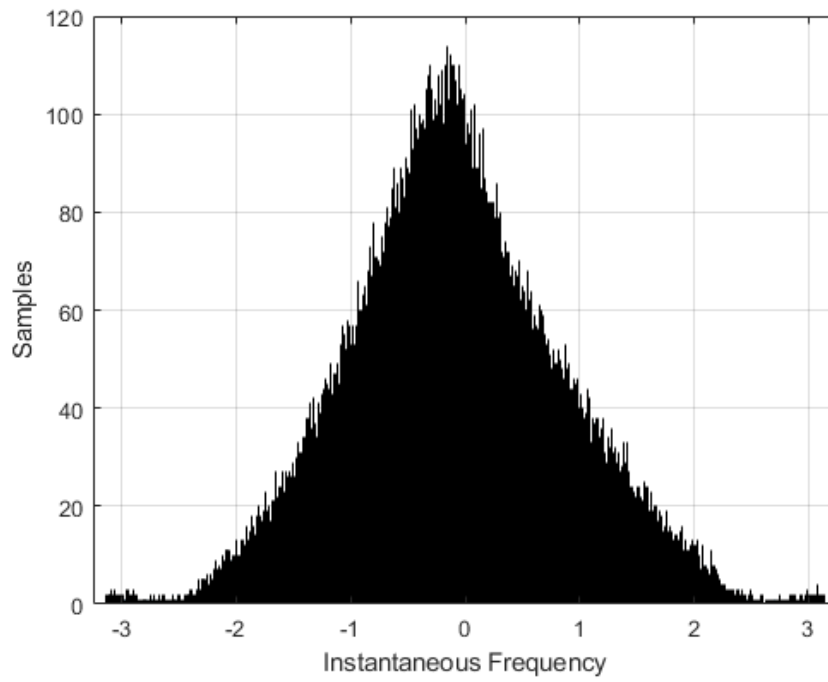


Figure 2.34: Instantaneous frequency distribution for notched FTE captured in loopback.

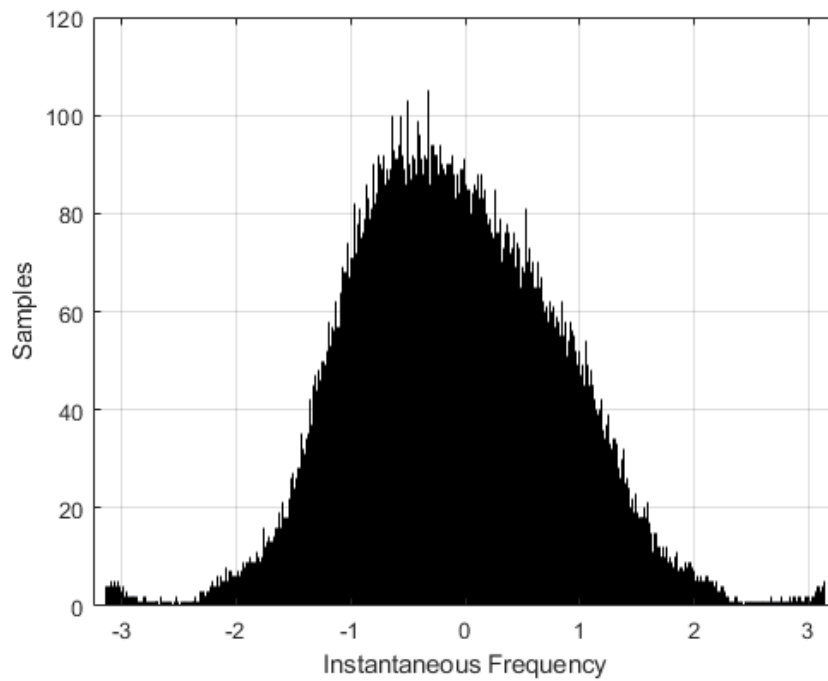


Figure 2.35: Instantaneous frequency distribution for notched Log-FTE captured in loopback.

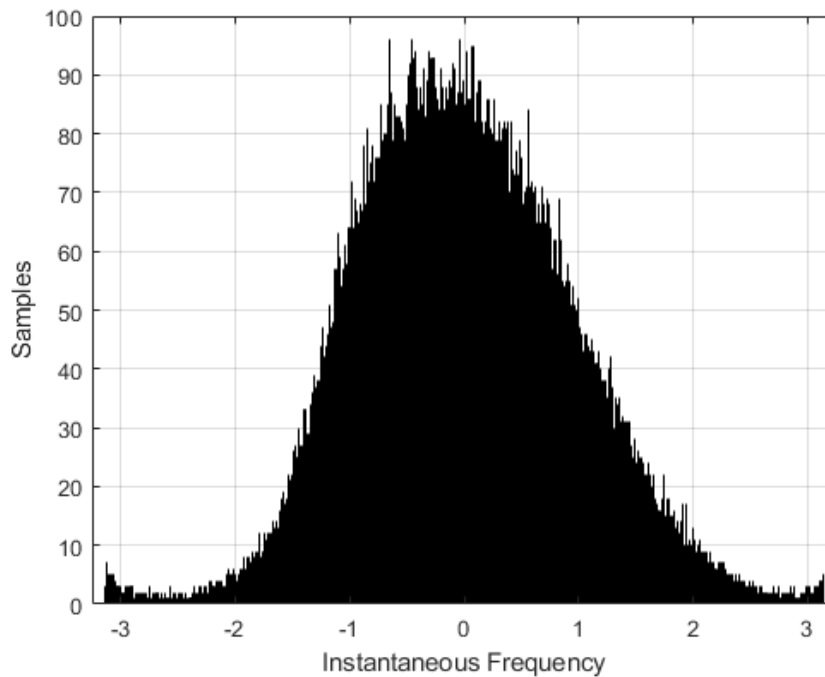


Figure 2.36: Instantaneous frequency distribution for notched TTE captured in loopback.

Table 2.13 shows show the mean, variance, and 99th percentile values for each of the distributions in simulation and loopback respectively. PRO-FM, FTE, and Log-FTE have notably shifted means towards the side of the spectrum without a notch, while less notably so with TTE.

Table 2.13: Instantaneous frequency metrics for various notched waveform classes captured in loopback.

Waveform (Loopback)	PRO-FM	FTE	Log-FTE	TTE
Mean	-0.1073	-0.9510	-0.1088	-0.0159
Variance	0.7888	0.6975	0.6488	-0.7116
99th Percentile	2.515	2.116	2.000	2.280

2.4.2 Spectrogram Analysis

To characterize the behavior of the notch temporally throughout the waveform, they must be viewed in a fully 2D joint time frequency transform. First, the waveforms are studied using the STFT-based spectrogram previously shown in 2.2.2.

Unlike the symmetric Gaussian spectral random FM waveforms, the presence of a notch will greatly alter the behavior of the spectrogram. For notched random FM waveforms, three regimes of notch behavior exist depending on the window size used [33].

- Large window size: When the window is large enough, the notch is visibly present during all times in the waveform.
- Medium window size: When the window size decreases, the notch will narrow and appear as a series of nulls across time.
- Small window size: When the window size decreases further, the spectrogram will match up to the instantaneous frequency of the waveform, with no notch present.

As previously noted, the sampling frequency and oversampling factor used will greatly the time window percentages in which these various behaviors occur.

Figure 2.37 shows an example spectrogram of a PRO-FM waveform using a 20% of pulse width wide window, where the horizontal axis is time and the vertical axis is frequency. The notch can be seen clearly throughout the entirety of the waveform. Figure 2.38 shows a spectrogram of a PRO-FM waveform using a 5% of pulse width wide window. Though the notch region is still present, it more closely resembles a series of nulls than a continuous low energy region. Lastly, figure 2.39 shows a spectrogram of a PRO-FM waveform using 1% of pulse width wide window. While the frequency resolution is coarse, the spectrogram resembles the instantaneous frequency of the waveform, with no spectral notch visibly present.

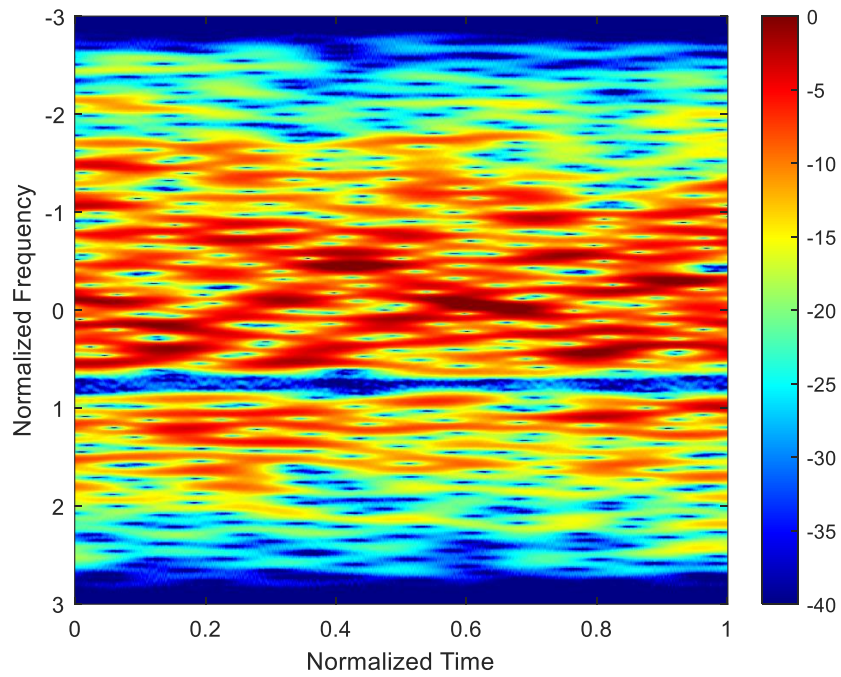


Figure 2.37: Spectrogram of a notched PRO-FM waveform using a 20% time window

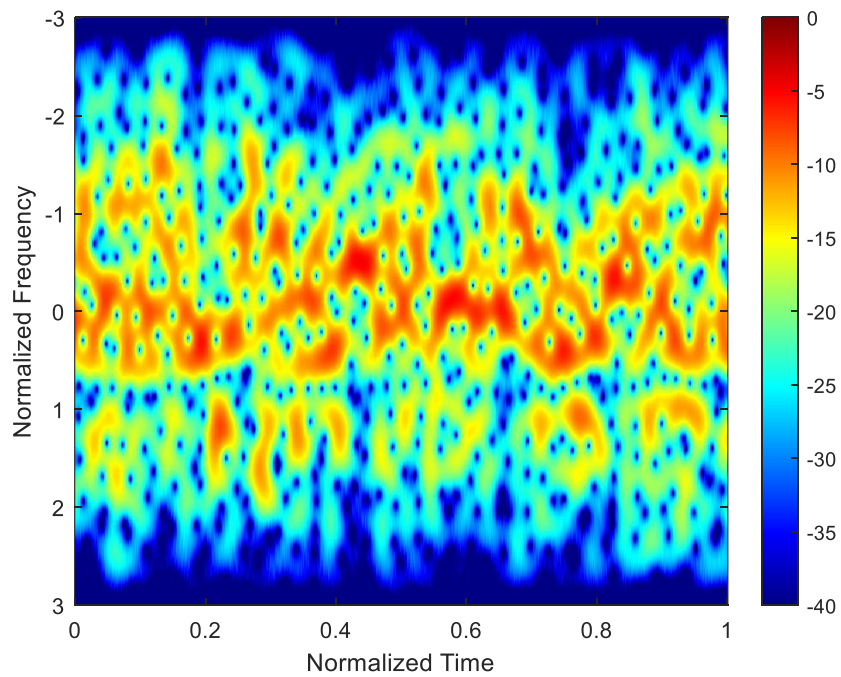


Figure 2.38: Spectrogram of a notched PRO-FM waveform using a 5% time window

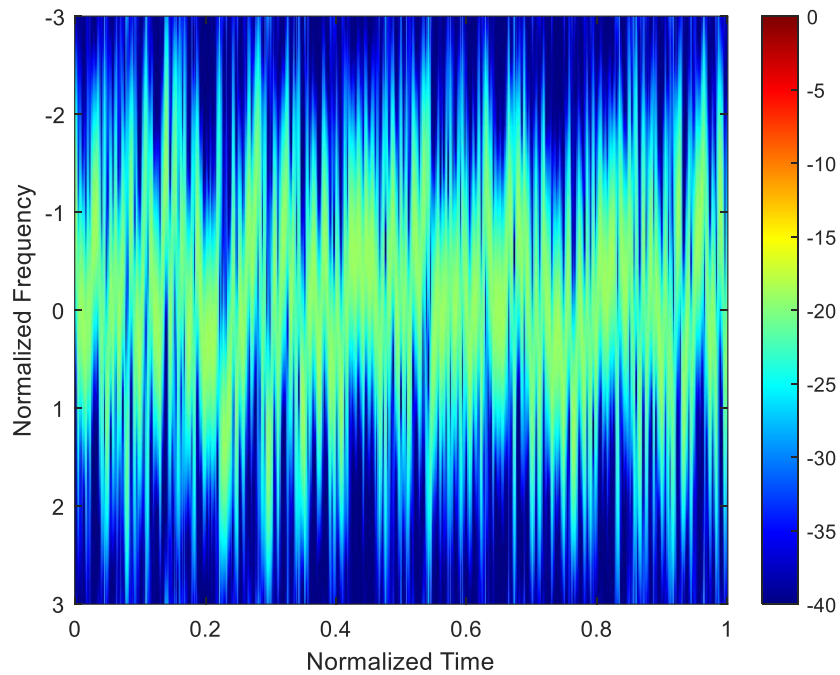


Figure 2.39: Spectrogram of a notched PRO-FM waveform using a 1% time window

To further quantify the results, similar metrics to those used in section 2.3.2 are utilized to characterize the spectrogram notches. Both notch depth and width are computed again, but they are averaged over the time axis as well. They are computed regardless of whether or not the notch is visible in the transform, as it is still insightful to determine if less energy is placed in that region of the spectrogram.

Table 2.14 shows the results of the analysis for a 10% time window, while Table 2.15 shows the results for a 1% time window. Notably, the notch is present in all of the 10% window spectrograms, even though FTE isn't nearly as deep as the rest. For the 1% case, no significant notch is present, though all the waveforms consistently show less energy in the expected notch region than would be observed for an unnotched waveform.

Table 2.14: Spectrogram metrics for various notched waveform classes using 10% time window.

Waveform (Loopback)	PRO-FM	FTE	Log-FTE	TTE
Mean Roll-off Level (dB)	-53.64	-53.60	-53.93	-53.91
Roll-off Level Variance (dB)	0.0728	0.0728	0.0885	0.1470
Mean Percent OOB	41.32%	38.56%	38.47%	38.23%
Percent OOB Variance	0.0157%	0.0154%	0.0125%	0.0331%
Mean Notch Depth (dB)	17.95	8.89	16.79	13.06
Notch Depth Variance (dB)	1.45	1.51	1.34	4.23
Mean Notch Width	7.56%	7.08%	7.54%	7.53%
Notch Width Variance	1.02E-6	1.21E-4	2.23E-06	2.49E-06

Table 2.15: Spectrogram metrics for various notched waveform classes using 1% time window.

Waveform (Loopback)	PRO-FM	FTE	Log-FTE	TTE
Mean Roll-off Level (dB)	-39.08	-39.71	-40.42	-40.95
Roll-off Level Variance (dB)	0.1687	0.2255	0.1739	0.3518
Mean Percent OOB	45.33%	43.65%	43.23%	43.10%
Percent OOB Variance	0.0070%	0.0327%	0.0279%	0.0521%
Mean Notch Depth (dB)	1.27	1.14	1.27	0.53
Notch Depth Variance (dB)	0.18	0.17	0.21	0.27

Mean Notch Width	0%	0%	0%	0%
Notch Width Variance	0	0	0	0

2.5 Traditional FM Design Perspective

After studying these classes of random FM waveforms, the results for the notched waveforms might appear counterintuitive based on traditional waveform design. Specifically, these waveforms represent a departure from the well-known principle of stationary phase (PSP) which was previously discussed.

So why doesn't the PSP seem to apply to the notched random FM waveforms? The PSP makes an assumption about the waveform, namely, that the instantaneous frequency $f(t)$ as a function of time is the inverse of group delay $T(f)$. These quantities and this relationship can be written as:

$$f(t) = T^{-1}(f), \quad (2.3)$$

where

$$f(t) = \frac{1}{2\pi} \frac{d\phi}{dt} \quad (2.4)$$

and

$$T(f) = -2\pi \frac{d\phi}{df} \quad (2.5)$$

When the instantaneous frequency is monotonically increasing or decreasing, this assumption can reasonably be made, as a one-to-one relationship between instantaneous frequency and group delay will be present so the inverse of group delay will exist. However, if the instantaneous frequency is not monotonic, then the relationship is no longer one-to-one but rather one-to-many. Therefore, an inverse will not exist, and this assumption underlying the PSP no

longer holds. This is noticeably the case with random FM waveforms, as their instantaneous frequency will be randomly distributed, almost never being entirely monotonic and crossing over the same instantaneous frequency many times. With respect to spectrally notched random FM, the mechanism which causes the deep spectral notches is not a result of the PSP, but something else [33].

Looking back on what was observed in several of the time-frequency distributions, it was clear that the notch was only apparent over time intervals that were sufficiently long enough. Specifically, when studying the spectrograms of different window lengths, the spectral notch became more prominent as the time window of the spectrogram increased. What is observed is a notch formation that is achieved through means of cancellation over the pulse width. The instantaneous frequency of these notched waveforms creates time-frequency distributions which destructively interfere in the notched spectral bands at sufficiently long time intervals.

2.6 Waveform Analysis Conclusions

The data obtained from the Monte Carlo simulation metrics and experimental testing provide quantitative insight into the variation of random FM waveform classes. However, it is also valuable to determine key trends observed from the data, given the imperfections potentially present in the data (imperfect bandwidth match, random number generator behavior, measurement hardware effects, etc.)

- Random FM waveforms exhibit relatively consistent behavior for a given spectral template, even if no inherent template is specified in the design.

- Optimized waveforms tend to behave more similarly to each other than they do algorithmically generated waveforms. The same is true for algorithmically generated waveforms.
- The optimized waveforms tend to have more varying instantaneous frequency functions than the algorithmically generated ones. This underlying behavior is the most probable cause for the difference in the two sets of waveform classes.
- The greatest difference between waveform classes can be seen in their instantaneous frequency distributions, suggesting that joint time-frequency methods are the most effective way at observing subtleties of random FM waveforms.
- Both waveform class and hardware are limiting components to spectral containment of waveforms. The waveforms exhibited significant variation in spectral containment in simulation but were limited by the hardware when observed in loopback.
- The notches formed by random FM waveform are the result of a cancellation effect, contrary to those formed by quickly chirping through the notch band.
- The notches are only present at sufficiently long time-scales; the notch disappears as the time window of observation decreases.

3. Instantaneous Frequency Estimation of Random FM.

In section 2, the waveforms that were studied were generated in simulation or recovered in a loopback capture. However, the same approach cannot be use to recover the waveforms from freespace, especially in the presence of interference and noise. Here, methods for estimating the instantaneous frequency of random FM in open air are shown.

3.1 Instantaneous Frequency Estimation using the Spectrogram

It is possible to try and used the angle-based instantaneous frequency approach utilized in section 2.2.1. However, in the presence of noise, multipath, or other interference, this method will fail, since the angle-based IF estimation treats the signal as mono-component, as compared to a multi-component signal that an open-air capture would be. Therefore, a joint time-frequency method is more effective at estimating the IF of a random FM signal. Using small time-windows, the spectrogram tends to put the majority of its energy at the frequency value of the instantaneous frequency for a given point in time. Therefore, by estimating the center of the energy across frequency, one should be able to obtain the instantaneous frequency.

3.1.1 Bayesian Estimation of Instantaneous Frequency using the Spectrogram

The question arises on what exactly is the center of a particular time cut of the spectrogram? Here, several statistical measures of central tendency are used [39], namely, the arithmetic mean, median, and mode. More appropriately, these estimators utilize the following cost function from Bayesian risk estimation given as:

$$C(\boldsymbol{\varepsilon}|\mathbf{x}) = \sum_n p^n |\boldsymbol{\varepsilon}_n|^p \quad (3.1)$$

From this cost function, the median corresponds to $p = 1$, the mean corresponds to the MMSE estimate $p = 2$, and the mode corresponds to the MAP estimate $p = \infty$. Once the IF has been estimated across each time bin, these N instantaneous frequency estimates form a vector \mathbf{f} , that can be reconstructed into a discrete, random FM waveform by using:

$$\tilde{\mathbf{s}} = \exp(j\mathbf{L}\mathbf{f}) \quad (3.2)$$

Where \mathbf{L} is a lower diagonal matrix of ones.

Figure 3.1 shows the reconstructed PRO-FM waveform from IF estimation using the three estimators. While the estimate is relatively poor using $p = 1$ or $p = 2$, the $p = \infty$ estimator, or the mode (max) is a close approximation to the PRO-FM waveform.

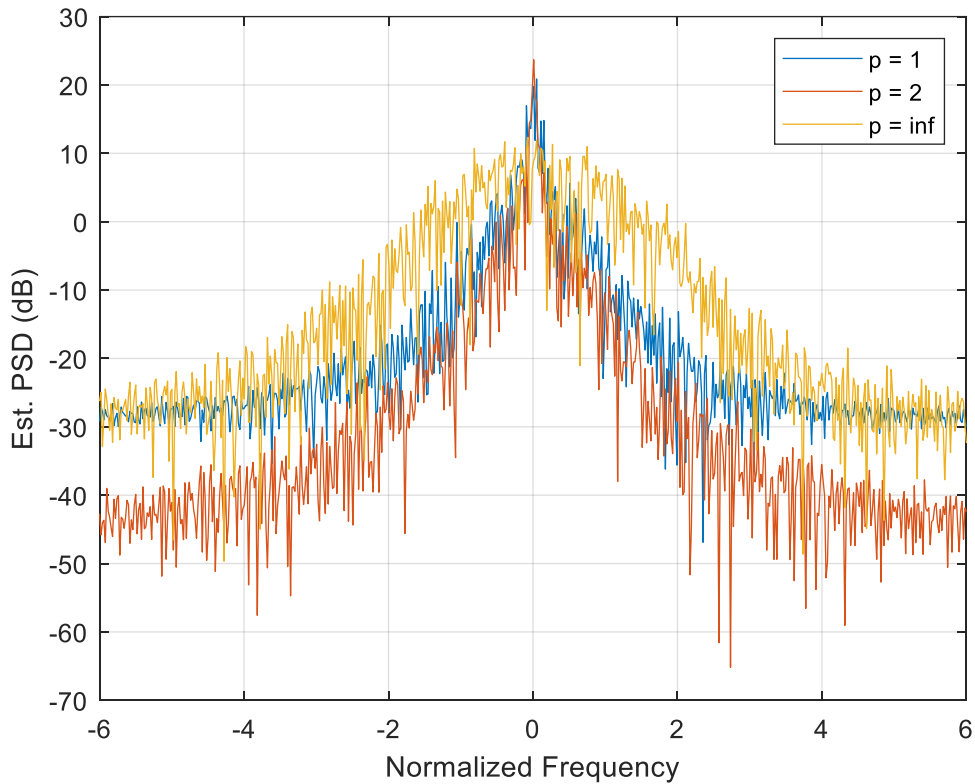


Figure 3.1: Estimated spectrum from different estimators on the spectrogram.

3.1.2 Reiterative Bayesian Estimation of Instantaneous Frequency using the Spectrogram.

The initial estimate provided by the median and mean across frequency provides a poor reconstruction of the initial signal. While the estimator using the mode is somewhat effective at estimating the instantaneous frequency, it is not perfect. However, a reiterative approach can substantially improve the estimation [32]. Here, a reiterative estimation approach is applied to estimate the signals true IF.

Recall the reconstructed signal in (1) which is now denoted as $\tilde{\mathbf{s}}_0$, which can be constructed from the vector of IF estimates f_0 . The original signal can be modulated by the conjugate of the reconstructed signal to obtain a residual signal by:

$$\mathbf{r}_1 = \mathbf{s} \odot \tilde{\mathbf{s}}_0 \quad (3.3)$$

Where \mathbf{r}_1 is the first residual of \mathbf{s} . The spectrogram of the residual signal is computed, and the instantaneous frequency estimate is computed from the residual spectrogram, resulting in f_1 . This can reconstruct a new residual signal \mathbf{r}_2 in the same way that \mathbf{r}_1 was computed. This can be performed reiteratively for K iterations where:

$$\mathbf{r}_k = \mathbf{r}_{k-1} \odot \exp(j\mathbf{L}\mathbf{f}_{k-1}) \quad (3.4)$$

After K iterations, the original signal can be reconstructed by:

$$\hat{\mathbf{s}} = \exp(j\mathbf{L}\sum_{k=0}^{K-1} \mathbf{f}_k) \quad (3.5)$$

So that after a sufficient number of iterations, the residual signal will simply be a constant across time, and thus the reiterative estimate should converge on the IF of the signal.

Figures 3.2 to 3.4 show the original PSD of a PRO-FM signal captured in loopback, the reconstruction of the first estimate, and reconstruction of the tenth iterative estimate of the IF, with figure 3.2 using the $p = 1$ estimator, figure 3.3 using the $p = 2$ estimator, and figure 3.4 using the

$p = \infty$ estimator. It is clear from the figures that, while the initial estimate may be poor, after 10 iterations, each estimator converges upon the true signal.

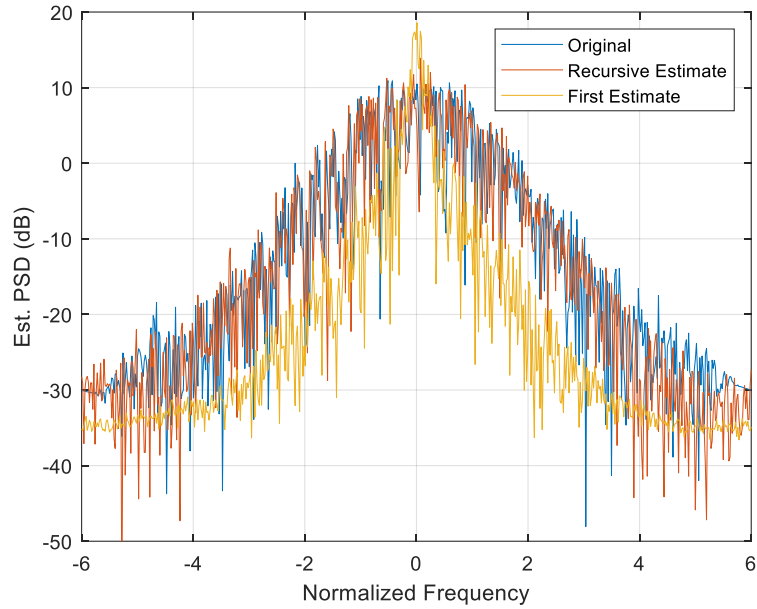


Figure 3.2: Reiterative spectrum estimate using the $p = 1$ estimator for 10 iterations.

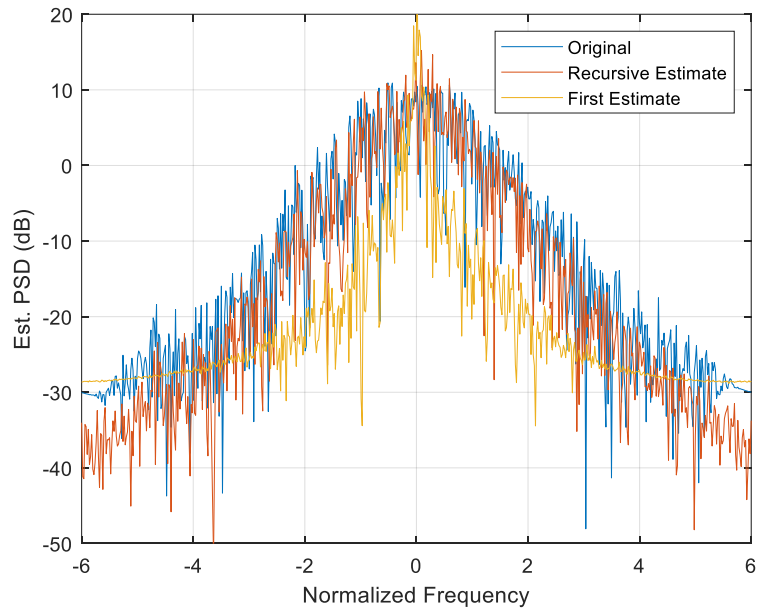


Figure 3.3: Reiterative spectrum estimate using the $p = 2$ estimator for 10 iterations.

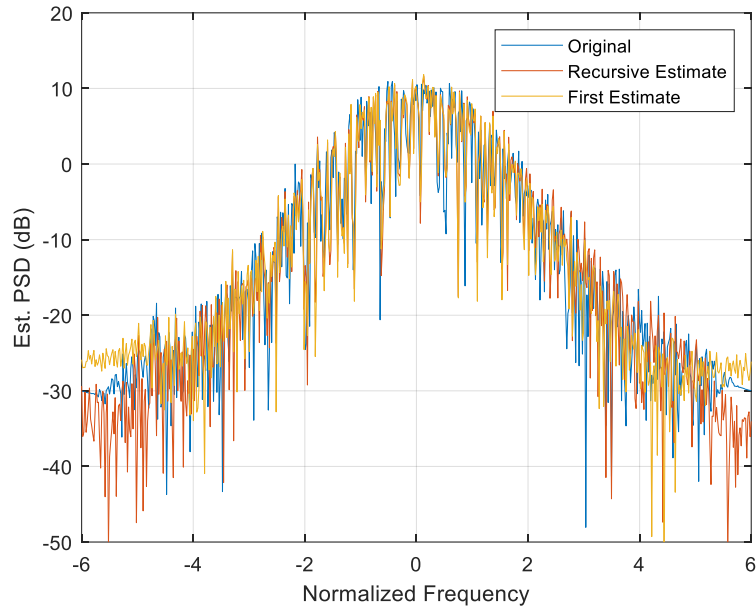


Figure 3.4: Reiterative spectrum estimate using the $p = \infty$ estimator for 10 iterations.

Figure 3.5 shows a comparison of the mean squared error (MSE) for each of the 3 estimators on average for 1,000 PRO-FM waveforms captured in loopback. The estimation was applied for 100 iterations, with the performance evaluated at each iteration. While the MAP estimator performs the best initial guess, it is not well suited for reiterative estimates on the spectrogram. The median and MMSE estimates, however, start off significantly more poorly, but converge to more accurate estimates after a number of iterations. However, in all cases, a point is reached where the iterative approach no longer can improve the IF estimate.

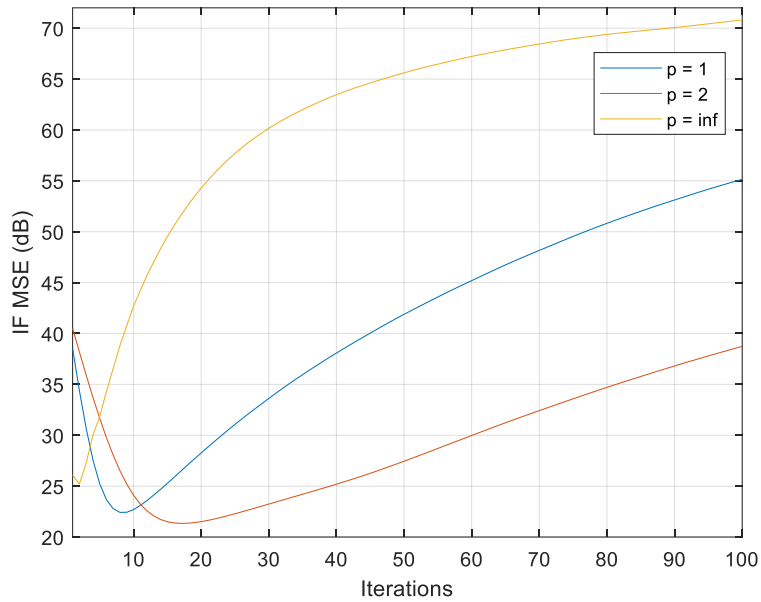


Figure 3.5: Comparison of estimators versus iterations on PRO-FM.

The estimators in all cases tend to perform better with smoother phase functions. Figure 3.6 shows a comparison of the MSE for each of the 3 estimators on average for 1,000 CE-OFDM waveforms captured in loopback. Again, the estimation was applied for 100 iterations, with the performance evaluated at each iteration.

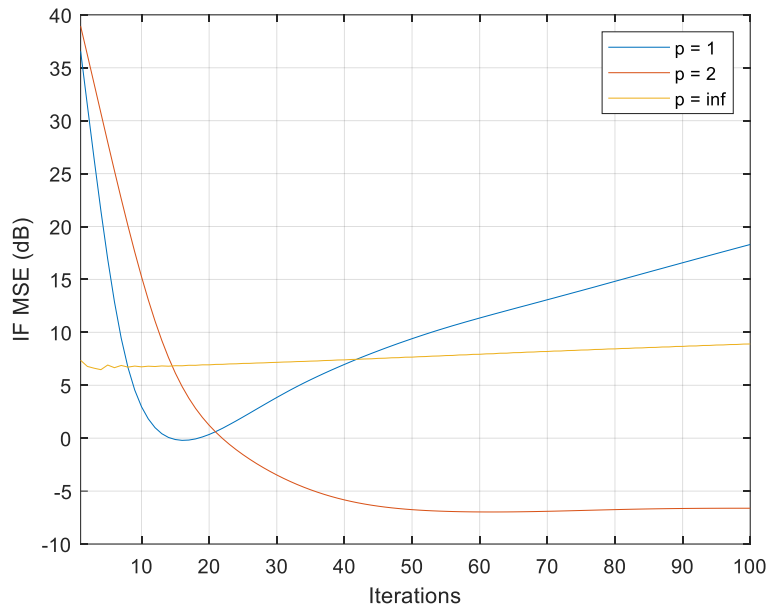


Figure 3.6: Comparison of estimators versus iterations on PRO-FM.

4. Conclusions & Future Work

Waveform diverse designs can be analyzed in many different domains to observe various properties about the waveform classes. Variations in performance can be observed between these classes of waveforms even when controlled to the same desired spectral template. The choice of optimization impacts many of these metrics, providing more noise-like waveforms than those that do not utilize optimization. The effects of hardware on the different waveform classes were also observed to deviate from their simulated forms.

The use of joint time-frequency analysis provided the deepest insights into the various waveform behaviors. This suggests that joint time-frequency methods are the most effective way at observing subtle behaviors of the waveforms. These results demonstrate the importance of the observation time scale in correctly understanding the waveforms spectral interaction. This behavior is most readily observed in the notched waveforms, where the formation and depth of the notch was dependent on the observation time scale. This is due to the cancellation behavior of the notches across the length of the waveform. The histograms, spectrograms, and WVDs of the notched waveforms clearly show that the waveform does not simply chirp through the notched region.

The insights provided by the analysis were leveraged to accurately estimate the instantaneous frequency profiles of the random FM waveforms using a reiterative approach. The choice of estimator was shown to impact both the accuracy and convergence rate of the estimation. The use of time-frequency estimation can provide accurate estimation even in the presence of noise and interference, providing an alternative to filter based approaches which may alter the subtleties of the waveform classes.

The use of joint time-frequency techniques provides additional tools for not only understanding existing waveform classes, but in the processing algorithms and future designs. Future work should include leveraging these insights to improve the design of existing random FM approaches or developing entirely novel ones. Utilizing the analysis performed in this work on a wider array of hardware may also better characterize alterations to the waveforms due to hardware as opposed to their particular design approach.

References

- [1] M. A. Richards, J. Scheer, W. A. Holm, and W. L. Melvin, *Principles of modern radar*. Citeseer, 2010.
- [2] S. Mitra and T. Acharya, "Gesture Recognition: A Survey," *IEEE Transactions on Systems, Man, and Cybernetics, Part C (Applications and Reviews)*, vol. 37, no. 3, pp. 311-324, May 2007
- [3] Norbert Wiener, *Time Series*. M.I.T. Press, Cambridge, Massachusetts. p. 42, 1964.
- [4] N. Levanon, E. Mozeson, *Radar Signals*, Wiley-IEEE Press, 2004.
- [5] *Random FM autocorrelation fuze system*, Sept. 1980.
- [6] L. Guosui, G. Hong, Z. Xiaohua and S. Weimin, "The present and future of random signal
- [7] S.R.J. Axelsson, "Noise radar using random phase and frequency modulation", *IEEE Trans. Geoscience & Remote Sensing*, vol. 42, no. 11, pp. 2370-2384, Nov. 2004.
- [8] L. Pralon, B. Pompeo and J.M. Fortes, "Stochastic analysis of random frequency modulated waveforms for noise radar systems", *IEEE Trans. Aerospace & Electronic Systems*, vol. 51, no. 2, pp. 1447-1461, Apr. 2015.
- [9] L. Pralon, G. Beltrao, B. Pompeo, M. Pralon and J.M. Fortes, "Near-thumbtack ambiguity function of random frequency modulated signals", *IEEE Radar Conf.*, May 2017.
- [10] S.D. Blunt, J.K. Jakobosky, C.A. Mohr, P.M. McCormick, J.W. Owen, B. Ravenscroft, C. Sahin, G.D. Zook, C.C. Jones, J.G. Metcalf, and T. Higgins, "Principles & Applications of Random FM Radar Waveform Design," *IEEE Aerospace & Electronic Systems Magazine*, vol. 35, no. 10, pp. 20-28, Oct. 2020.
- [11] M.B. Heintzelman, T.J. Kramer, S.D. Blunt, "Experimental Evaluation of Super-Gaussian-Shaped Random FM Waveforms," *IEEE Radar Conference*, New York City, NY, 21-25 Mar. 2022.

- [12] T.J. Kramer, M.B. Heintzleman, S.D. Blunt, "On the Repeated Use of Random FM Waveforms," IEEE Radar Conference, New York City, NY, 21-25 Mar. 2022.
- [13] C.A. Mohr, S.D. Blunt, "Designing Random FM Radar Waveforms with Compact Spectrum," IEEE International Conference on Acoustics, Speech & Signal Processing (ICASSP), Toronto, Canada, 6-11 June 2021.
- [14] T.J. Kramer, S.D. Blunt, "Time-Frequency Analysis of Spectrally-Notched Random FM Waveforms," 2020 IEEE International Radar Conference, Washington, DC, 27-30 Apr. 2020.
- [15] C.A. Mohr, P.M. McCormick, and S.D. Blunt, "Optimized Complementary Waveform Subsets within an FM Noise Radar CPI," IEEE Radar Conference, Oklahoma City, OK, 23-27 Apr. 2018.
- [16] J.W. Owen, C.A. Mohr, B.H. Kirk, S.D. Blunt, A.F. Martone, K.D. Sherbondy, "Demonstration of Real-Time Cognitive Radar using Spectrally-Notched Random FM Waveforms," 2020 IEEE International Radar Conference, Washington, DC, 27-30 Apr. 2020.
- [17] J. Nocedal, S. Wright, *Numerical Optimization*, Springer, 2006.
- [18] S. D. Blunt, M. R. Cook, J. Jakobosky, J. De Graaf, and E. Perrins, "Polyphase-coded FM (PCFM) radar waveforms, part i: implementation," IEEE Transactions on Aerospace and Electronic Systems, vol. 50, no. 3, pp. 2218–2229, July 2014
- [19] J. Jakobosky, S. D. Blunt, and B. Himed, "Waveform design and receive processing for non-recurrent nonlinear FMCW radar," in *2015 IEEE Radar Conference (RadarCon)*, pp. 1376-1381, May 2015.
- [20] J. Jakobosky, S. D. Blunt, and B. Himed, "Spectral-shape optimized FM noise radar for pulse agility," in *2016 IEEE Radar Conference (RadarConf)*, pp. 1-6, May 2016.

- [21] C. A. Mohr, P. M. McCormick, S. D. Blunt, and C. Mott, "Spectrally-efficient FM noise radar waveforms optimized in the logarithmic domain," in *2018 IEEE Radar Conference (RadarConf18)*, pp. 0839-0844, April 2018.
- [22] C. A. Mohr and S. D. Blunt, "FM noise waveforms optimized according to a temporal template error (TTE) metric," in *2019 IEEE Radar Conference (RadarConf)*, pp. 1-6, Apr 2019.
- [23] S. D. Blunt and E. L. Mokole, "Overview of radar waveform diversity," *IEEE Aerospace and Electronic Systems Magazine*, vol. 31, pp. 2-42, November 2016.
- [24] A. L. Drozd, et. al., "Multiobjective joint optimization and frequency diversity for efficient utilization of the RF transmission hyperspace," *2004 International Waveform Diversity and Design Conference*, Nov. 2004.
- [25] G. Zook, P. M. McCormick, S. D. Blunt, C. Allen, and J. Jakabosky, "Dual-polarized FM noise radar," in *International Conference on Radar Systems (Radar 2017)*, pp. 1-5, Oct 2017.
- [26] C. A. Mohr and S. D. Blunt, "Design and generation of stochastically defined, pulsed FM noise waveforms," in *2019 International Conference on Radar (RADAR)*, pp. 1-6, Sep 2019.
- [27] C.-D. Chung and S.-M. Cho, "Constant-envelope orthogonal frequency division multiplexing modulation", Proc. APCC/OECC, Oct. 1999.
- [28] S.C. Thompson, A.U. Ahmed, J.G. Proakis and J.R. Zeidler, "Constant envelope OFDM phase modulation: spectral containment signal space properties and performance", IEEE Military Communications Conf., Oct./Nov. 2004.
- [29] S.C. Thompson et al., "Constant envelope OFDM", IEEE Trans. Communications, vol. 56, no. 8, pp. 1300-1312, Aug. 2008.

- [30] M.P. Wylie-Green, E. Perrins and T. Svensson, "Introduction to CPM-SC-FDMA: a novel multi-access power-efficient transmission scheme", *IEEE Trans. Communications*, vol. 59, no. 7, pp. 1904-1915, July 2011.
- [31] E. R. Biehl, C. A. Mohr, B. Ravenscroft and S. D. Blunt, "Assessment of Constant Envelope OFDM as a Class of Random FM Radar Waveforms," *2020 IEEE Radar Conf.*, 2020, Sep 2020.
- [32] B. Boashash, *Time-Frequency Signal Analysis and Processing*, 2016.
- [33] T.J. Kramer, S.D. Blunt, "Time-Frequency Analysis of Spectrally-Notched Random FM Waveforms," *2020 IEEE International Radar Conference*, Washington, DC, 27-30 Apr. 2020.
- [34] L. Cohen, "Time-frequency distributions – a review," *Proc. IEEE*, vol. 77, no. 7, Jul. 1989.
- [35] E. N. Fowle, "The design of FM pulse compression signals", *IEEE Trans. Information Theory*, vol. 10, no. 1, pp. 61-67, Jan. 1964.
- [36] J. Owen, C. Mohr, B. Ravenscroft, S. Blunt, B. Kirk, A. Martone, "Real-Time Experimental Demonstration and Evaluation of Open-Air Sense-and-Notch Radar," *IEEE Radar Conference*, New York City, NY, 21-25 Mar. 2022.
- [37] J.W. Owen, B. Ravenscroft, B.H. Kirk, S.D. Blunt, C.T. Allen, A.F. Martone, K.D. Sherbondy, and R.M. Narayanan, "Experimental Demonstration of Cognitive Spectrum Sensing & Notching for Radar," *IEEE Radar Conference*, Oklahoma City, OK, 23-27 Apr. 2018.
- [38] J. Jakabosky, S.D. Blunt, and A. Martone, "Incorporating Hopped Spectral Gaps into Nonrecurrent Nonlinear FMCW Radar Emissions," *IEEE Intl. Workshop on Computational Advances in Multi-Sensor Adaptive Processing*, Cancun, Mexico, 13-16 Dec. 2015.
- [39] Weisberg H.F., *Central Tendency and Variability*, 1992.